SOME ELECTRO-ACOUSTIC EFFECTS
IN CADMIUM SULFIDE

SOME ELECTRO-ACOUSTIC EFFECTS
IN CADMIUM SULFIDE

PROEFSCHRIFT

TER VERKRIJGING VAN DE GRAAD VAN DOCTOR
IN DE WISKUNDE EN NATUURWETENSCHAPPEN
AAN DE RIJKSUNIVERSITEIT TE UTRECHT, OP
GEZAG VAN DE RECTOR MAGNIFICUS
PROF. DR. M. A. BOUMAN, VOLGENS BESLUIT VAN
HET COLLEGE VAN DECANEN IN HET OPENBAAR
TE VERDEDIGEN OP WOENSDAG 24 MAART 1982
DES NAMIDDAGS TE 4.15 UUR

DOOR

WIM WESTERA

GEBOREN OP 20 APRIL 1954 TE DOESBURG

PROMOTOREN: PROF. DR. R. J. J. ZIJLSTRA
PROF. DR. C. TH. J. ALKEMADE

EPPUR SI MUOVE

(en tòch beweegt zij zich)

Galileo Galileï

C O N T E N T S

Voorwoord

In dit voorwoord wil ik graag iedereen bedanken, die in de afgelopen vier jaar op de één of andere manier een bijdrage heeft geleverd aan de totstandkoming van dit proefschrift. In het bijzonder wil ik bedanken:

— mijn promotoren Rijk Zijlstra en Cees Alkemade voor de talloze diskussies en voor hun kritische houding bij het op schrift stellen van de resultaten van dit onderzoek,

— Harry Slaper, Menno van Dijk, Toine Geelen en Gerhard Dalhoeven voor de bergen werk, die zij als student verzet hebben,

— Frans Wollenberg voor het oplossen van de vele, bijna onoplosbare technische problemen,

— mijn kollega's Jitze van der Meulen en Daan Frenkel, en mijn oud-kollega's Hans Timmermans, Dick van Eck en Gijs Bosman voor de vele vruchtbare diskussies,

— Sheila McNab voor de vele taal-adviezen,

— Greetje Hollander voor het foutloze typewerk,

— Marian Oskam voor het puntgave tekenwerk,

— niet te vergeten mijn ouders, die mij in de gelegenheid stelden een goede opleiding te volgen,

— en tenslotte Ite, wier bijdrage aan dit onderzoek niet is weg te denken.

Wim

1

CHAPTER   I

GENERAL INTRODUCTION

In a piezoelectric semiconductor free charge carriers may interact strong-
ly with acoustic waves. An acoustic wave propagating in such a crystal will be
accompanied by a piezoelectric field, which produces a periodic variation in
the electric potential. As the free charge carriers tend to seek the potential
minima, this potential wave modulates the space-charge distribution. If the
drift velocity of the carriers is smaller than the sound velocity, acoustic
energy is thereby transferred to the carriers, and the acoustic wave is at-
tenuated. However, if an applied electric field causes the drift velocity of
the carriers to exceed the sound velocity, energy is transferred from the
carriers to the sound wave, resulting in the amplification of the sound wave.
This sound-amplification process is called the *electro-acoustic effect*, or
acousto-electric effect. We prefer the former term, because the cause, i.e.
the application of a sufficiently high *electric* field, should precede the
effect, i.e. the amplification of *acoustic* waves.

The electro-acoustic amplification of sound waves is selective with re-
spect to the polarization direction, the propagation direction as well as to
the frequency of the sound waves [1, 2]. Clearly, only acoustic waves that pro-
duce piezoelectric fields, i.e. piezoelectrically active acoustic waves, can
be amplified. In general the number of piezoelectrically active modes is re-
stricted due to the particular crystal symmetry. The frequency range suitable
for the amplification of acoustic waves is restricted to the range where space-
charge waves can be built up. If the frequency of the acoustic wave is much
lower than the dielectric-relaxation frequency f_c ($f \ll f_c$), the free carriers
redistribute themselves quickly enough to cancel the piezoelectric field pro-
duced by the wave; at frequencies much higher than the carrier-diffusion fre-
quency f_D ($f \gg f_D$), carrier diffusion counteracts the build-up of space-charge
waves. In both cases the interaction between acoustic waves and free charge
carriers is absent. It follows therefore that optimum amplification occurs at
intermediate frequencies, determined by f_c and f_D.

In 1962 White [3] gave a linear classical continuum description of the electro-acoustic effect by extending the theory of elastic wave propagation in piezoelectric semiconductors as given in 1961 by Hutson et al. [4], to the case where an electric field is applied. White did indeed find a maximum in the amplification coefficient at a frequency given by $f_m = (f_c \cdot f_D)^{\frac{1}{2}}$. One year earlier, the first experimental results on electro-acoustic amplification were reported by Hutson et al. [5] for photoconducting single crystals of hexagonal CdS. In addition to the amplification of injected acoustic waves they also observed the amplification of acoustic waves originating from the thermal background. A subordinate difficulty in most experiments on this subject is that the electrical bias has to be applied in pulses of short duration to avoid excessive Joule heating.

Brillouin-scattering studies [6-8] of the growth of the acoustic flux in semiconducting CdS have made it clear that the linear theory applies only in the weak-flux region. At higher acoustic flux intensities the frequency of maximum gain has been found to be an order of magnitude lower than that predicted by White's theory. This frequency down-shift is ascribed to non-linearities in the interaction between the acoustic waves and the space-charge waves. These nonlinearities also give rise to other effects; these may include current saturation, current oscillations, large current fluctuations and ac-impedance effects. These effects as well as the sound-amplification process itself are usually referred to as *electro-acoustic effects*. In this thesis we shall use the term electro-acoustic effect in both contexts.

So far there has been a great deal of controversy about which type of acoustic wave, transverse or longitudinal, is amplified in piezoelectric semi-conductors such as CdS and the crystallographically similar ZnO. Because in these materials the sound velocity of longitudinal waves is more than twice that of transverse waves, the determination of the critical electric field strength E_c marking the onset of the electro-acoustic effect, can, in principle, be used to discriminate between the two types of waves. The critical field E_c is equal to v_s/μ, where v_s is the sound velocity and μ the carrier drift-mobility. However, the considerable spread in the literature values for the carrier drift-mobility in CdS and ZnO gives rise to ambiguous results for the sound velocity as calculated from the measured E_c. (It should be noted that both CdS and ZnO are always n-type.) In the following we shall give a brief summary of statements on this problem made in the literature.

We shall distinguish between two experimental configurations [2]: if the

4

electric field is applied parallel to the c-axis one refers to the *longitudinal configuration*; if the electric field is applied perpendicular to the c-axis one refers to the *transverse configuration*. It should be realized that these names can be very misleading.

In 1962 Smith [9] investigated electro-acoustic current saturation in CdS in both configurations. He found that the critical field E_c as obtained from the onset of current saturation was the same in both configurations. He concluded that longitudinal acoustic waves are amplified in both configurations. In 1963 McFee [10] concluded from his experimental data on current saturation in ZnO and CdS that transverse waves are amplified in both configurations. He suggested that in the longitudinal configuration the amplified transverse waves are off-axis waves, i.e. waves whose wave vectors make finite angles with the c-axis, because the latter waves are piezoelectrically active, in contrast with transverse on-axis waves [2]. Subsequently Moore et al. [11, 12] reported that for both configurations longitudinal waves are amplified in CdS. They [12] obtained E_c from the onset field of current saturation and determined explicitly the electron Hall-mobility to obtain the sound velocity.

In 1967 Wettling [13] measured the frequency shift of the Brillouin-scattered light in CdS using a Fabry-Perot interferometer. Since the theoretical values of the frequency shift as calculated from the Brillouin-scattering formulas depend on the value of the sound velocity, Wettling deduced the sound velocity of the amplified acoustic waves by comparing the experimental frequency-shift with the calculated one. He concluded that in the transverse configuration transverse waves are amplified and that longitudinal waves are amplified in the longitudinal configuration. He also came to the same conclusion through measurements of the polarization of the Brillouin-scattered light. However, from similar Brillouin-scattering experiments on ZnO as reported one year later Wettling et al. [14] concluded that transverse waves are amplified in both configurations. In view of the crystallographic similarity of ZnO and CdS these results confuse rather than clarify.

In 1967 Moore [15] measured electro-acoustic current fluctuations in CdS in the longitudinal configuration. From the onset field of the current fluctuations he inferred that longitudinal waves are amplified. In 1968 Moore [16] used the effect of strain-induced optical birefringence in CdS to obtain a direct image of the amplified acoustic waves. He concluded that in both configurations transverse waves are amplified.

5

Several authors [17-19] have reported data on Brillouin-scattering by transverse waves in both configurations.

Recently Gielen and Zijlstra [20, 21] concluded from the onset field of electro-acoustic current fluctuations in CdS that longitudinal waves are amplified in the longitudinal configuration.

From resonances in the ac impedance occurring at frequencies that are related to the transit time of the amplified acoustic waves Westera, Zijlstra and van Dijk [22, 23] were able to find the sound velocity. The sound velocities thus obtained in CdS samples in the longitudinal configuration were close to the velocity of transverse waves.

So far it is commonly accepted that in the transverse configuration it is transverse waves that are amplified. The dispute about which waves are amplified in the longitudinal configuration will be settled in Chapter III of this thesis, where measurements on the ac impedance are combined with measurements on current saturation in CdS samples.

Usually the amplified acoustic flux has been found to be concentrated in macroscopic travelling domains starting at the carrier-injecting contact and propagating with the sound velocity in the direction of the carrier drift. The occurrence of travelling acoustic domains involves macroscopic electrical current oscillations with a period equal to the domain transit-time, and a highly non-uniform distribution of the electric field. The formation of these domains is probably due to shock excitation during the turn-on transient of the electrical bias-pulse [24-26]. Domain excitation can be suppressed by using bias pulses with relatively long rise-times ($\gtrsim$ 1 μs); some authors [9, 15] have argued that the use of relatively short samples ($\lesssim$ 3 mm) may also be helpful in avoiding domain formation. In the absence of travelling acoustic domain-formation stable current saturation occurs. The amplified acoustic flux, which originates from the thermal background, is then found to be continuously distributed over the sample [24, 25], and the electric field is found to be uniform [9, 15]. In a study of the electro-acoustically amplified thermal flux the occurrence of shock excitation should be avoided, as it involves the injection of a large, poorly defined acoustic disturbance. So far, however, most Brillouin-scattering studies reported in the literature deal mainly with the growth of the acoustic flux in these acoustic domains, so there is a lack of experimental data on a domain-less type of amplified flux.

In this thesis we report Brillouin-scattering data and experimental data on current saturation, ac impedance and current noise for CdS single crystals

6

where the electric field is parallel to the c-axis, and the amplified thermal flux is continuously distributed over the sample. Since there is rotational symmetry around the current direction in the longitudinal configuration, the mathematical analysis of the electro-acoustic phenomena can be simplified considerably. In the transverse configuration, however, the analysis becomes more complicated because of the lack of rotational symmetry around the current direction, particularly when an appreciable amount of off-axis flux is present [2, 18].

The investigations reported in this thesis form part of the research project on non-Ohmic charge transport in semiconductors under high electric-field conditions, which is being carried out by the research group "Fysische Fluktuatieverschijnselen" of the Physics Department, State University of Utrecht. Since the trend in technology is towards a further miniaturization of devices (chips, micro-chips), effects at high electric field strengths will become more and more important. Although we have restricted ourselves here to the case of piezoelectric semiconductors, some of the theoretical results reported in Chapter II may have wider applications.

By using a simple model we avoided the need for nonlinear equations to describe current saturation, current fluctuations and ac-impedance effects. We assumed that groups of electrons in the conduction band can become trapped in deep potential troughs that are associated with the amplified acoustic waves. Clearly, the trapping of supersonically drifting charge carriers in these potential troughs gives rise to current saturation, because trapped carriers are forced to move only with the sound velocity. This mechanism of current saturation was proposed already in 1962 by Smith [9]. The large current fluctuations are described by random trapping and de-trapping of whole groups of charge carriers in these deep potential troughs. This mechanism of current fluctuations was proposed in 1967 by Moore [15].

With the help of the theoretical model outlined above, expressions for the spectral current-noise intensity, the ac impedance and the current-voltage (IV-) characteristic are derived in Chapter II. In Chapter III experimental data on current saturation and ac impedance in CdS are presented and compared with the theoretical results of Chapter II. In Chapter IV our experimental data on electro-acoustic current fluctuations in CdS are shown and discussed in terms of the potential-trough model of Chapter II. Brillouin-scattering data of the amplified acoustic flux in CdS are presented in Chapter V. These data are interpreted in terms of White's linear theory [3] adapted by taking a

reduction of the free carrier concentration, caused by the trapping of carriers in potential troughs, into account.

Chapters II, III, IV and V have all been accepted for publication in "Physica-B". Since this thesis is a compilation of papers, each chapter can be read independently.

Some preliminary theoretical and experimental results on current saturation and ac impedance have already been published [22, 23]. Preliminary results including those on Brillouin-scattering, ac impedance, current fluctuations and current saturation have also been published recently [27].

References

[1] J.H. McFee in "Physical Acoustics", Vol. IV, part A, ed. by W.P. Mason, Academic Press, New York and London (1966), p. 1.
[2] N.I. Meyer and M.H. Jørgensen in "Festkörperprobleme X", ed. by O. Madelung, Pergamon Vieweg (1970), p. 21.
[3] D.L. White, J. Appl. Phys. 33 (1962) 2547.
[4] A.R. Hutson and D.L. White, J. Appl. Phys. 33 (1962) 40.
[5] A.R. Hutson, J.H. McFee and D.L. White, Phys. Rev. Lett. 7 (1961) 237.
[6] J. Zucker and S. Zemon, Appl. Phys. Lett. 9 (1966) 398.
[7] B.W. Hakki and R.W. Dixon, Appl. Phys. Lett. 14 (1969) 185.
[8] M. Bruun, W. Wettling and N.I. Meyer, Phys. Lett. 31A (1970) 31.
[9] R.W. Smith, Phys. Rev. Lett. 9 (1962) 87.
[10] J.H. McFee, J. Appl. Phys. 34 (1963) 1548.
[11] A.R. Moore, Phys. Rev. Lett. 12 (1964) 47.
[12] A.R. Moore and R.W. Smith, Phys. Rev. 138 (1965) 1250.
[13] W. Wettling, Phys. Lett. 25A (1967) 193.
[14] W. Wettling and M. Bruun, Phys. Lett. 27A (1968) 123.
[15] A.R. Moore, J. Appl. Phys. 38 (1967) 2327.
[16] A.R. Moore, Appl. Phys. Lett. 13 (1968) 126.
[17] M. San'ya, M. Yamada, C. Hamaguchi and J. Nakai, Jap. J. Appl. Phys. 13 (1974) 611.
[18] O. Keller, Phys. Rev. B 10 (1974) 1585.
[19] J. Attal and J.P. Laurenti, J. Phys. C, Solid State Phys. 7 (1974) 1160.
[20] P.A. Gielen and R.J.J. Zijlstra, Physica 95B (1978) 347.
[21] P.A. Gielen and R.J.J. Zijlstra, Physica 103B (1981) 165.
[22] W. Westera, R.J.J. Zijlstra and M.A. van Dijk, Phys. Lett. 78A (1980) 371.
[23] W. Westera and R.J.J. Zijlstra, Physica 106B (1981) 33.
[24] S. Zemon, J.H. Wasko, L.L. Hope and J. Zucker, Appl. Phys. Lett. 11 (1967) 40.
[25] A. Many and U. Gelbart, Appl. Phys. Lett. 19 (1971) 192.
[26] M.B.N. Butler, Rep. Prog. Phys. 37 (1974) 421.
[27] R.J.J. Zijlstra and W. Westera in "Proceedings of the Sixth International Conference on Noise in Physical Systems", ed. by P.H.E. Meijer, R.D. Mountain and R.J. Soulen, NBS-SP614 (1981), p. 276.

C H A P T E R   I I

THEORY OF ELECTRO-ACOUSTIC EFFECTS

IN HEXAGONAL PIEZOELECTRIC SEMICONDUCTORS

Abstract — A theoretical model is presented to describe electro-acoustic effects
in single crystalline materials. The calculations, which are essentially linear,
are based on the assumption that the electro-acoustic effects can be described
by the trapping of bunches of free charge carriers in two types of potential
troughs. One type of trough is associated with acoustic waves, which are ampli-
fied from the thermal background, travelling in the direction of the drifting
carriers; the second type is associated with waves with large amplitudes
travelling in the opposite direction. We assumed that the two types of troughs
are independent, and that they are created and annihilated at random throughout
the crystal.

   Expressions are derived for the IV-characteristic, the current noise, the
ac impedance and the wave attenuation coefficients. In these calculations the
anisotropy of the crystal is taken into account. When space charge, diffusion
and the displacement current are neglected, the calculated noise spectra con-
sist of two Lorentzians. The ac impedance, which is calculated without making
these approximations, shows two low-frequency roll-offs and resonances that are
related to the transit time of potential troughs.

   Finally some remarks on dispersion effects are made.

II.1. Introduction

   The first theoretical description of the electro-acoustic effect, i.e. the
amplification of travelling acoustic waves in piezoelectric semiconductors
where an electric drift field is applied, was given in 1962 by White [1] in the
form of a linear classical continuum theory. Some years later Brillouin-
scattering studies of the growth of the acoustic flux in semiconducting CdS [2,
3] showed that this linear theory applies only in the weak acoustic-flux region.
At higher acoustic flux intensities, however, the frequency of maximum amplifi-
cation of acoustic waves was found to be an order of magnitude lower than pre-
dicted by the theory. The failure of the linear theory is due to the appearance
of essentially nonlinear effects at higher acoustic flux intensities. These
effects may include current saturation, large current fluctuations, ac-impedance

9

effects, parametric down-conversion of waves, electro-acoustic domain formation, current oscillations and so on [4, 5]. We shall direct our attention mainly to current saturation, current fluctuations and ac-impedance effects.

Several authors [6, 7] have tried to describe the nonlinear effects. Since, however, this is very difficult when starting from basic principles, many of these phenomena are not yet understood. Already in 1962 Smith [8] proposed that the observed current saturation is due to the bunching of free charge carriers in potential troughs, which are coupled to the amplified acoustic waves via the piezoelectric effect. Accordingly, in 1967 Moore [9] avoided the need for non-linear equations to describe the large current fluctuations by suggesting that these fluctuations are caused by the random creation and annihilation of potential troughs. The expression obtained by Moore for the current-noise spectrum gave a reasonable explanation for his experimental data. Subsequently Friedman [10] and Nakamura [11, 12], using different approaches, were less successful in describing these experimental data.

In 1978 Zijlstra and Gielen [13] modified Moore's calculation by accounting for transit-time effects in a one-dimensional local description. They neglected the dielectric-displacement and the diffusion current in the expression for the current density. In addition they assumed space-charge neutrality and also assumed that the creation and annihilation rates of troughs are independent of the electric field strength. The resulting transit-time effects in the current noise, however, are very sensitive to the choice of the boundary conditions. Since the boundary conditions which they chose imply an inconsistency at low frequencies, their calculated result for the current noise should be considered doubtful. Furthermore their calculation resulted in a frequency-independent impedance. Experimentally, however, the ac impedance of electro-acoustically active CdS turned out to be frequency dependent [14].

In 1965 Greebe [15] used the linear small-signal gain theory to calculate the effects that boundary conditions have on the impedance of semiconducting piezoelectric plates. His results, however, were not applicable to electro-acoustically active semiconductors.

Recently Westera, Zijlstra and van Dijk [5, 16] derived an expression for the ac impedance, starting from the trough model, while taking into account diffusion, space charge, the displacement current, the electric-field dependence of the trough creation and annihilation rates and anisotropy effects. The result was in good agreement with the experimental data on CdS. It was found, however, that the relaxation times derived from additional current-noise

10

spectra [17] differed markedly from those obtained from the ac impedance [18]. This inconsistency can be removed by introducing into the theory two types of potential troughs, with two corresponding relaxation times. This theory, which will be treated here, is again a local description and essentially linear. Furthermore, anisotropy and dispersion effects are taken into account. It should be noted that this theory holds for crystals where a continuous amplified acoustic flux is present (i.e. where no travelling electro-acoustic domains occur). For a comparison of this theory with experimental results on CdS, the reader is referred to [17-19].

In section II.2 the basic equations for our calculations are introduced. In section II.3 the equations for the stationary state are given. In section II.4 the spectral current-noise intensity is calculated. An expression for the ac impedance is derived in section II.5. In section II.6 expressions for the acoustic attenuation coefficients are given; some concluding remarks on the effects of dispersion of the acoustic waves are presented in section II.7.

II.2. Basic Equations

A classical continuum description is applicable, if it is assumed that the free carrier inter-collision time is small on the time scale considered, and the mean free path of free charge carriers is much smaller than the wavelengths involved in the sound-amplification process.

We consider an n-type homogeneous piezoelectric semiconducting crystal, where the electric field is applied along a symmetry axis, the x_3-axis. In the case of CdS the x_3-axis coincides with the c-axis. Together with the x_1- and x_2-axis the x_3-axis forms a Cartesian coordinate system. The sample is provided with Ohmic contacts at $x_3 = 0$ and $x_3 = L$, where L is the contact spacing.

When the drift velocity of the electrons exceeds the sound velocity, acoustic waves, originating from the thermal background and travelling in the direction of the drifting electrons, are amplified. As a result potential troughs which propagate with the sound velocity are spontaneously created and annihilated throughout the crystal. Note that the creation and annihilation occurs at random because of the incoherence of the thermal background waves.

Since it is known from the literature [16, 20] that under these conditions transverse off-axis waves are amplified rather than longitudinal on-axis waves, our calculation must include the anisotropic propagation characteristics of acoustic waves as well as the anisotropy of the piezoelectric and dielectric

11

properties. We shall consider acoustic waves with an arbitrary polarization and propagation direction and show how the general form of the piezoelectric relations and the wave equation can be reduced to the more simple one-dimensional form (cf. [4]).

There is experimental evidence [17, 18] that two relaxation mechanisms are involved in the electric phenomena to be described. Relaxation times obtained from current-noise spectra are considerably smaller than those obtained from ac-impedance measurements. Therefore we shall introduce two types of potential troughs, each with a different decay time.

If the electric field is applied along the c-axis, the amplification (or attenuation) coefficient for acoustic waves is a function of the angle between the wave vector and the c-axis, the off-axis angle δ [4, 21]. Therefore, acoustic waves with wave vectors lying on a cone centred around the c-axis, with a half-cone angle δ, are amplified to the same extent. If the crystal end-surface at $x_3 = L$ (anode) acts as a perfect mirror, the wave vectors of reflected acoustic waves also lie on a cone, with the same half-cone angle δ. Although the amplification coefficient of acoustic waves is generally not a delta-function of the off-axis angle, it is in practice sufficiently peaked at a favourable piezoelectrically active direction [19, 21] to allow us to consider waves travelling in this direction only. Therefore the stationary acoustic-energy distribution is built up by forward-travelling (amplified) waves and backward-travelling (attenuated) waves, with the same preferential off-axis angle δ.

It should be noticed that the ultimate acoustic amplitudes near the cathode may largely exceed the amplitudes of the original thermal waves, because of net acoustic round-trip gain. McFee [22] observed net acoustic round-trip gain during the build-up of the acoustic flux in CdS. His observations were in accordance with White's [1] linear theory. When the net round-trip gain is reduced to unity due to some nonlinear loss mechanism a stationary state is reached.

We now introduce two types of potential troughs: one type of trough is formed by forward-travelling acoustic waves, the second by backward-travelling waves. In [18] it is shown that the trough velocity is given by the group velocity of the amplified (and attenuated) acoustic waves. As a result of the elastic anisotropy and the electro-acoustic dispersion (cf. section 7, [20]) the direction and magnitude of the group velocity may differ markedly from the direction and magnitude of the phase velocity.

12

To simplify the calculation we consider a system of acoustic waves, which travel in a fixed wave-vector direction $\vec{\kappa}$ only. Ultimately we are only interested in the motion of the troughs projected on the x_3-axis.

From White's calculation [1] it appears that piezoelectric stiffening has only a slight effect on the phase velocity of acoustic waves. Therefore acoustic waves travelling in opposite directions have approximately the same absolute phase velocity. This conclusion also applies to the group velocity. If the velicity of the potential troughs associated with forward-travelling acoustic waves is denoted by $\vec{v}_g$, the backward-travelling troughs in our system will thus travel with $-\vec{v}_g$. For the theoretical description the nature of $\vec{v}_g$ is irrelevant; it can be either a phase or a group velocity.

In the following analysis we use the sign convention: $V > 0$ while $E < 0$ and $I < 0$, where V is the applied voltage, E the electric field strength and I the electric current.

Let n_d be the local, instantaneous density of free electrons in the conduction band, and n_{s_1} and n_{s_2} the local, instantaneous density of electrons trapped in potential troughs which travel towards the anode and the cathode, respectively. When the total local electron density in the conduction band is denoted by n, we have

$$n = n_d + n_{s_1} + n_{s_2} \quad .$$ (1)

Gauss's equation yields

$$\frac{\partial D_i}{\partial x_i} = - q(n - \bar{n}) \quad ,$$ (2)

where D_i is the i-th component of the dielectric-displacement vector, x_i the corresponding component of the position vector and $-q$ the electron charge. The time average of n is denoted by $\bar{n}$ and is assumed to be equal to the thermal-equilibrium density of free charge carriers. This assumption, which implies that there is no space charge in the stationary state, is supported by potential-probe measurements, which showed that the electric field is uniform even in the electro-acoustically active regime [8, 9]. It should be noted that in eq. (2) we have to carry out a summation over repeated subscripts (Einstein convention); here i is a subscript running from 1 to 3. The equation for the total current density $\vec{j}$ becomes for our system:

13

$$j_i = - qn_d v_{d_i} - qn_{s_1} v_{g_i} + qn_{s_2} v_{g_i} + qD_{n_{ij}} \frac{\partial n_d}{\partial x_j} + \frac{\partial D_i}{\partial t} \quad , \tag{3}$$

where $D_{n_{ij}}$ are tensor elements describing the anisotropic diffusion, t is time, $\vec{v}_d$ the drift velocity and $\pm\vec{v}_g$ the velocity of the potential troughs. Here we have assumed that only the free carriers can contribute to diffusion and that the diffusion-tensor elements are equal to their thermal-equilibrium values.

In addition we have, since $\vec{j}$ is solenoidal

$$\frac{\partial j_i}{\partial x_i} = 0 \quad , \tag{4}$$

the piezoelectric relations

$$T_{ij} = c_{ijkl} S_{kl} - e_{kij} E_k \quad , \tag{5}$$

$$D_i = \varepsilon_{ij} E_j + e_{ijk} S_{jk} \quad , \tag{6}$$

Newton's second law

$$\frac{\partial T_{ik}}{\partial x_k} = \rho \frac{\partial^2 u_i}{\partial t^2} \quad , \tag{7}$$

and

$$S_{ij} = \tfrac{1}{2}\left(\frac{\partial u_i}{\partial x_j} + \frac{\partial u_j}{\partial x_i}\right) \quad , \tag{8}$$

where T_{ij} and S_{ij} are elements of the stress and strain tensor, respectively, and c_{ijkl}, e_{ijk} and ε_{ij} are the elastic, piezoelectric and dielectric tensor elements, respectively. $\vec{E}$ is the electric field strength vector, ρ the mass density and $\vec{u}$ the spatial-displacement vector.

If p_1 and b_1 are the creation and annihilation rate per unit volume of forward-travelling troughs, respectively, the Master Equation for the density of these troughs, n_{t_1}, reads:

14

$$\frac{\partial n_{t_1}}{\partial t} = P_1 - b_1 - v_{g_i} \frac{\partial n_{t_1}}{\partial x_i} \qquad . \tag{9}$$

Analogously the Master Equation for the density of backward-travelling troughs, n_{t_2}, reads

$$\frac{\partial n_{t_2}}{\partial t} = P_2 - b_2 + v_{g_i} \frac{\partial n_{t_2}}{\partial x_i} \qquad . \tag{10}$$

In addition we make the approximation that each forward-travelling trough contains N_1 electrons and each backward-travelling trough N_2 electrons, where N_1 and N_2 do not depend explicitly on $\vec{x}$. Then the densities of trapped electrons become:

$$n_{s_1} = N_1 \cdot n_{t_1} \tag{11}$$

and

$$n_{s_2} = N_2 \cdot n_{t_2} \qquad . \tag{12}$$

II.3. The Stationary State

If the electric field strength is applied along the x_3-axis we have

$$\frac{\partial \bar{E}_k}{\partial x_j} = 0 \qquad , \qquad \qquad \text{unless } k = j = 3 \qquad . \tag{13}$$

Because of the crystal symmetry it is reasonable to assume that the static spatial displacement and strain components, $\bar{u}_i$ and $\bar{S}_{ij}$, depend only on x_3. Then we obtain (cf. eq. (8)):

$$\bar{S}_{ij} = 0 \qquad , \qquad \qquad \text{unless } i = 3 \text{ or } j = 3 \qquad , \tag{14}$$

and

$$\frac{\partial \bar{S}_{ij}}{\partial x_k} = 0 \qquad , \qquad \qquad \text{unless } k = 3 \qquad . \tag{15}$$

15

In the stationary state eq. (7) yields

$$\frac{\partial \overline{T}_{ij}}{\partial x_j} = 0 \qquad . \tag{16}$$

With the help of eqs. (5) and (16) we find

$$c_{ijkl} \frac{\partial \overline{S}_{kl}}{\partial x_j} - e_{kij} \frac{\partial \overline{E}_k}{\partial x_j} = 0 \qquad . \tag{17}$$

Furthermore, in crystals with a hexagonal symmetry, such as those of CdS, we have $c_{333k} = c_{33k3} = 0$, unless k = 3. With the help of eqs. (13)-(15), eq. (17) then becomes for i = 3:

$$\frac{\partial \overline{E}_3}{\partial x_3} = \frac{c_{3333}}{e_{333}} \frac{\partial \overline{S}_{33}}{\partial x_3} \qquad . \tag{18}$$

From eqs. (2) and (6) we find

$$\varepsilon_{ij} \frac{\partial \overline{E}_j}{\partial x_i} + e_{ijk} \frac{\partial}{\partial x_i} \overline{S}_{jk} = 0 \qquad . \tag{19}$$

Since for hexagonal crystals $e_{33k} = e_{3k3} = 0$ unless k = 3, we obtain from eq. (19) with the help of eqs. (13)-(15):

$$\frac{\partial \overline{E}_3}{\partial x_3} = \frac{e_{333}}{\varepsilon_{33}} \frac{\partial}{\partial x_3} \overline{S}_{33} \qquad . \tag{20}$$

From eqs. (18) and (20) we can conclude that

$$\frac{\partial \overline{E}_3}{\partial x_3} = \frac{\partial}{\partial x_3} \overline{S}_{33} = 0 \qquad . \tag{21}$$

Note that this result is a consequence of the assumption of space-charge neutrality in the stationary state (cf. eq. (2)).

Equation (21), means among other things, that we are dealing with a uniform electric field strength $\overline{E}_3$. Thence $\overline{v}_{d_3}$ is also independent of x_3, so

16

$$\bar{v}_{d_3} = -\mu_{33}\bar{E}_3 = \mu_{33}\frac{\bar{V}}{L} \quad , \tag{22}$$

where μ_{ij} are the free electron mobility-tensor elements and $\bar{V}$ is the voltage applied to the sample.

Since the sample is assumed to be homogeneous, we can put

$$\frac{\partial \bar{n}}{\partial x_i} = 0 \quad . \tag{23}$$

In the stationary state the diffusion contribution to the current density can be omitted. In view of the translational symmetry along the x_1- and x_2-axis we can write:

$$\frac{\partial \bar{n}_d}{\partial x_i} = \frac{\partial \bar{n}_{s_1}}{\partial x_i} = \frac{\partial \bar{n}_{s_2}}{\partial x_i} = 0 \qquad \text{for } i = 1, 2 \quad . \tag{24}$$

Combining eqs. (1)-(4), (23) and (24) yields

$$(\bar{v}_{d_3} - v_{g_3}) \frac{\partial \bar{n}_{s_1}}{\partial x_3} = -(\bar{v}_{d_3} + v_{g_3}) \frac{\partial \bar{n}_{s_2}}{\partial x_3} \quad . \tag{25}$$

If we assume that the kinetics of the two types of troughs are statistically independent, it follows that the only possible solution of eq. (25) is given by

$$\frac{\partial \bar{n}_{s_1}}{\partial x_3} = \frac{\partial \bar{n}_{s_2}}{\partial x_3} = \frac{\partial \bar{n}_d}{\partial x_3} = 0 \quad . \tag{26}$$

The assumption of the statistical independence of the two types of troughs is inspired by the idea that the creation and annihilation of potential troughs is solely determined by the random distribution of acoustic wave amplitudes and phases.

Note that for the derivation of eq. (26) the assumption of space-charge neutrality in the stationary state (cf. eq. (2)) again plays an important role.

If we use eqs. (3), (4), (22), (23) and (26) we find for the electric current in the stationary state the following expression

$$\overline{I} = - \left(\frac{qA\mu_{33}\overline{n}_d}{L}\right) \cdot \overline{V} - qAv_{g_3}(\overline{n}_{s_1} - \overline{n}_{s_2}) \quad , \tag{27}$$

where A is the cross-sectional area of the crystal (= the contact area). Expression (27) is also valid when the field strength is below the threshold for amplification, since in that case $\overline{n}_d = \overline{n}$ and $\overline{n}_{s_1} = \overline{n}_{s_2} = 0$. It follows then that eq. (27) reduces to Ohm's law.

It should be noted that $\overline{n}_d$, $\overline{n}_{s_1}$, $\overline{n}_{s_2}$ and v_{g_3} generally depend on $\overline{V}$.

For amplification of an acoustic wave with off-axis angle δ, the component of the drift velocity $\vec{v}_d$ along the phase velocity $\vec{v}_s(\delta)$ should exceed the phase velocity [4, 21]. With eq. (22) this condition for electro-acoustic amplification is given by

$$\overline{V} > \frac{v_s(\delta) \cdot L}{\cos\delta \cdot \mu_{33}} \quad , \tag{28}$$

where $v_s(\delta) = |\vec{v}_s(\delta)|$. In the case of CdS [20, 21], or ZnO [20] the threshold voltage V_c for the amplification of sound waves is determined by on-axis waves ($\delta = 0$), according to

$$V_c = \frac{v_s(0) \cdot L}{\mu_{33}} \quad . \tag{29}$$

Equation (29) holds for both longitudinal and transverse piezoelectrically active sound waves, although the electro-mechanical coupling factor for the transverse on-axis waves happens to be zero. For transverse waves, the off-axis angle of maximum amplification increases at increasing voltage until it saturates at 30° (in CdS and ZnO). This occurs because there is a maximum in the electro-mechanical coupling factor at this angle [4, 21]. This implies that v_{g_3} occurring in eq. (27) depends essentially on the applied voltage $\overline{V}$. As will be shown in section II.7, electro-acoustic dispersion may cause v_{g_3}, if $\vec{v}_g$ is identified with the group velocity, to become voltage dependent even at a fixed off-axis angle.

Finally we find from the Master Equations (eqs. (9) and (10)), and from eqs. (11), (12) and (24), that the stationary state values of the creation and annihilation rates are equal:

$$\overline{p}_1 = \overline{b}_1 \qquad \text{and} \qquad \overline{p}_2 = \overline{b}_2 \quad . \tag{30, 31}$$

18

II.4. The Current Noise

In this section we present the calculation of the spectral current-noise intensity. To simplify the calculation we assume that space-charge neutrality prevails. This assumption seems valid on a time-scale which is large compared to the dielectric-relaxation time. Furthermore diffusion and the displacement current are neglected. Due to these assumptions the spectral current-noise intensity can be calculated without using the piezoelectric relations (eqs. (5) and (6)), Newton's second law (eq. (7)) and eq. (8). This implies that the elastic, dielectric and piezoelectric anisotropy is not taken into account explicitly. For a further discussion of the validity of these assumptions we refer to the end of section II.5.

We recall that the basic equations presented in section II.2 hold for a system of waves travelling in a fixed wave vector direction $\vec{\kappa}$. In general $\vec{\kappa}$ is characterized by an off-axis angle δ and an azimuth angle ϕ. Because we neglect space charge, diffusion and the displacement current, the calculation can be simplified substantially by averaging the fluctuating quantities a priori over the azimuth angle ϕ. Thus the contribution of all wave vectors lying on a cone, with half-cone angle δ, centred around the c-axis is taken into account. Furthermore, the fluctuating quantities are averaged over the cross-sectional area. The averaged quantities obtained in this way are indicated by ' . So when $y(x_1,x_2,x_3,\phi,\delta,t)$ is a fluctuating local quantity, $y'(x_3,\delta,t)$ is defined by

$$y' = \frac{1}{A} \iint_A \{ \frac{1}{2\pi} \int_0^{2\pi} y \, d\phi \} \, dx_1 dx_2 \qquad . \tag{32}$$

From this consideration it follows that y' is independent of x_1, x_2 and ϕ. In the following we shall rewrite our equations in terms of these averaged quantities. Note that these quantities are still local with respect to x_3.

For small deviations Δ from the stationary state we find that by linearizing eq. (3) and using eq. (32), for $i = 3$,

$$\Delta j_3' = - q\bar{n}_d \Delta v_{d_3}' - q\bar{v}_{d_3} \Delta n_d' - qv_{g_3} \Delta n_{s_1}' + qv_{g_3} \Delta n_{s_2}' \qquad . \tag{33}$$

Here we have neglected the ac-conductivity contribution of trapped electrons. Space-charge neutrality yields with the help of eq. (1):

$$\Delta n_d' = - \Delta n_{s_1}' - \Delta n_{s_2}' \qquad . \tag{34}$$

Because of the symmetry around the x_3-axis, we can write

$$\Delta v_{d_3}' = - \mu_{33} \Delta E_3' \qquad . \tag{35}$$

From eqs. (33), (34) and (35) we obtain

$$\Delta j_3' = q(\bar{v}_{d_3} - v_{g_3}) \Delta n_{s_1}' + q(\bar{v}_{d_3} + v_{g_3}) \Delta n_{s_2}' + q\mu_{33} \bar{n}_d \Delta E_3' \qquad . \tag{36}$$

For the fluctuations in the creation and annihilation rates of forward-travelling troughs, we can write in first-order approximation:

$$\Delta p_1' - \Delta b_1' = - \frac{\Delta n_{t_1}'}{\tau_1} + \left[\frac{\partial}{\partial E_3} (p_1 - b_1) \right]_{\Delta E_3 = 0} \Delta E_3' + L_{p_1}' - L_{b_1}' \qquad , \tag{37}$$

where

$$\tau_1^{-1} = - \left[\frac{\partial}{\partial n_{t_1}} (p_1 - b_1) \right]_{\Delta n_{t_1} = 0} \qquad ,$$

and τ_1 is the mean lifetime of the fluctuations in the density of forward-travelling troughs, and

$$L_{p_1}' = (\Delta p_1')_{\substack{\Delta n_{t_1} = 0 \\ \Delta E_3 = 0}} \qquad \text{and} \qquad L_{b_1}' = (\Delta b_1')_{\substack{\Delta n_{t_1} = 0 \\ \Delta E_3 = 0}} \qquad ,$$

are Langevin source-functions, which formally describe the spontaneous, random fluctuations in the creaction and annihilation rate, respectively. Analogously we can write for backward-travelling troughs

$$\Delta p_2' - \Delta b_2' = - \frac{\Delta n_{t_2}'}{\tau_2} + \left[\frac{\partial}{\partial E_3} (p_2 - b_2) \right]_{\Delta E_3 = 0} \Delta E_3' + L_{p_2}' - L_{b_2}' \tag{38}$$

where

20

$$\tau_2^{-1} = - \left[\frac{\partial}{\partial n_{t_2}} (p_2 - b_2) \right]_{\Delta n_{t_2} = 0} \qquad ,$$

and

$$L'_{p_2} = (\Delta p'_2)_{\substack{\Delta n_{t_2} = 0 \\ \Delta E_3 = 0}} \qquad \text{and} \qquad L'_{b_2} = (\Delta b'_2)_{\substack{\Delta n_{t_2} = 0 \\ \Delta E_3 = 0}} \qquad .$$

In eqs. (37) and (38) we have accounted for the field dependence of the creation and annihilation rates.

Although the number of electrons per trough, N_1 and N_2, might be functions of the electric field strength $\vec{E}$, so that local fluctuations $\Delta\vec{E}$ would induce local fluctuations ΔN_1 and ΔN_2, we assume that the fluctuations ΔN_1 and ΔN_2 can be neglected. This assumption is reasonable since the sudden trapping and de-trapping of a whole group $(N_1, N_2 \gg 1)$ of electrons is the main reason for the occurrence of current fluctuations. Thence eqs. (11) and (12) yield

$$\Delta n'_{s_1} = N_1 \Delta n'_{t_1} \qquad , \tag{39}$$

and

$$\Delta n'_{s_2} = N_2 \Delta n'_{t_2} \qquad . \tag{40}$$

From eqs. (9), (37) and (39) we obtain:

$$\frac{\partial}{\partial t} \Delta n'_{s_1} = - \frac{\Delta n'_{s_1}}{\tau_1} + N_1 \left[\frac{\partial}{\partial E_3} (p_1 - b_1) \right]_{\Delta E_3 = 0} \Delta E'_3 - v_{g_3} \frac{\partial}{\partial x_3} \Delta n'_{s_1} + N_1 (L'_{p_1} - L'_{b_1}) \quad . \tag{41}$$

Equations (10), (38) and (40) yield:

$$\frac{\partial}{\partial t} \Delta n'_{s_2} = - \frac{\Delta n'_{s_2}}{\tau_2} + N_2 \left[\frac{\partial}{\partial E_3} (p_2 - b_2) \right]_{\Delta E_3 = 0} \Delta E'_3 + v_{g_3} \frac{\partial}{\partial x_3} \Delta n'_{s_2} + N_2 (L'_{p_2} - L'_{b_2}) \quad . \tag{42}$$

Making a Fourier analysis we obtain from eqs. (36), (41) and (42) (Fourier

transformed quantities are denoted by tilde):

$$\tilde{j}_3' = \frac{qN_1(\overline{v}_{d_3} - v_{g_3})}{(1/\tau_1 + i\omega)}(\tilde{L}_{p_1}' - \tilde{L}_{b_1}') + \frac{qN_2(\overline{v}_{d_3} + v_{g_3})}{(1/\tau_2 + i\omega)}(\tilde{L}_{p_2}' - \tilde{L}_{b_2}')$$

$$- \frac{q(\overline{v}_{d_3} - v_{g_3})}{(1/\tau_1 + i\omega)} v_{g_3} \frac{d}{dx_3}\tilde{n}_{s_1}' + \frac{q(\overline{v}_{d_3} + v_{g_3})}{(1/\tau_2 + i\omega)} v_{g_3} \frac{d}{dx_3}\tilde{n}_{s_2}'$$

$$+ \left\{ \left[\frac{qN_1(\overline{v}_{d_3} - v_{g_3})}{(1/\tau_1 + i\omega)} \left[\frac{\partial}{\partial E_3}(p_1 - b_1) \right]_{\Delta E_3 = 0} \right. \right.$$

$$\left. + \frac{qN_2(\overline{v}_{d_3} + v_{g_3})}{(1/\tau_2 + i\omega)} \left[\frac{\partial}{\partial E_3}(p_2 - b_2) \right]_{\Delta E_3 = 0} + q\mu_{33}\overline{n}_d \right\} \tilde{E}_3' \qquad . \qquad (43)$$

Before this first-order differential equation is solved, it is advisable to choose suitable boundary conditions. Mechanical boundary conditions, such as zero stress at the boundaries corresponding to free end-surfaces, must be translated into boundary conditions for the electron densities if they are to be useful in eq. (43). This can be done by using the space-charge-neutrality condition. From eq. (8) it follows that at all positions (cf. eq. (12))

$$\Delta S_{ij}' = 0 \qquad\qquad\qquad \text{unless } i = 3 \text{ or } j = 3. \qquad (44)$$

Considering free end-surfaces we put:

$$\Delta T_{ij}'(x_3) = 0 \qquad\qquad\qquad \text{at } x_3 = 0 \text{ and } x_3 = L. \qquad (45)$$

It then follows for $i = j = 3$ from eq. (5) that

$$c_{3333}\Delta S_{33}'(x_3) - e_{333}\Delta E_3'(x_3) = 0 \quad \text{at } x_3 = 0 \text{ and } x_3 = L. \qquad (46)$$

Here we have used $c_{33k3} = c_{333k} = 0$ unless $k = 3$, and $e_{k33} = 0$ unless $k = 3$, in crystals with a hexagonal symmetry. From Gauss's equation (eq. (2)) we obtain in the case of space-charge neutrality

22

$$\frac{\partial}{\partial x_3} \Delta D_3'(x_3) = 0 \qquad \text{or} \qquad \Delta D_3'(0) = \Delta D_3'(L) \qquad . \tag{47}$$

With eq. (6) it then follows that

$$\varepsilon_{33} \Delta E_3'(0) + e_{333} \Delta S_{33}'(0) = \varepsilon_{33} \Delta E_3'(L) + e_{333} \Delta S_{33}'(L) \qquad . \tag{48}$$

Here, we have used $\varepsilon_{3k} = 0$ unless $k = 3$, and $e_{33k} = e_{3k3} = 0$ unless $k = 3$, in hexagonal crystals.

Combining eqs. (46) and (48) we find that

$$\Delta E_3'(0) = \Delta E_3'(L) \qquad . \tag{49}$$

This electrical boundary condition corresponds to the mechanical boundary condition in eq. (45) for $i = j = 3$. From eq. (4) we have

$$\frac{\partial}{\partial x_3} \Delta j_3' = 0 \qquad . \tag{50}$$

By using eqs. (36), (49) and (50) we find

$$(\bar{v}_{d_3} - v_{g_3})(\Delta n_{s_1}'(L) - \Delta n_{s_1}'(0)) = -(\bar{v}_{d_3} + v_{g_3})(\Delta n_{s_2}'(L) - \Delta n_{s_2}'(0)) \qquad . \tag{51}$$

Since we assumed that the two types of potential troughs are statistically independent, it follows that fluctuations $\Delta n_{s_1}'$ cannot be affected by fluctuations $\Delta n_{s_2}'$. Therefore, the only solution of eq. (51) is given by

$$\Delta n_{s_1}'(L) = \Delta n_{s_1}'(0) \qquad , \tag{52}$$

and

$$\Delta n_{s_2}'(L) = \Delta n_{s_2}'(0) \qquad . \tag{53}$$

In order to derive the ac short-circuited current fluctuations, we put

$$\tilde{V} = - \int_0^L \tilde{E}_3' \, dx_3 \equiv 0 \qquad . \tag{54}$$

23

By integrating eq. (43) and using eqs. (50) and (52)-(54) we obtain the following solution for the Fourier-transformed current fluctuations:

$$\tilde{I}_3 = A \cdot \tilde{j}_3' = \frac{qN_1(\overline{v}_{d_3} - v_{g_3})}{(1/\tau_1 + i\omega)L} \int_0^L \iint_A (\tilde{L}''_{p_1} - \tilde{L}''_{b_1}) dx_1 dx_2 dx_3$$

$$+ \frac{qN_2(\overline{v}_{d_3} + v_{g_3})}{(1/\tau_2 + i\omega)L} \int_0^L \iint_A (\tilde{L}''_{p_2} - \tilde{L}''_{b_2}) dx_1 dx_2 dx_3 \quad , \tag{55}$$

where the averaging of the local source-functions over the azimuth angle ϕ is denoted by ".

If the following assumptions are made:

i)   the fluctuations in L''_{p_1}, L''_{p_2}, L''_{b_1} and L''_{b_2} are uncorrelated;

ii) there is a delta-function space-correlation for each Langevin source-function (L''_{p_1}, L''_{p_2}, L''_{b_1}, L''_{b_2});

iii) the noise in the source functions is shot noise;

we obtain for the spectral cross-intensities of fluctuations in $(L''_{p_1} - L''_{b_1})$ at frequency f [13]:

$$S_{(L''_{p_1} - L''_{b_1})}(\vec{x}, \vec{x}^*, f) = 4\overline{b}_1 \, \delta(x_1 - x_1^*) \delta(x_2 - x_2^*) \delta(x_3 - x_3^*) \quad . \tag{56}$$

We used $\overline{p''_1} = \overline{b''_1} = \overline{b}_1$. Analogously we find:

$$S_{(L''_{p_2} - L''_{b_2})}(\vec{x}, \vec{x}^*, f) = 4\overline{b}_2 \, \delta(x_1 - x_1^*) \delta(x_2 - x_2^*) \delta(x_3 - x_3^*) \quad . \tag{57}$$

From eqs. (55)-(57) we obtain for the spectral current-noise intensity S_I:

$$S_I(f) = 4\overline{b}_1 N_1^2 q^2 (\overline{v}_{d_3} - v_{g_3})^2 \frac{A}{L} \frac{\tau_1^2}{1 + \omega^2 \tau_1^2} + 4\overline{b}_2 N_2^2 q^2 (\overline{v}_{d_3} + v_{g_3})^2 \frac{A}{L} \frac{\tau_2^2}{1 + \omega^2 \tau_2^2} \quad . \tag{58}$$

When we use (cf. [13])

$$\overline{b}_1 = \frac{\overline{n}_{t_1}}{\tau_1} = \frac{\overline{n}_{s_1}}{N_1 \tau_1} \quad , \tag{59}$$

$$\overline{b}_2 = \frac{\overline{n}_{s_2}}{N_2 \tau_2} \quad , \tag{60}$$

and

$$\tau_t = L/v_{g_3} \quad , \tag{61}$$

being the transit time for the potential troughs, the expression for the spectral current-noise intensity becomes:

$$S_I(f) = 4qN_1(q\overline{n}_{s_1} v_{g_3} A)\left(\frac{\overline{v}_{d_3} - v_{g_3}}{v_{g_3}}\right)^2 \frac{\tau_1/\tau_t}{1+\omega^2\tau_1^2}$$

$$+ 4qN_2(q\overline{n}_{s_2} v_{g_3} A)\left(\frac{\overline{v}_{d_3} + v_{g_3}}{v_{g_3}}\right)^2 \frac{\tau_2/\tau_t}{1+\omega^2\tau_2^2} \quad . \tag{62}$$

From eq. (62) we see that the current-noise spectra contain two Lorentzian spectra with different weighting factors and, generally, different roll-off frequencies. It is concluded that at voltages slightly above V_c, where $\overline{v}_{d_3} \approx v_{g_3}$, the noise is caused mainly by the second term, which describes backward-travelling troughs. At increasing voltage, both Lorentzians may contribute, depending on the relative magnitude of the weighting factors. As a consequence of considering an ac-shorted circuit, the field dependence of p_1, b_1, p_2 and b_2 has no influence on the current noise (cf. eqs. (43) and (54)). An important difference between these results and earlier calculations [9, 13] is, that $\overline{n}_{s_1}$ and $\overline{n}_{s_2}$ are allowed to be voltage dependent. It should be noted that, as indicated in sect. II.3, v_{g_3} is voltage dependent as well. Because of these additional voltage-dependences the magnitude of the current noise is generally not proportional to $(\overline{V} - V_c)^2$; earlier calculations [9, 13] predicted that the current noise is proportional to $(\overline{V} - V_c)^2$. Note that eq. (62) does not describe any potential-trough transit-time effects.

The result of the spectral current-noise intensity, presented in eq. (62), suggests that the calculation can be simplified by considering total numbers of free and trapped electrons only (cf. [9]). However, we believe that the treatment given in this section in terms of averaged local quantities is preferable, because it allows us to adjust the boundary conditions to changing experimental

25

conditions. Furthermore the influence of a spatial correlation in the spontaneous fluctuations in the creation and annihilation rates can be investigated.

A comparison with experimental results is presented in [17].

II.5. The ac Impedance

In the calculation given in this section we extend Greebe's impedance calculation of piezoelectric plates [15] by including trough creation and annihilation processes. We extend our earlier calculation [5, 16] by assuming that two types of troughs exist and that the trough velocity may differ from the phase velocity of the acoustic waves.

In this section the effects of space charge, diffusion and the displacement current are taken into account, because the ac impedance can be calculated without neglecting these effects. Thus, the elastic, dielectric and piezoelectric anisotropies are taken into account with respect to the propagation direction and polarization of the acoustic waves. Before calculating the ac impedance, it will be usefull to examine more closely the sound-wave-induced electric field strength wave [23-25].

Consider a sound wave which moves along a crystal direction $\vec{\kappa}$. The sound-wave-induced electric field strength wave is given by

$$\vec{E}_{ind}(\vec{x},t) = \vec{E}_{ind_0} e^{i(\omega t - \vec{k} \cdot \vec{x})} \quad , \tag{63}$$

where $\vec{E}_{ind_0}$ is an electric field amplitude, independent of $\vec{x}$ and t, ω is the angular frequency of the sound wave, and

$$\vec{k} = (k_{RE} + i k_{IM}) \vec{\kappa} \quad . \tag{64}$$

Note that $\vec{k}$ may be a complex vector, the real part of which $(k_{RE} \vec{\kappa})$ is the ordinary wave vector, whereas the imaginary part $(k_{IM} \vec{\kappa})$ describes the amplification of the sound wave. Maxwell's equations yield

$$\vec{\nabla} \times (\vec{\nabla} \times \vec{E}_{ind}) = - \mu_0 \cdot \vec{\mu}_r \cdot \frac{\partial}{\partial t} \vec{J}_{ind} \quad , \tag{65}$$

where μ_0 is the vacuum permeability, $\vec{\mu}_r$ the relative-permeability tensor and

26

$\vec{j}_{ind}$ is the induced total current density. If we assume that $\vec{\mu}_r$ is the unit tensor, we find the following expression from eqs. (63) and (65):

$$- k^2 \cdot \vec{E}_{ind} + \vec{k} \cdot (\vec{k} \cdot \vec{E}_{ind}) = - \mu_0 \cdot i\omega \vec{j}_{ind} \qquad , \qquad (66)$$

where

$$k^2 = (\vec{k} \cdot \vec{k}) \qquad .$$

If we assume that $\left| k_{IM}/k_{RE} \right| \ll 1$, i.e. the amplification factor is close to unity over one wavelength, and use $\omega^2/k_{RE}^2 = v_s^2$ with $v_s = \left| \vec{v}_s \right|$ the acoustic phase velocity, eq. (66) can be rewritten as

$$\vec{E}_{ind} - \vec{\kappa}(\vec{\kappa} \cdot \vec{E}_{ind}) = v_s^2 \cdot \frac{i\mu_0}{\omega} \vec{j}_{ind} \qquad . \qquad (67)$$

The left-hand side of eq. (67) is the transverse component of $\vec{E}_{ind}$. To estimate the order of magnitude of this component, we approximate $\vec{j}_{ind}$ by $(\sigma_0 \cdot \vec{E}_{ind})$, where σ_0 is a typical conductivity for the samples under study. Equation (67) now becomes:

$$\frac{\left| \vec{E}_{ind} - \vec{\kappa}(\vec{\kappa} \cdot \vec{E}_{ind}) \right|}{\left| \vec{E}_{ind} \right|} = v_s^2 \frac{\mu_0 \sigma_0}{\omega} \qquad (68)$$

By inserting reasonable values for the unknowns in the right-hand side of eq. (68), it can be shown that for all practical cases the magnitude of the transverse electric field component can be neglected with respect to $\left| \vec{E}_{ind} \right|$. (For example, when we use $v_s = 2 \times 10^3$ ms^{-1}, $\mu_0 = 1.26 \times 10^{-6}$ Hm^{-1}, $\sigma_0 < 100$ Ω^{-1}m^{-1} and $\omega > 10^5$ s^{-1}, the right-hand side becomes smaller than 5×10^{-3}.) Therefore for the acoustic-wave-induced electric field strength we may write in good approximation:

$$\vec{E}_{ind} = E_{ind} \cdot \vec{\kappa} \qquad . \qquad (69)$$

For small deviations Δ from the stationary state we find from eq. (1) the following expression for the electron densities:

27

$$\Delta n = \Delta n_d + \Delta n_{s_1} + \Delta n_{s_2} \quad . \tag{70}$$

By linearizing the Master Equations (eqs. (9) and (10)) we obtain (disregarding the Langevin source-functions, as we are only interested in the ac impedance):

$$\frac{\partial}{\partial t} \Delta n_{t_1} = - \frac{\Delta n_{t_1}}{\tau_1} + \left[\frac{\partial}{\partial E_i} (p_1 - b_1) \right]_{\Delta E_i = 0} \Delta E_i - v_{g_j} \frac{\partial}{\partial x_j} \Delta n_{t_1} \quad , \tag{71}$$

and

$$\frac{\partial}{\partial t} \Delta n_{t_2} = - \frac{\Delta n_{t_2}}{\tau_2} + \left[\frac{\partial}{\partial E_i} (p_2 - b_2) \right]_{\Delta E_i = 0} \Delta E_i + v_{g_j} \frac{\partial}{\partial x_j} \Delta n_{t_2} \quad . \tag{72}$$

The linearized equation for deviations in the total current density from the stationary state value becomes (cf. eq. (3)):

$$\Delta j_i = - q\bar{n}_d \Delta v_{d_i} - q\bar{v}_{d_i} \Delta n_d - qv_{g_i} (\Delta n_{s_1} - \Delta n_{s_2}) + qD_{n_{ij}} \frac{\partial}{\partial x_j} \Delta n_d + \frac{\partial}{\partial t} \Delta D_i. \tag{73}$$

In this equation the ac conductivity of the trapped electrons is neglected (cf. [5, 16]).

Equations (2), (4)-(8), (11), (12) and (70)-(73) form a set of 12 linear homogeneous differential equations with 12 variables, $\Delta\vec{T}$, $\Delta\vec{S}$, $\Delta\vec{E}$, $\Delta\vec{D}$, $\Delta\vec{u}$, $\Delta\vec{j}$, Δn, Δn_d, Δn_{s_1}, Δn_{s_2}, Δn_{t_1} and Δn_{t_2}, which can be solved by looking for solutions of the type $\exp[i(\omega t - \vec{k}\cdot\vec{x})]$. When $k = 0$ we find a trivial solution. When the polarization of the acoustic wave is denoted by the unit vector $\vec{\pi}$, and when eq. (69) is used the dispersion relation for $k \neq 0$ becomes after some algebra (note that i when not used as a subscript is the imaginary unity):

$$\rho\omega^2 = c'k^2 \quad , \tag{74}$$

where $\vec{k} = k\cdot\vec{\kappa}$,

$c' = c[1 + K_e^2 \Phi]$,

$c = \kappa_i \pi_j c_{ijkl} \pi_k \kappa_l$ the effective elastic constant,

$K_e = [\frac{e^2}{\varepsilon c}]^{\frac{1}{2}}$ the effective electro-mechanical coupling factor,

$e = \kappa_i e_{ijk} \pi_j \kappa_k$ the effective piezoelectric constant (we used

28

$$e_{ijk} = e_{ikj} \text{ in hexagonal crystals}),$$

$$\varepsilon = \kappa_i \varepsilon_{ij} \kappa_j \qquad \text{the effective dielectric constant,}$$

$$\Phi = \left[1 + \frac{q\mu\bar{n}_d + \dfrac{\alpha_1(1+i\dfrac{k \cdot D_n}{(\bar{v}_{d_j} - v_{g_j})\kappa_j})}{1/\tau_1 + i(\omega - k_i v_{g_i})} + \dfrac{\alpha_2(1+i\dfrac{k \cdot D_n}{(\bar{v}_{d_k} + v_{g_k})\kappa_k})}{1/\tau_2 + i(\omega + k_1 v_{g_1})}}{\varepsilon(k^2 D_n + i(\omega - k_m \bar{v}_{d_m}))} \right]^{-1}$$

$$(i, j, k, 1, m = 1, 2, 3) \qquad ,$$

$$\mu = \kappa_i \mu_{ij} \kappa_j \qquad \text{the effective mobility,}$$

$$D_n = \kappa_i D_{n_{ij}} \kappa_j \qquad \text{the effective diffusion constant,}$$

$$\alpha_1 = qN_1(\bar{v}_{d_i} - v_{g_i})\kappa_i \left(\frac{\partial}{\partial E_j}(p_1 - b_1)\right)_{\Delta E_j = 0} \cdot \kappa_j \qquad ,$$

$$\alpha_2 = -qN_2(\bar{v}_{d_i} + v_{g_i})\kappa_i \left(\frac{\partial}{\partial E_j}(p_2 - b_2)\right)_{\Delta E_j = 0} \cdot \kappa_j \qquad .$$

From eq. (74) we see that all electro-acoustic effects on wave propagation are described by an effective elastic constant c'. The solution of eq. (74) can now be simplified if it is assumed that the coupling between the acoustic waves and the electrons is small. (For instance in CdS the maximum value of K_e^2, which is in fact a measure for the ratio of the piezoelectric force and the elastic force, is approximately 0.05.) In other words, the electronic amplification will not change the acoustic wave amplitudes by more than a few per cent over one wavelength. In fact this has already been assumed before, to arrive at eq. (69). Accordingly we assume

$$|K_e^2 \Phi| \ll 1 \qquad . \tag{75}$$

Since the value of Φ is still unknown, condition (75) should be verified for consistency. Experimental results [5, 16] show that condition (75) is apparently satisfied. This small-coupling approximation implies that c' (and therefore k as well) contains only a relatively small imaginary part. If condition (75) holds, eq. (74) becomes a quadratic equation in k with solutions given by

(we used $v_{s_0} = (c/\rho)^{\frac{1}{2}}$, the unstiffened phase velocity [4]):

$$k = k'_- \underset{\sim}{\sim} \frac{\omega}{v_{s_0}} (1 - \tfrac{1}{2}K_e^2 \Phi') \qquad (76)$$

and

$$k = k'' \underset{\sim}{\sim} \frac{-\omega}{v_{s_0}} (1 - \tfrac{1}{2}K_e^2 \Phi'') \qquad . \qquad (77)$$

Putting $k' \underset{\sim}{\sim} \omega/v_s$ in the expression for Φ' and $k'' \underset{\sim}{\sim} - \omega/v_s$ in the expression for Φ'' (in fact this means that the imaginary parts of k' and k'' are neglected) and introducing the angular electron-diffusion frequency $\omega_D = v_s^2/D_n$, we find

$$\Phi' = \frac{\gamma - i \frac{\omega}{\omega_D}}{\gamma - i \left\{ \frac{\omega}{\omega_D} + \frac{1}{\varepsilon\omega} \left[\frac{\alpha_1 (1+i\frac{\omega}{\omega_D} \frac{v_s}{(\overline{v}_{d_i} - v_{g_i})\kappa_i})\tau_1}{(1 + i\omega\theta'\tau_1)} + \frac{\alpha_2 (1+i\frac{\omega}{\omega_D} \frac{v_s}{(\overline{v}_{d_j} + v_{g_j})\kappa_j})\tau_2}{(1 + i\omega\theta''\tau_2)} + q\mu\overline{n}_d \right] \right\}} \qquad (78)$$

where $\quad \theta' = 1 - \dfrac{v_{g_i}\kappa_i}{v_s} \qquad ,$

and $\quad \theta'' = 1 + \dfrac{v_{g_i}\kappa_i}{v_s} = 2 - \theta' \qquad ,$

are factors related to the electro-acoustic dispersion (cf. section II.7). Furthermore we used

$$\gamma = 1 - \frac{\overline{v}_{d_i}\kappa_i}{v_s} \qquad ,$$

being the drift parameter [21].
For Φ'' we obtain:

30

$$\Phi'' = \frac{2 - \gamma - i\frac{\omega}{\omega_D}}{2-\gamma-i\left\{\frac{\omega}{\omega_D} + \frac{1}{\varepsilon\omega}\left[\dfrac{\alpha_1\left(1-i\frac{\omega}{\omega_D}\dfrac{v_s}{(\bar{v}_{d_i}-v_{g_i})\kappa_i}\right)\tau_1}{(1 + i\omega\theta''\tau_1)} + \dfrac{\alpha_2\left(1-i\frac{\omega}{\omega_D}\dfrac{v_s}{(\bar{v}_{d_j}+v_{g_j})\kappa_j}\right)\tau_2}{(1 + i\omega\theta'\tau_2)} +q\mu\bar{n}_d\right]\right\}}$$

$$(80)$$

Once we have found the dispersion relations (eqs. (76) and (77)) the solution of our basic equations for any variable $\Delta\vec{y}(\vec{x},t)$, be it a tensor, vector or scalar quantity, at given angular frequency can be written as a linear combination of plane waves with wave numbers $k = 0$ representing a solution uniform over space, $\vec{k} = k'\vec{\kappa}$ representing a plane wave travelling along $\vec{\kappa}$, and $\vec{k} = k''\vec{\kappa}$ representing a plane wave travelling in the opposite direction. So in general we have:

$$\Delta\vec{y}(\vec{x},t) = \Delta\vec{y}_0 e^{i\omega t} + \Delta\vec{y}' e^{i(\omega t-\vec{k}'\cdot\vec{x})} + \Delta\vec{y}'' e^{i(\omega t-\vec{k}''\cdot\vec{x})} \quad , \qquad (81)$$

where $\Delta\vec{y}_0$, $\Delta\vec{y}'$ and $\Delta\vec{y}''$ are independent of $\vec{x}$ and t.

We now return to our basic equations to derive some useful relations between the plane-wave amplitudes of our variables for each mode separately. For $k = 0$ it follows from eq. (8) that

$$(\Delta S_0)_{ij} = 0 \quad . \qquad (82)$$

From eqs. (6), (69) and (82) it follows that

$$\kappa_i(\Delta D_0)_i = \varepsilon\Delta E_0 \quad . \qquad (83)$$

Here we used eq. (69)

$$(\Delta E_0)_i = \Delta E_0 \cdot \kappa_i \quad . \qquad (84)$$

From eqs. (5), (82) and (84) we find

$$\pi_i\kappa_j(\Delta T_0)_{ij} = - e\Delta E_0 \quad . \qquad (85)$$

31

From eqs. (11), (12), (70)-(73), (83) and the definitions in eq. (74) it follows that for $i = 3$

$$(\Delta j_0)_3 = (q\mu_{33}\bar{n}_d + \frac{\alpha_1\tau_1}{1+i\omega\tau_1} + \frac{\alpha_2\tau_2}{1+i\omega\tau_2} + i\omega\varepsilon_{33})\Delta E_0 \cdot \kappa_3 \qquad . \qquad (86)$$

Here we also made use of the fact that the off-diagonal elements of the mobility and the dielectric tensor are zero.

For $k = k'$ we find from eqs. (5), (7), (8) and (74) that

$$\pi_i\kappa_j(\Delta T')_{ij} = - \frac{e}{\phi' \cdot K_e^2}\Delta E' \qquad , \qquad (87)$$

and from eq. (4) that

$$(\Delta j')_i = 0 \qquad . \qquad (88)$$

Analogously we obtain for $k = k''$ that

$$\pi_i\kappa_j(\Delta T'')_{ij} = - \frac{e}{\phi''K_e^2}\Delta E'' \qquad , \qquad (89)$$

and that

$$(\Delta j'')_i = 0 \qquad . \qquad (90)$$

The choice of boundary conditions allows us to determine the relative magnitude of the three modes occurring in eq. (81). For two free end-surfaces we take the boundary conditions to be:

$$\pi_i\kappa_j[(\Delta T_0)_{ij} + (\Delta T')_{ij}e^{-i\vec{k}'\cdot\vec{x}} + (\Delta T'')_{ij}e^{-i\vec{k}''\cdot\vec{x}}]e^{i\omega t} \equiv 0 \qquad (91)$$

at the cathode, $x_3 = 0$, and at the anode, $x_3 = L$.

So far, the results obtained only describe the behaviour of acoustic waves with a fixed wave-vector direction $\vec{\kappa}$. If we realize that the results should be averaged over the azimuth angle ϕ, it follows that the only important components of the electric field strength and the current density are along the x_3-axis.

32

By integrating the x_3-component of the electric field strength along the direction of the trough velocity we find for the alternating voltage with angular frequency ω, developed between the contacts:

$$\Delta V = - \int_0^L [\Delta E_0 + \Delta E'e^{-i\vec{k}'\cdot\vec{r}} + \Delta E''e^{-i\vec{k}''\cdot\vec{r}}] e^{i\omega t} \kappa_3 dx_3 \qquad , \qquad (92)$$

where $\vec{r}$ is a position vector along the direction of the trough velocity. The magnitude of the phase factor $(\vec{k}'\cdot\vec{r})$ at the anode $(x_3 = L)$ is found to be (we use $\vec{g} = \vec{r}/r$ is a unit vector along $\vec{r}$):

$$\vec{k}'\cdot\vec{r} = k'r \, \vec{\kappa}\cdot\vec{g} = k'L \frac{\vec{\kappa}\cdot\vec{g}}{g_3} \qquad . \qquad (93)$$

Thus it is convenient to introduce L_{eff} by defining

$$L_{eff} = L \cdot \frac{\vec{\kappa}\cdot\vec{g}}{g_3} \qquad . \qquad (94)$$

From eq. (91) we obtain with the help of eqs. (85), (87) and (89):

$$\Delta E' = K_e^2 \Phi' \left[\frac{e^{-ik''L_{eff}} - 1}{e^{-ik'L_{eff}} - e^{-ik''L_{eff}}} \right] \Delta E_0 \qquad , \qquad (95)$$

and

$$\Delta E'' = K_e^2 \Phi'' \left[\frac{e^{-ik'L_{eff}} - 1}{e^{-ik'L_{eff}} - e^{-ik''L_{eff}}} \right] \Delta E_0 \qquad . \qquad (96)$$

With the help of eqs. (92), (95) and (96) ΔV can be expressed in ΔE_0. By integrating the x_3-component of the current density over the cross-sectional area we find with eqs. (86), (88) and (90) that the total current ΔI is given by

$$\Delta I = A \cdot (q\mu_{33}\bar{n}_d + \frac{\alpha_1 \tau_1}{1+i\omega\tau_1} + \frac{\alpha_2 \tau_2}{1+i\omega\tau_2} + i\omega\varepsilon_{33}) \Delta E_0 \cdot \kappa_3 \cdot e^{i\omega t} \qquad . \qquad (97)$$

33

The ac small-signal impedance at angular frequency ω can be calculated with

$$Z(\omega) = - \frac{\Delta V}{\Delta I} \quad . \tag{98}$$

We finally obtain

$$Z(\omega) = \frac{L}{A(q\mu_{33}\bar{n}_d + \frac{\alpha_1\tau_1}{1+i\omega\tau_1} + \frac{\alpha_2\tau_2}{1+i\omega\tau_2} + i\omega\varepsilon_{33})}$$

$$\times \left\{ 1 + iK_e^2(k'\Phi''- k''\Phi') \frac{(e^{-ik'L_{eff}} - 1)(e^{-ik''L_{eff}} - 1)}{L_{eff}k'\cdot k''(e^{-ik'L_{eff}} - e^{-ik''L_{eff}})} \right\} \quad . \tag{99}$$

Substituting reasonable values for the unknowns in eq. (99), we find that the term containing K_e^2 contributes significantly only at frequencies given by

$$f = f_1 = (21 + 1) \frac{v_s}{2L_{eff}} \quad ; \quad 1 = 0, 1, 2, 3, \ldots \ . \tag{100}$$

This is easily seen by putting $k' \backsim \omega/v_s$ and $k'' \backsim -\omega/v_s$ in eq. (99). It then follows that

$$Z(\omega) \backsim \frac{L}{A(q\mu_{33}\bar{n}_d + \frac{\alpha_1\tau_1}{1+i\omega\tau_1} + \frac{\alpha_2\tau_2}{1+i\omega\tau_2} + i\omega\varepsilon_{33})} \cdot \left\{ 1 - K_e^2 \frac{v_s}{\omega L_{eff}} (\Phi'+\Phi'') tg(\frac{\omega L_{eff}}{2v_s}) \right\} \quad . \tag{101}$$

Considering that $v_s / \omega L_{eff} \backsim 1$ in all practical cases, and that condition (75) holds, it follows that $|Z(\omega)|$ will show narrow maxima at frequencies given by eq. (100). In sect. II.7 it will be shown that L_{eff}/v_s is equal to the trough transit-time.

We recall that the ac impedance was calculated with the help of plane waves with wave vectors lying on a cone with half-cone angle δ. In practice however it is known that waves with different off-axis angles are involved in the sound-amplification process [26]. This distribution of off-axis angles causes the narrow resonances predicted by eq. (100) to be smoothed out somewhat.

34

This smoothing out will occur because a distribution of off-axis angles corresponds to a distribution of trough velocities, and thus to a distribution of trough transit-times (cf. [5, 16]).

In section II.4 the current noise was calculated. In this calculation the effect of space charge was neglected among other things. As was pointed out in section II.4 this neglect removes the piezoelectric coupling of acoustic waves and electric fields. When we put $K_e^2 = 0$ in the expression for the ac impedance (eq. (99) or (101)), $Z(\omega)$ remains unchanged except for frequencies close to the resonance frequencies given by eq. (100): in fact, the transit-time resonances disappear. Therefore it is concluded that the absence of transit-time resonances in the expression for the current noise (eq. (62)) may be due to the fact that space-charge neutrality was assumed. Apparently, the condition that only frequencies small compared to the dielectric-relaxation frequency are considered is not sufficient to allow the assumption of space-charge neutrality. Yet, we assume that the current noise, apart from transit-time effects, can be described by eq. (62).

A further discussion about the resonance frequencies given by eq. (100) will be presented in section II.7. Apart from these resonances, the behaviour of $Z(\omega)$, as given by eq. (99), is of interest in three limiting cases for our ac-impedance measurements:

$$\text{i)} \quad Z(\omega) \longrightarrow \frac{L}{A(q\mu_{33}\bar{n}_d + \alpha_1\tau_1 + \alpha_2\tau_2)} \quad \text{for } \omega \to 0 \quad ; \tag{102}$$

$$\text{ii)} \quad Z(\omega) \longrightarrow \frac{L}{i\omega A\varepsilon_{33}} \tag{103}$$

$$\text{for } \omega \gg \left| \frac{q\mu_{33}\bar{n}_d + \dfrac{\alpha_1\tau_1}{1+i\omega\tau_1} + \dfrac{\alpha_2\tau_2}{1+i\omega\tau_2}}{\varepsilon_{33}} \right| \quad ,$$

which corresponds to the ac impedance of a device with capacity $C = \varepsilon_{33}A/L$;

$$\text{iii)} \quad Z(\omega) \approx \frac{L}{Aq\mu_{33}\bar{n}_d} \tag{104}$$

at intermediate frequencies, where

35

$$\left| \frac{\alpha_1 \tau_1}{1+i\omega\tau_1} + \frac{\alpha_2 \tau_2}{1+i\omega\tau_2} + i\omega\varepsilon_{33} \right| \ll q\mu_{33}\bar{n}_d \quad .$$

Furthermore, at low frequencies we generally have two roll-offs, determined by the relaxation times τ_1 and τ_2; at intermediate frequencies we expect a plateau, which is determined by free carriers only (this is a consequence of the assumption that the ac conductivity of trapped electrons can be neglected); at high frequencies we find the familiar dielectric roll-off. Measurements of the ac impedance of CdS single crystals will be discussed in [18].

II.6. The Attenuation Coefficients

From the calculation of the ac impedance presented in section II.5 one can obtain some additional interesting results. The imaginary parts of the wave numbers k' and k" (cf. eqs. (76) and (77)) yield the attenuation coefficients α_e' of waves travelling along $\vec{\kappa}$, and $\alpha_e"$ of waves travelling in the opposite direction, respectively. (Note that amplification occurs when the attenuation coefficient is negative.) It turns out that

$$\alpha_e'(\omega) = - \text{Im}(k') = \frac{K_e^2}{2\varepsilon v_{s_0}} \cdot \frac{\gamma\sigma_1' - \frac{\omega}{\omega_D}\sigma_2'}{(\gamma + \frac{\sigma_2'}{\varepsilon\omega})^2 + (\frac{\omega}{\omega_D} + \frac{\sigma_1'}{\varepsilon\omega})^2} \quad , \tag{105}$$

where

$$\sigma_1' = q\mu\bar{n}_d + \frac{\alpha_1\tau_1(1 + \frac{\omega^2\tau_1\theta'}{\omega_D(\theta'-\gamma)})}{1 + \omega^2\tau_1^2\theta'^2} + \frac{\alpha_2\tau_2(1 + \frac{\omega^2\tau_2\theta"}{\omega_D(\theta"-\gamma)})}{1 + \omega^2\tau_2^2\theta"^2} \quad ,$$

and

$$\sigma_2' = \frac{\alpha_1\tau_1(\frac{\omega}{\omega_D(\theta'-\gamma)} - \omega\tau_1\theta')}{1 + \omega^2\tau_1^2\theta'^2} + \frac{\alpha_2\tau_2(\frac{\omega}{\omega_D(\theta"-\gamma)} - \omega\tau_2\theta")}{1 + \omega^2\tau_2^2\theta"^2} \quad .$$

36

Analogously we find

$$\alpha_e''(\omega) = \text{Im}(k'') = \frac{K_e^2}{2\varepsilon v_{s_0}} \cdot \frac{(2-\gamma)\sigma_1'' - \frac{\omega}{\omega_D}\sigma_2''}{(2-\gamma+\frac{\sigma_2''}{\varepsilon\omega})^2 + (\frac{\omega}{\omega_D}+\frac{\sigma_1''}{\varepsilon\omega})^2} \qquad , \qquad (106)$$

where

$$\sigma_1'' = q\mu\bar{n}_d + \frac{\alpha_1\tau_1(1 - \frac{\omega^2\tau_1\theta''}{\omega_D(\theta'-\gamma)})}{1 + \omega^2\tau_1^2\theta''^2} + \frac{\alpha_2\tau_2(1 - \frac{\omega^2\tau_2\theta'}{\omega_D(\theta''-\gamma)})}{1 + \omega^2\tau_2^2\theta'^2} \qquad ,$$

and

$$\sigma_2'' = \frac{-\alpha_1\tau_1(\frac{\omega}{\omega_D(\theta'-\gamma)} + \omega\tau_1\theta'')}{1 + \omega^2\tau_1^2\theta''^2} - \frac{\alpha_2\tau_2(\frac{\omega}{\omega_D(\theta''-\gamma)} + \omega\tau_2\theta')}{1 + \omega^2\tau_2^2\theta'^2} \qquad .$$

Due to the complexity of the expressions (105) and (106) no simple predictions about the voltage and frequency dependence of the attenuation coefficients can be given without detailed knowledge of the various, generally voltage-dependent parameters. We confine ourselves to some general remarks.

The magnitude of the attenuation coefficients appears to be very sensitive to the magnitude of the dispersion factors θ' and θ'' (cf. eq. (78)). In the following section it will be shown that both θ' and θ'' are essentially frequency dependent as a consequence of electro-acoustic frequency-dispersion.

It should be noted that these expressions reduce to White's much simpler results for the linear attenuation coefficients [1], if we put $\alpha_1\tau_1 = 0$, $\alpha_2\tau_2 = 0$ and replace $(q\mu\bar{n}_d)$ by the conductivity $(q\mu\bar{n})$.

II.7. Dispersion Effects

In this section we present the calculation of the group velocity $\vec{v}_g$ of an acoustic wave packet, resulting from a collection of plane acoustic waves with wave vectors close to $\vec{k} = k \cdot \vec{\kappa}$ (k is real). The group velocity of this wave packet is then found with

$$\vec{v}_g = \vec{\nabla}_{\vec{k}} \, \omega(\vec{k}) \qquad . \tag{107}$$

When we use

$$\omega(\vec{k}) = \vec{k} \cdot \vec{v}_s = k v_s \qquad , \tag{108}$$

eq. (107) becomes:

$$\vec{v}_g = \vec{\nabla}_{\vec{k}} (k v_s) \qquad . \tag{109}$$

Because of rotational symmetry around the c-axis, using the off-axis angle δ, we can rewrite eq. (109) as

$$\vec{v}_g = (v_s + k \, \frac{\partial v_s}{\partial k}) \vec{\kappa} + \frac{\partial v_s}{\partial \delta} \vec{\kappa}_\delta \qquad , \tag{110}$$

where $\vec{\kappa}_\delta$ is a unit vector perpendicular to $\vec{k}$, lying in the plane of $\vec{k}$ and the x_3-axis, defined by:

$$\vec{\kappa}_\delta = \frac{\vec{\kappa} \times (\vec{\kappa} \times \vec{x}_{3_0})}{|\vec{\kappa} \times (\vec{\kappa} \times \vec{x}_{3_0})|} \tag{111}$$

$\vec{x}_{3_0}$ is a unit vector along the x_3-axis (c-axis).

In general the phase velocity $\vec{v}_s$ will be a function of k and δ. In fact, because v_s is determined by the real part of the elastic constant, we find, with the help of the definitions in eq. (74), that

$$v_s = v_{s_0} [1 + \tfrac{1}{2} K_e^2 \cdot Re(\Phi)] \qquad . \tag{112}$$

38

We recall that v_{s_0} is the unstiffened phase velocity given by
$v_{s_0} = (\kappa_i \pi_j c_{ijkl} \pi_k \kappa_l / \rho)^{\frac{1}{2}}$. By substituting eq. (112) into eq. (110) we obtain:

$$\vec{v}_g = v_s \left\{ 1 + \frac{k}{v_{s_0}} \frac{\partial}{\partial k} v_{s_0} + \tfrac{1}{2}k \frac{v_{s_0}}{v_s} K_e^2 \frac{\partial}{\partial k} (\text{Re } (\Phi)) \right\} \vec{\kappa}$$

$$+ v_s \left\{ \frac{1}{v_{s_0}} \frac{\partial}{\partial \delta} v_{s_0} + \tfrac{1}{2} \frac{v_{s_0}}{v_s} \frac{\partial}{\partial \delta} (K_e^2 \cdot \text{Re}(\Phi)) \right\} \vec{\kappa}_\delta \qquad . \qquad (113)$$

The various terms in this equation can be identified as follows:

$$\frac{k}{v_{s_0}} \frac{\partial}{\partial k} v_{s_0} \cdot \vec{\kappa} \qquad \qquad \text{— elastic frequency-dispersion,}$$

$$\tfrac{1}{2}k \frac{v_{s_0}}{v_s} K_e^2 \frac{\partial}{\partial k} (\text{Re}(\Phi)) \cdot \vec{\kappa} \qquad \qquad \text{— electro-acoustic frequency-dispersion,}$$

$$\frac{1}{v_{s_0}} \frac{\partial}{\partial \delta} v_{s_0} \cdot \vec{\kappa}_\delta \qquad \qquad \text{— elastic angular-dispersion,}$$

$$\tfrac{1}{2} \frac{v_{s_0}}{v_s} \frac{\partial}{\partial \delta} (K_e^2 \cdot \text{Re}(\Phi)) \cdot \vec{\kappa}_\delta \qquad \qquad \text{— electro-acoustic angular-dispersion.}$$

The elastic frequency-dispersion can be neglected, since in the continuum approximation (usually valid for elastic waves with frequencies below 10^2 or 10^3 GHz) v_{s_0} is independent of k [27].

The elastic angular-dispersion can be calculated if the elastic constants are known. For instance, one finds for CdS [26] that the elastic angular-dispersion for transverse waves (T_2-mode) has a maximum at $\delta = 20°$. In that case the angle between the direction of the group velocity and the c-axis is $38°$. For longitudinal waves the elastic angular-dispersion is somewhat less pronounced.

It is much more complicated to calculate the electro-acoustic dispersion effects. The reason is that the function ϕ defined in eq. (74), which is needed for the calculation of $\vec{v}_g$, contains $\vec{v}_g$. Therefore it will be necessary to use

39

numerical methods to find $\vec{v}_g$. Keller [26] has estimated under some limiting conditions, the magnitude of the electro-acoustic dispersion using the linear theory of White [1]. It has been shown that electro-acoustic angular dispersion depends strongly on the acoustic frequency. The electro-acoustic frequency-dispersion generally depends on the acoustic frequency, and on the direction and is of the order of K_e^2.

Important quantities appearing in the attenuation coefficients (cf. section II.6) are the dispersion factors θ' and θ'', defined in eq. (78). From eqs. (78) and (113) it is found that

$$\theta' = -\tfrac{1}{2}K_e^2 \cdot k \cdot \frac{\partial}{\partial k}(\text{Re}(\Phi)) \qquad , \qquad (114)$$

$(\theta'' = 2 - \theta')$. To find θ' (and θ''), eq. (114) should be solved (note that the function Φ contains θ' and θ''; cf. eq. (78)). Additional complications in the evaluation of θ' and θ'' are the frequency and directional dependence of these quantities, as can be seen from eq. (114).

When we use Keller's estimate [26] of the electro-acoustic frequency-dispersion, it is found that

$$|\theta'| \lesssim K_e^2/4 \qquad ; \qquad \theta'' \approx 2 \qquad . \qquad (115)$$

It can be shown that the magnitude of the attenuation coefficients (cf. section II.6) is strongly dependent on $|\theta'|$, even if $|\theta'| \ll K_e^2/4$.

Finally we discuss the resonance frequencies predicted in the ac impedance, which are given by eq. (100). If we use eqs. (94), (100) and (113), and neglect the elastic and electro-acoustic frequency-dispersion in the phase velocity, we find for the resonance frequencies

$$f_1 = (21 + 1)\frac{v_{g_3}}{2L} = \frac{(21 + 1)}{2}\tau_t^{-1} \qquad ; \qquad 1 = 0, 1, 2, 3, \ldots\ldots , \qquad (116)$$

where τ_t is the trough transit-time as defined in eq. (61).

As will be discussed in [18], the effect of electro-acoustic dispersion may influence the magnitude of the trough transit-velocity v_{g_3}.

References

[1] D.L. White, J. Appl. Phys. 33 (1962) 2547.
[2] W. Wettling and M. Bruun, Phys. Stat. Sol. 34 (1969) 221.
[3] B.W. Hakki and R.W. Dixon, Appl. Phys. Lett. 14 (1969) 185.
[4] N.I. Meyer and M.H. Jørgensen, in "Festkörperprobleme X", ed. by
    O. Madelung, Pergamon Vieweg, 1970, pp. 21-124.
[5] W. Westera, R.J.J. Zijlstra and M.A. van Dijk, Phys. Lett. 78A (1980) 371.
[6] P.K. Tien, Phys. Rev. 171 (1968) 970.
[7] E.M. Conwell and A.K. Ganguly, Phys. Rev. B 4 (1971) 2535.
[8] R.W. Smith, Phys. Rev. Lett. 9 (1962) 87.
[9] A.R. Moore, J. Appl. Phys. 38 (1967) 2327.
[10] L. Friedman, Phys. Rev. 174 (1968) 737.
[11] K. Nakamura, J. Phys. Soc. Japan 39 (1975) 860.
[12] K. Nakamura, J. Phys. Soc. Japan 40 (1976) 350.
[13] R.J.J. Zijlstra and P.A. Gielen, Physica 95B (1978) 190.
[14] P.A. Gielen and R.J.J. Zijlstra, Physica 95B (1978) 347.
[15] C.A.A.J. Greebe, Philips Res. Repts. 20 (1965) 1.
[16] W. Westera and R.J.J. Zijlstra, Physica 106B (1981) 33.
[17] W. Westera, Chapter IV of this thesis.
[18] W. Westera, Chapter III of this thesis.
[19] W. Westera, Chapter V of this thesis.
[20] O. Keller, Phys. Stat. Sol. (a) 16 (1973) 87.
[21] A.R. Moore, R.W. Smith and P. Worcester, IBM J. Res. Developm. 13 (1969)
    503.
[22] J.H. McFee, J. Appl. Phys. 34 (1963) 1548.
[23] J.J. Kyame, J. Acoust. Soc. Am. 21 (1949) 159.
[24] J.J. Kyame, J. Acoust. Soc. Am. 26 (1954) 990.
[25] A.R. Hutson and D.L. White, J. Appl. Phys. 33 (1962) 40.
[26] O. Keller, Phys. Stat. Sol. (a) 8 (1971) 61.
[27] M. Born and K. Huang, Dynamical theory of crystal lattices, Clarendon
    Press, Oxford, 1968.

C H A P T E R   I I I

AC AND DC CONDUCTION IN ELECTRO-ACOUSTICALLY ACTIVE CdS

Abstract — The ac impedance, in the frequency range 400 kHz to 100 MHz, and current saturation were investigated in electro-acoustically active semiconducting and photoconducting CdS single crystals. The measurements were carried out under pulsed-bias conditions to avoid excessive Joule heating. The experimental results are discussed in terms of our previously published theory. The latter is based on a model according to which bunches of conduction electrons can be trapped and detrapped in potential troughs associated with acoustic waves which are amplified from the thermal background. The ac-impedance data show two low-frequency roll-offs obscured by potential-trough transit-time resonances. At frequencies above 10 MHz an impedance plateau is observed. Theoretical results for the ac impedance could be fitted to the experimental results. From the observed resonance frequencies we were able to determine the potential-trough transit-time. The velocity of potential troughs was found to correspond to the group velocity of amplified transverse acoustic waves. No essential differences between semiconducting and photoconducting samples were observed. Furthermore it was found that the off-axis angle of maximum sound amplification is very sensitive to acoustic scattering losses at the sample boundaries. Experimental data at 77 K did not differ essentially from data at room temperature.

III.1. Introduction

Current saturation in piezoelectric semiconductors has been a subject of continuous interest, ever since Smith [1] in 1962 reported the first experimental data on CdS, CdSe and GaAs. The observed current saturation could be related to the amplification of acoustic waves originating from the thermal background, as was first reported by Hutson et al. [2] in 1961. In 1962 White [3] gave a linear continuum theory for the amplification of acoustic waves in piezoelectric semiconductors. Current saturation, however, is not described by this theory. Smith [1], following a suggestion of Rose, proposed that the current saturation was caused by trapping of free charge carriers in potential troughs associated with the amplified acoustic waves via the piezoelectric effect.

43

So far no systematic experimental data have been reported on the ac impedance of these devices under current-saturation conditions. Some ac-impedance spectra were presented in 1978 by Gielen and Zijlstra [4]. However, because the electrical contacts on their CdS platelets covered only a small part of the end-surfaces, the electric current was mainly determined by the ohmic, unsaturated fringe area. As a consequence, the observed current saturation was very weak, and no associated ac-impedance effects were observed either.

In 1980 Westera, Zijlstra and van Dijk [5, 6] calculated the ac impedance of electro-acoustically active semiconductors. Their calculation was based on the trapping and detrapping of groups of free charge carriers in potential troughs which move with the sound velocity. Experimental results, which showed a low-frequency roll-off related to the potential-trough lifetime and resonances related to the trough transit-time, were in good agreement with the theoretical predictions.

Additional measurements of current-noise spectra [7], however, showed significantly smaller trough lifetimes than those obtained from ac-impedance data. To account for this discrepancy, Westera [8] extended the impedance calculation by introducing two types of potential troughs, one related to waves travelling in the direction of the drifting carriers (forwards) and the other to waves travelling in the opposite direction (backwards), each with a different relaxation time.

The aim of this paper is to compare systematically experimental data on current saturation and ac impedance for semiconducting and photoconducting CdS single crystals with the theory given in [8]. Furthermore we shall use the value of the trough transit-time, which can be obtained from the resonances in the ac impedance, to distinguish between the amplification of transverse and longitudinal waves. So far there has been considerable controversy about which type of acoustic wave is amplified in some photoconducting CdS samples in which the electric field is parallel to the c-axis. From the observed relatively high threshold fields for the occurrence of ultrasonic amplification some authors [1, 4, 9] have concluded that longitudinal on-axis waves are amplified. Others [3, 10] believe that transverse off-axis waves are amplified and that the threshold field is raised by the existence of bound electron states in the forbidden energy gap.

The theoretical results of [8] are summarized in section III.2, the experimental arrangement is described in section III.3, and experimental results are presented and discussed in section III.4.

44

III.2. Theory

On the assumption that the observed electro-acoustic effects can be de-
scribed by the trapping of bunches of free charge carriers in potential troughs
associated with the amplified acoustic waves, Westera [8] gave a linear classi-
cal continuum theory of the electro-acoustic effect, which took anisotropy and
dispersion effects into account. In this section we shall summarize these
theoretical results.

We consider an n-type homogeneous piezoelectric semiconducting single
crystal, where the electric field is applied along a symmetry axis, the x_3-axis.
In the case of CdS the x_3-axis coincides with the c-axis. The sample is sup-
plied with Ohmic contacts at $x_3 = 0$ (cathode) and $x_3 = L$ (anode), where L is
the contact spacing. These contacts are spread uniformly over the end-surfaces.
It is assumed that two types of potential troughs are present and that the
kinetics of the two types of troughs are independent. One type of trough is
associated with forward-travelling (amplified) waves; the second type with
backward-travelling (attenuated) waves. Therefore the two types of troughs
have opposite velocity components along the x_3-axis. In section III.4 it will
be shown that the trough velocity can be associated with the group velocity of
the acoustic waves.

It is assumed that the first type of trough contains N_1 and the second
type N_2 electrons per trough, with N_1 and N_2 independent of x_3. Furthermore it
is assumed that the stationary-state value of the total local electron density
n in the conduction band is equal to the thermal-equilibrium density of free
charge carriers. This assumption implies that there is space-charge neutrality
in the stationary state. Then, it follows that $\bar{n}_{s_1}$ and $\bar{n}_{s_2}$, and therefore $\bar{n}_d$
as well, are independent of x_3, where $\bar{n}_{s_1}$ and $\bar{n}_{s_2}$ are the average local densi-
ties of bunched electrons in the two types of troughs respectively, and $\bar{n}_d$ is
the average free electron density. The average total density of electrons in
the conduction band is given by

$$\bar{n} = \bar{n}_d + \bar{n}_{s_1} + \bar{n}_{s_2} \quad . \tag{1}$$

The following sign convention is used: V > 0 while E < 0 and I < 0, where
V is the applied voltage, E the electric field strength and I the electric
current.

Under these conditions it is found that the equation for the current-

voltage (IV-) characteristic reads [8]:

$$\bar{I} = - \left(\frac{qA\mu_{33}\bar{n}_d}{L}\right) \bar{V} - qAv_{g_3}(\bar{n}_{s_1} - \bar{n}_{s_2}) \qquad , \qquad (2)$$

where A is the contact area, -q the electron charge, μ_{33} an element of the electron-mobility tensor and v_{g_3} the component of the trough velocity along the x_3-axis. It should be noted that in general $\bar{n}_d$, $\bar{n}_{s_1}$, $\bar{n}_{s_2}$ and v_{g_3} depend on $\bar{V}$.

The threshold voltage V_c for amplification of acoustic waves is determined by the phase velocity of on-axis waves (wave-vector direction along the c-axis). So we have

$$V_c = \frac{v_s(0)L}{\mu_{33}} \qquad , \qquad (3)$$

where $v_s(0)$ denotes the phase velocity of on-axis waves.

When $\bar{V} < V_c$ we have $\bar{n}_d = \bar{n}$, and $\bar{n}_{s_1} = \bar{n}_{s_2} = 0$. So, eq. (2) reduces to Ohm's law

$$\bar{I} = - \frac{\bar{V}}{R} \qquad , \qquad (4)$$

where

$$R = \frac{L}{qA\mu_{33}\bar{n}} \qquad . \qquad (5)$$

The ac impedance was calculated by considering plane-wave solutions with a wave vector in the direction of the unit vector $\vec{\kappa}$, and by assuming that the amplification of a wave is close to unity over one wavelength. If the crystal end-surfaces are free, the ac impedance Z is found to be given by:

$$Z(\omega) = \frac{L}{A\left(q\mu_{33}\bar{n}_d + \frac{\alpha_1\tau_1}{1+i\omega\tau_1} + \frac{\alpha_2\tau_2}{1+i\omega\tau_2} + i\omega\varepsilon_{33}\right)} \times \{1 + \Psi(\omega)\} \qquad , \qquad (6)$$

where ω is the angular frequency, and

ε_{33} is an element of the permittivity tensor.

46

τ_1 and τ_2 are the mean lifetimes of fluctuations in the trough densities n_{t_1} and n_{t_2}. If p_1 and b_1 are the creation and annihilation rate per unit volume of forward-travelling troughs, respectively, τ_1 is given by

$$\tau_1 = - \left[\frac{\partial}{\partial n_{t_1}} (p_1 - b_1) \right]_{\Delta n_{t_1} = 0}^{-1} \qquad . \qquad (7)$$

Analogously τ_2 is given by

$$\tau_2 = - \left[\frac{\partial}{\partial n_{t_2}} (p_2 - b_2) \right]_{\Delta n_{t_2} = 0}^{-1} \qquad . \qquad (8)$$

In addition we have

$$\alpha_1 = q N_1 (\overline{v}_{d_i} - v_{g_i}) \cdot \kappa_i \left[\frac{\partial}{\partial E_j} (p_1 - b_1) \right]_{\Delta E_j = 0} \cdot \kappa_j \qquad , \qquad (9)$$

and

$$\alpha_2 = - q N_2 (\overline{v}_{d_i} + v_{g_i}) \cdot \kappa_i \left[\frac{\partial}{\partial E_j} (p_2 - b_2) \right]_{\Delta E_j = 0} \cdot \kappa_j \qquad (10)$$

(summation over repeated indices; Einstein convention), where $\overline{v}_{d_i}$ is the i-th component of the drift velocity given by

$$\overline{v}_{d_i} = - \mu_{ij} \overline{E}_j \qquad , \qquad (11)$$

where μ_{ij} are elements of the electron-mobility tensor.
Obviously the quantities α_1 and α_2 are related to the field dependence of the trough creation and annihilation rates. Finally $\Psi(\omega)$ is a complicated complex function of ω, which describes the trough transit-time effects. It is found that $\Psi(\omega)$ contributes significantly only at frequencies given by

$$f = f_1 = \frac{(21 + 1)}{2} \tau_t^{-1} \qquad ; \qquad 1 = 0, 1, 2, 3, \ldots \qquad , \qquad (12)$$

where $\tau_t = L/v_{g_3}$ is the trough transit-time. Consequently $|Z(\omega)|$ will be found

47

to show maxima at frequencies given by eq. (12).

Three limiting cases are of interest for our impedance measurements:

(i)   When $\omega \to 0$ we obtain from eq. (6) for the differential resistance R_d in the IV-characteristic:

$$R_d = Z(0) = \frac{L}{A(q\mu_{33}\bar{n}_d + \alpha_1\tau_1 + \alpha_2\tau_2)} \quad ; \tag{13}$$

(ii)   When $\omega \gg \left| \dfrac{q\mu_{33}\bar{n}_d + \dfrac{\alpha_1\tau_1}{1+i\omega\tau_1} + \dfrac{\alpha_2\tau_2}{1+i\omega\tau_2}}{\varepsilon_{33}} \right|$, we find

$$Z(\omega) \approx \frac{L}{i\omega A\varepsilon_{33}} \quad , \tag{14}$$

which corresponds to the impedance of a device with capacity
$C = \varepsilon_{33}A/L$;

(iii) At intermediate frequencies, where

$$\left| \frac{\alpha_1\tau_1}{1+i\omega\tau_1} + \frac{\alpha_2\tau_2}{1+i\omega\tau_2} + i\omega\varepsilon_{33} \right| \ll q\mu_{33}\bar{n}_d \quad ,$$

we find an impedance plateau which is given by

$$Z(\omega) = \frac{L}{Aq\mu_{33}\bar{n}_d} \quad . \tag{15}$$

III.3. Experimental Arrangement

The devices used for our measurements were obtained from Eagle-Picher Industries, Inc.. We used both semiconducting and photoconducting single crystals of hexagonal n-type CdS.

To make Brillouin-scattering experiments possible at a later stage some crystal side-faces were mechanically polished to a flatness of approximately

48

$\frac{1}{4}$ µm. Unpolished surfaces, being several orders of magnitude less flat than polished ones, can be expected to cause considerable acoustic scattering losses, since the wavelengths of the amplified acoustic waves having frequencies around 1 GHz are about 2 µm.

The samples were supplied with two In-evaporated Ohmic contacts in such a way that the applied electric field was orientated along the c-axis (the longitudinal configuration). The In-contacts covered the end-surfaces completely. Prior to the In-evaporation at 10^{-8} Pa, the contact surfaces were chemically cleaned and subjected to a 20 minute low-energy (0.5 keV) Ar-ion bombardment. After the In-deposition the crystals were heated for about one hour at 150°C in a nitrogen atmosphere [4]. Thin copper wires were connected to the crystal contacts by tiny droplets of a two-component silver epoxy.

In table 1 the dimensions, dark-conductivity at room temperature, and surface characteristics of the semiconducting (s) and photoconducting (p) CdS crystals are listed. The sample lengths were kept smaller than 3×10^{-3} m to suppress electro-acoustic domain formation, which would give rise to a highly non-uniform and non-stationary electric field distribution in the samples. It is known from potential-probe experiments [1, 9] that in these short crystals the electric field is uniform even under current-saturation conditions.

Except for the crystals s_3, s_4 and s_5, which are attached to a sample holder at a small area on one of the side faces to permit Brillouin-scattering

Table 1. Dimensions, dark-conductivity at room temperature and surface characteristics of the semiconducting (s) and photoconducting (p) CdS samples.

Sample	L (mm)	A (mm^2)	Dark conductivity ($\Omega^{-1}m^{-1}$)	Polished faces (mm^2)
s_1	1.76	1.24×0.55	6.6×10^{-1}	—
s_2	1.84	1.27×0.59	5.6×10^{-1}	—
s_3	1.63	1.78×0.48	9.5×10^{-1}	1.78×1.63 — faces 1.78×0.48 — faces
s_4	1.76	1.24×0.43	6.6×10^{-1}	1.76×1.24 — faces
s_5	2.79	1.43×0.37	2.3	all faces
s_6	1.76	2.53×0.97	1.3	—
p_1	1.65	2.14×2.20	2.3×10^{-3}	—
p_2	1.14	1.81×0.76	5.5×10^{-1}	—

experiments, the samples were suspended freely in space by the copper wires. Obviously this experimental arrangement provides free end-surfaces, in accordance with the boundary conditions used in the calculations ([8], cf. section III.2).

To control the conductivity of photoconducting crystals the samples were illuminated from the side with filtered light from a quartz-halogen lamp or with light from a Krypton laser. The optical wavelengths were such that no band-to-band transitions were induced but the generation of carriers from local centres prevailed. Therefore the absorption coefficient of the light is small and the samples can be assumed to be homogeneously illuminated.

To avoid excessive Joule heating of the samples the high voltage was applied in pulses of 40 µs with a repetition rate of 4 Hz. The rise-times of these pulses were about 5 µs. The duration of these pulses was sufficient for the samples to reach a stationary state. Furthermore the samples were subjected to a room-temperature nitrogen or air flow.

The height of the voltage pulses was measured with a sample-and-hold circuit.

The experimental set-up for the ac-impedance measurements is shown in figure 1. Voltage pulses from the pulse generator were fed into the low-pass filter to suppress the higher harmonics of the pulses. To suppress the high broad-band noise generated by the electro-acoustic effect (cf. [7]) we used an HP 8558 B spectrum analyzer (input resistance 50 Ω) as a tunable band-pass filter. The high-pass filter protected the output stage of the signal generator against remaining transients of the voltage pulse. The IF-output (21.4 MHz) of the spectrum analyzer was fed into a switch (isolation > 110 dB) which only transmitted the signal between 5 and 35 µs after the onset of the bias pulse. The switch and the pulse generator were synchronised by the clock. The transmitted power was measured with an HP 8484 A power sensor combined with an HP 435 A power meter.

To determine the absolute value of the ac impedance $|Z|$ of the samples at a certain frequency we measured the power-meter deflection P_1 (with the signal generator switched on) and the background power P_2 (signal generator switched off). The latter power was caused by the electro-acoustic current fluctuations and the noise of our measuring circuit. Thereupon we interchanged Z and the ohmic reference impedance R_{ref} (cf. figure 1), and measured P_3 (signal generator switched on) and background power P_4 (signal generator switched off). It can be shown that
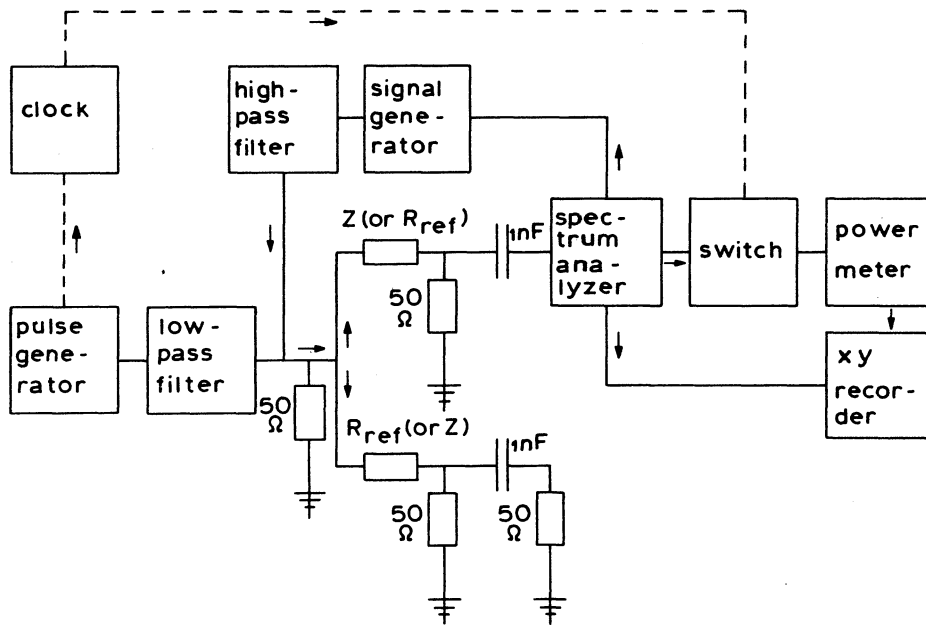
50

Figure 1. Experimental set-up for measurement of the absolute value of the ac impedance $|Z|$ of the sample under pulsed-bias conditions.

$$|Z + Z_s|^2 = \frac{P_3 - P_4}{P_1 - P_2} \cdot |R_{ref} + Z_s|^2 \quad , \tag{16}$$

where Z_s is the impedance in series with Z (or R_{ref}):

$$Z_s = R_0 \cdot \frac{1 + i\omega R_0 C_0}{1 + 2i\omega R_0 C_0} \quad , \tag{17}$$

where $R_0 = 50\ \Omega$ and $C_0 = 1$ nF.

If $|Z|$ and R_{ref} (which was always chosen to be of the same order of magnitude as $|Z|$) are large compared to $|Z_s|$ eq. (16) reduces to

$$|Z|^2 \simeq \frac{P_3 - P_4}{P_1 - P_2} \cdot R_{ref}^2 \quad . \tag{18}$$

The pulse length of 40 μs determines a fundamental low-frequency limit for the ac-impedance measurements. The low-frequency limit for our set-up turned out to be 400 kHz. The high-frequency limit for the ac-impedance measurements was 60 MHz to 100 MHz. This limit was set by the metal-film resistors which were used for reference, and by parasitic capacitances. The bandwidth of the spectrum analyzer was set at 300 kHz at frequencies below 10 MHz, and 1 MHz at frequencies above 10 MHz.

The signal generator was tuned automatically to the spectrum analyzer. Therefore, frequency-swept measurements were possible, using the frequency sweep of the spectrum analyzer. The power-meter deflection and the horizontal output of the spectrum analyzer (a measure for the operating frequency) were connected to an XY-recorder. The power-meter deflections P_1, P_2, P_3 and P_4 were recorded successively with frequency-sweep times of 500-1000 s.

The measuring procedure for the absolute value of the ac impedance under pulsed-bias conditions was checked by replacing the crystal by a known metal-film resistor. The results were in agreement with ac-impedance measurements obtained with other methods.

III.4. Experimental Results and Discussion

In this section we present and discuss the experimental results on semiconducting CdS (section III.4.1) and photoconducting CdS (section III.4.2). In section III.4.3 ac-impedance data will be used to study the effects of scattering losses at the crystal side-faces. In section III.4.4 data obtained at 77 K are shown.

III.4.1. *Semiconducting CdS*

In figure 2 pulsed measured IV-characteristics are shown for the semiconducting samples s_1, s_3 and s_5. The characteristics are ohmic at low voltages, whereas strong current saturation is observed at high voltages. The dc low-voltage conductivity $\sigma = q\mu_{33}\bar{n}$ is determined with eq. (5) from the slope R^{-1} of the ohmic part of the IV-characteristic. From the literature [4, 6] it is known that the voltage defined by the onset of the electro-acoustic current fluctuations is a better indication for the threshold voltage V_c (cf. eq. (3)) than the knee voltage in the IV-characteristic. Therefore to determine V_c we measured the current noise for each sample as a function of the applied voltage.
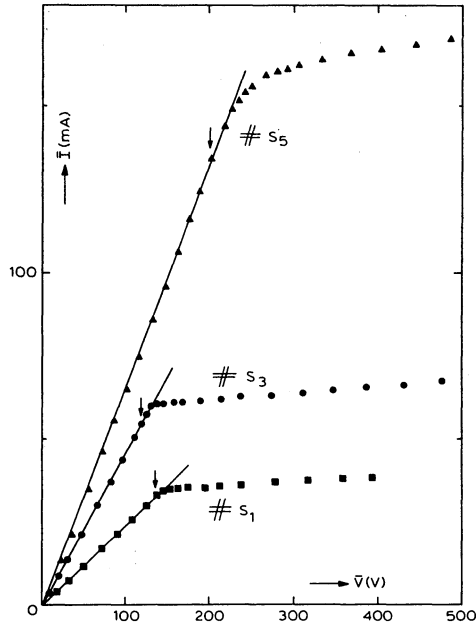
Figure 2. Current-voltage charac-
teristics for the semiconducting CdS
samples s_1, s_3 and s_5. The solid
lines represent Ohm's law. Arrows
indicate the onset of electro-
acoustic current fluctuations.

For details about these current-noise measurements we refer to [7].

The mobility values for CdS reported in the literature lie between
1.25×10^{-2} $m^2V^{-1}s^{-1}$ [11] and 3.88×10^{-2} $m^2V^{-1}s^{-1}$ [12] at room temperature.
For this reason in most cases it is not possible to distinguish between trans-
verse waves $(v_{s_0}(0) = 1.77 \times 10^3$ $ms^{-1})$ and longitudinal waves
$(v_{s_0}(0) = 4.41 \times 10^3$ $ms^{-1})$ by using the experimental value of V_c and eq. (3).

In figure 3 a typical result for the ac impedance as a function of fre-
quency is shown for crystal s_6 at $(\bar{V} - V_c)/V_c = 0.19$. We observe an impedance
plateau at frequencies above 10 MHz; this plateau corresponds to the plateau
expected from eq. (15). The differential dc-resistance R_d, which is indicated
by an arrow on the vertical scale, differs markedly from the plateau value
(cf. eq. (13)). Resonances, which appear to be the odd harmonics of
$(4.33 \pm 0.05) \times 10^5$ Hz, are indicated by vertical arrows. From the observed re-
sonances we find with eq. (12) a trough transit-velocity of
$v_{g_3} = (1.53 \pm 0.02) \times 10^3$ ms^{-1}. This result enables us to distinguish between
transverse and longitudinal acoustic waves.

The electro-mechanical coupling factor for longitudinal waves shows a
maximum for waves travelling along the c-axis [13]. Therefore, if longitudinal
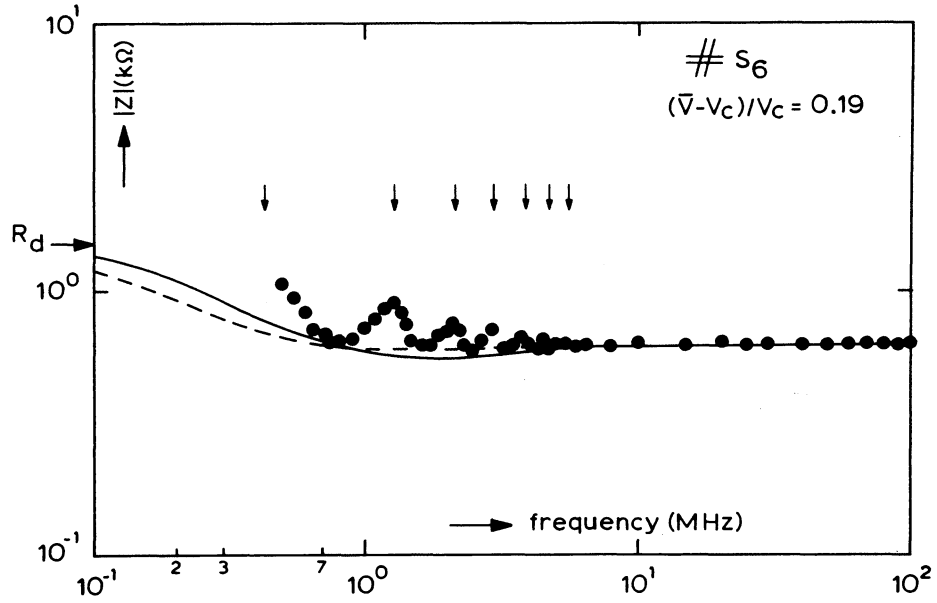acoustic waves are amplified in our samples these waves will be primarily

53

Figure 3. The absolute value of the ac impedance of sample s_6 at
$(\overline{V} - V_c)/V_c$ = 0.19. The value of the differential resistance R_d is indicated
on the vertical scale. The vertical arrows indicate odd harmonics of 4.33×10^5
Hz. The solid line and dashed line have been calculated with eq. (6), using
the parameters listed in table 2 (Appendix).

on-axis waves. Then, the associated trough-velocity, be it a phase or a group

velocity, will be on-axis as well, with a magnitude close to 4.4×10^3 ms^{-1}.

It is concluded that the trough transit-velocity v_{g_3} obtained from the re-

sonances in figure 3 cannot be explained by the amplification of longitudinal

waves. From the literature [13] it is known that transverse off-axis waves may

be amplified as well. The phase and group velocity of these waves have magni-

tudes around 2×10^3 ms^{-1}. The value of v_{g_3} = 1.53×10^3 ms^{-1} may thus be inter-

preted as the x_3-component of the phase or group velocity of transverse off-

axis waves.

The off-axis angle, δ, of maximum amplification increases with increasing

field strength until it saturates at 30°, because there is a maximum in the

electro-mechanical coupling factor for transverse waves at δ = 30° [13]. Due

to scattering losses at the crystal side-faces this saturation value will in

practice be somewhat lower than 30° [14, 15]. Note that δ is the angle between

the phase velocity and the c-axis [13-16].

54

If we were to interpret the observed trough transit-velocity $v_{g_3} = 1.53 \times 10^3$ ms^{-1} as the x_3-component of the (unstiffened) phase velocity of transverse off-axis waves [5, 6], we would find an off-axis angle of $\delta = 43°$. We used the elastic constants given in [17] and [18] to calculate the phase velocity as a function of the off-axis angle δ. It is concluded that the potential troughs do not move with the phase velocity, since the value of $\delta = 43°$, exceeding the saturation value of $30°$, is very unrealistic.

An alternative explanation is that the potential troughs move with the group velocity of transverse off-axis waves. Due to the elastic anisotropy in CdS the direction and magnitude of the group velocity may differ considerably from the direction and magnitude of the phase velocity. If we neglect the effects of electro-acoustic dispersion [8, 16], the direction and magnitude of the group velocity corresponding to a certain off-axis wave can be calculated using the elastic constants. We found that for an off-axis angle of $\delta = 25°$ the magnitude of the corresponding group velocity is 2.06×10^3 ms^{-1} and the angle between the group velocity and the c-axis is $42°$. Thus the x_3-component of this group velocity is 1.53×10^3 ms^{-1}. Since an off-axis angle of $\delta = 25°$ is quite acceptable we conclude that the potential troughs move with the group velocity of transverse off-axis waves.

The resonances that appear in figure 3 are much wider than those predicted by eq. (6). As was pointed out in [5, 6], however, we have in practice an angular distribution of amplified off-axis waves, which results in a distribution of transit velocities. This explains the smoothing out of the resonances as predicted by the theory, where only one type of off-axis angle was considered.

In view of the increasing current saturation with increasing applied voltage (cf. figure 1) we can expect α_1 in eq. (9) to be negative and α_2 in eq. (10) to be positive. (Note that E < 0 when V > 0.) The solid line in figure 3 was obtained with eq. (6) with $\Psi \equiv 0$ by setting $\tau_1 = 2.8 \times 10^{-7}$ s, $\tau_2 = 5.7 \times 10^{-8}$ s, $\alpha_1 = -3.4 \times 10^6$ $(\Omega ms)^{-1}$, $\alpha_2 = 5.5 \times 10^6$ $(\Omega ms)^{-1}$ and $q\mu_{33}\bar{n}_d = 1.14$ $(\Omega m)^{-1}$. In this calculation the impedance-plateau value, the differential resistance R_d and the relaxation time τ_2, which was obtained from current-noise data [7], were used as input constants. Since no broadened resonances are described by eq. (6) we used, at low frequencies, only the experimental data close to the local minima at frequencies that are in between the resonance frequencies. The values of τ_1 and α_1 (and therefore α_2) were adjusted by a least-squares fitting procedure. The thus obtained smooth solid

curve in figure 3 shows a minimum, which is caused by the two roll-offs: at
low frequencies we observe a roll-off due to forward-travelling troughs: with
increasing frequency this roll-off is counteracted by a (negative) roll-off
(or rather roll-on) due to backward-travelling troughs. It should be noted
that the errors in τ_1, α_1 and α_2 may be considerable due to the concealment of
the low frequency roll-offs by the transit-time resonances. The numerical
values of τ_1, α_1 and α_2 mentioned above, although obtained with a least-squares
fitting procedure, suggest a higher accuracy than can be obtained with the
available experimental data. To illustrate this we varied the parameters τ_1,
α_1 and α_2 somewhat. The dashed line in figure 3, which was calculated with eq.
(6) using $\tau_1 = 5.0 \times 10^{-7}$ s, $\tau_2 = 5.7 \times 10^{-8}$ s, $\alpha_1 = -1.6 \times 10^6$ $(\Omega ms)^{-1}$,
$\alpha_2 = 2.0 \times 10^6$ $(\Omega ms)^{-1}$ and $q\mu_{33}\bar{n}_d = 1.14$ $(\Omega m)^{-1}$, also provides quite an accepta-
ble fit to the measurements. Therefore, special care should be taken about
drawing quantitative conclusions from the magnitudes of the various parameters.
Nevertheless we can conclude that the relaxation time τ_2 of backward-travelling
troughs is considerably smaller than the relaxation time τ_1 of forward-travelling
troughs. This is what one would expect, since the strong attenuation of back-
ward-travelling potential waves will cause a decrease of the potential-trough
lifetime.

In figure 4 ac-impedance data obtained at different applied voltages are
shown for crystal s_3. The solid lines represent the best fits calculated with
the help of eq. (6), as discussed before. The values of α_1, α_2, τ_1, τ_2 and
$q\mu_{33}\bar{n}_d$ are listed in table 2 in the Appendix. The differential resistance R_d
turned out to be only weakly dependent on applied voltage (cf. figure 2). The
upper and lower value of R_d are indicated by arrows on the vertical scale. The
observed resonances are interpreted as the odd harmonics of
$(5.15 \pm 0.05) \times 10^5$ Hz, yielding a transit velocity of $(1.68 \pm 0.02) \times 10^3$ ms^{-1}.
It should be noted that in this case we cannot unambiguously distinguish be-
tween the phase and the group velocity. If, again, we assume that potential
troughs travel with the group velocity we find an off-axis angle of $13°$. This
value is considerably lower than the off-axis angle obtained for sample s_6.
From earlier reports it is known [14, 15] that the off-axis angle of maximum
amplification is strongly influenced by the dimensions of the sample, due to
boundary scattering. From the dimensions in table 1 it seems plausible that in
sample s_3 boundary scattering plays a more important role than in sample s_6.

Furthermore, it is observed that the resonances become less pronounced
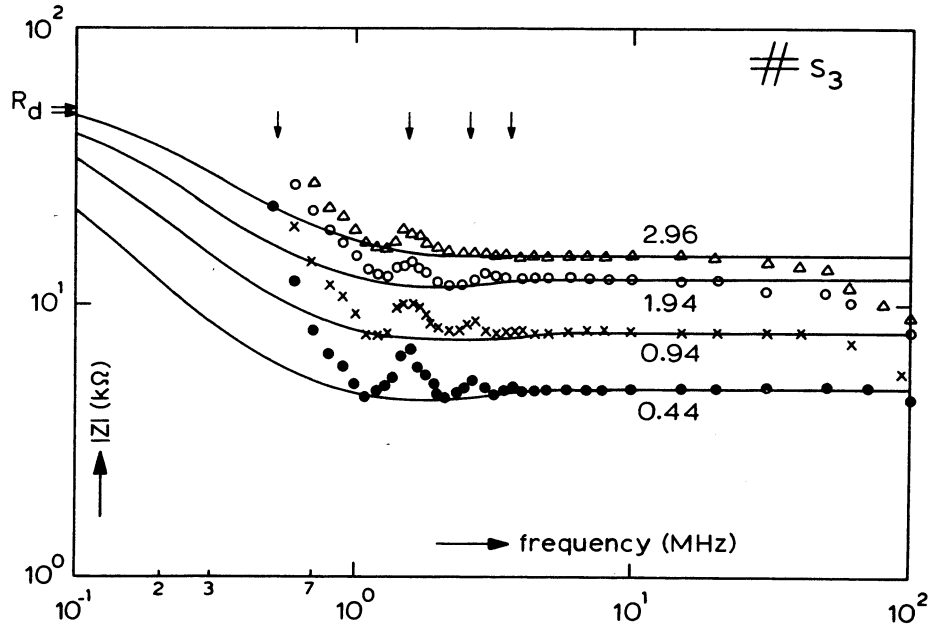with increasing voltage. Note that the increase in the impedance-plateau value

Figure 4. The absolute value of the ac impedance $|Z|$ of sample s_3, at different applied voltages. The values of $(\overline{V} - V_c)/V_c$ are indicated. The vertical arrows represent odd harmonics of 5.15×10^5 Hz. The upper and lower value of the differential resistance R_d are denoted by arrows on the vertical scale. The solid lines have been calculated with the help of eq. (6). The parameters used are listed in table 2 (Appendix).

with increasing voltage indicates that the trapping of carriers in potential troughs increases with increasing voltage. The observed high frequency roll-off may be due to an excess parasitic capacitance of approximately 1.4 pF parallel to Z (cf. figure 1).

In figure 5 we have plotted the value of the differential resistance R_d, obtained from the IV-characteristic, and the impedance-plateau value as a function of $\overline{V}/V_c$ for sample s_3.

When we use the measured IV-characteristic, and impedance-plateau values, we are able to calculate the electron densities $\overline{n}_d$, $\overline{n}_{s_1}$ and $\overline{n}_{s_2}$ as a function of the applied voltage. This was done with the help of eqs. (1), (2), (5) and (15). The mobility-tensor element μ_{33} was determined from the onset voltage of the electro-acoustic current fluctuations (cf. eq. (3)). In figure 6 the results of this calculation of the electron densities are given for sample s_3. For the value of v_{g_3} in eq. (2) we used 1.68×10^3 ms^{-1}, which was found from the
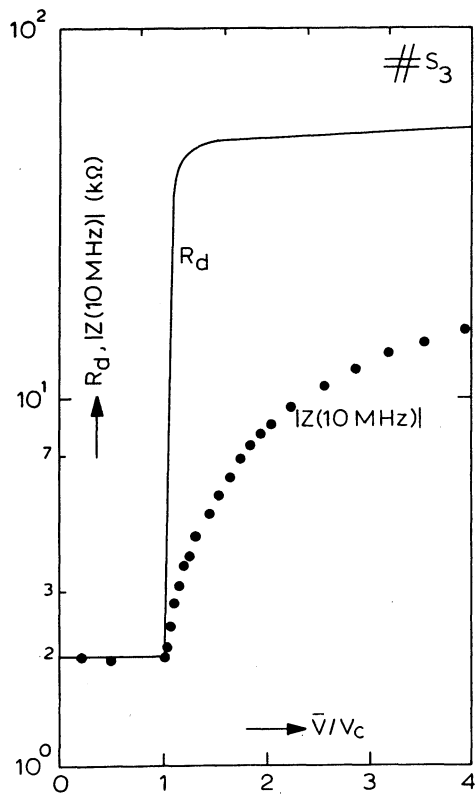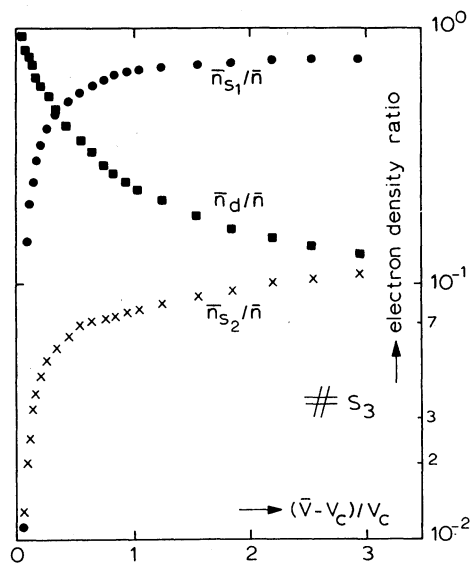
57

Figure 5. The differential re-
sistance (solid line) and the im-
pedance-plateau value at 10 MHz
(dots) as a function of $\overline{V}/V_c$ for
sample s_3.

Figure 6. The relative densities of
free and trapped electrons as a
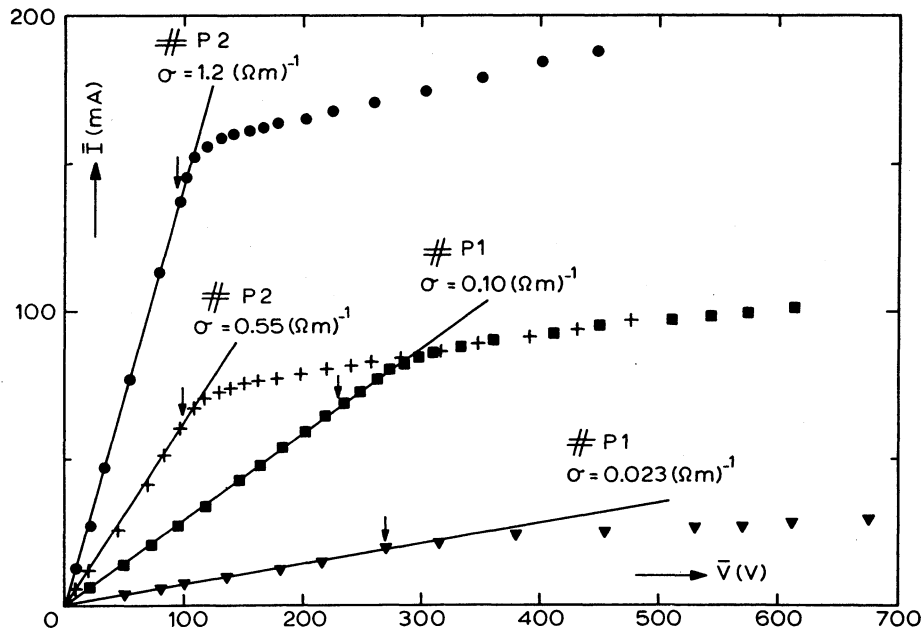function of $(\overline{V} - V_c)/V_c$ for sample
s_3.

Figure 7. Current-voltage characteristics for the photoconducting CdS samples p_1 and p_2 for different conductivities. The solid lines represent Ohm's law. Arrows indicate the onset of electro-acoustic current fluctuations.

resonance frequencies in figure 4. We observe a decrease of the free electron density with increasing voltage, whereas the density of both types of trapped electrons increases. Clearly the average trapping is dominated by the forward-travelling potential troughs. Similar results were obtained for the other samples.

II.4.2. *Photoconducting CdS*

In figure 7 IV-characteristics are shown for samples p_1 and p_2 for different conductivities. The results are similar to those obtained for semiconducting CdS (cf. figure 2).

Figure 8 shows the results of the impedance measurements on sample p_2, at different applied voltages. The sample conductivity was $\sigma = 1.2 \ (\Omega m)^{-1}$. The behaviour is found to be similar to that of the semiconducting samples: the plateau value increases steadily with increasing voltage, and resonances are observed, vanishing at higher voltages. At higher voltages the minimum in the
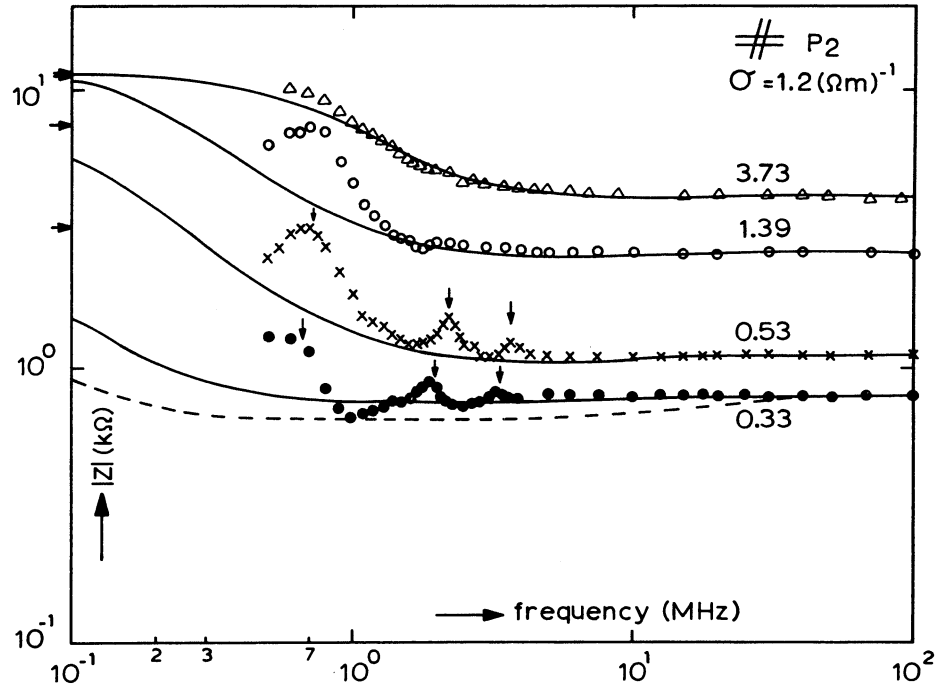
59

Figure 8. The absolute value of the ac impedance of sample p_2 ($\sigma = 1.2$ $(\Omega m)^{-1}$), at different applied voltages. The values of $(\bar{V} - V_c)/V_c$ are indicated. The magnitudes of the differential resistances R_d are indicated by arrows on the vertical scale. The vertical arrows represent the odd harmonics of 6.70×10^5 Hz and 7.32×10^5 Hz respectively. The solid lines and the dashed line have been calculated with the help of eq. (6). The parameters used are listed in table 2 (Appendix).

smooth curves disappears as well. Note that figure 8 shows a shift in the position of the resonances in the two lower curves. In the lower curve the resonances obviously coincide with the odd harmonics of 6.70×10^5 Hz, yielding a transit velocity of 1.53×10^3 ms^{-1}, whereas in the upper curve the resonance frequencies are given by the odd harmonics of 7.32×10^5 Hz, yielding

$v_{g_3} = 1.67 \times 10^3$ ms^{-1}. At first sight this is contrary to what one would expect, because, with increasing voltage, the off-axis angle of maximum sound amplification will increase until it reaches its saturation value. Therefore, with increasing voltage, the projection of the group velocity along the x_3-axis should become smaller [16]. However, a second, counteracting process may be of importance. Keller [16] showed, using White's linear theory, that the magnitude and direction of the group velocity are changed by electro-acoustic interaction.
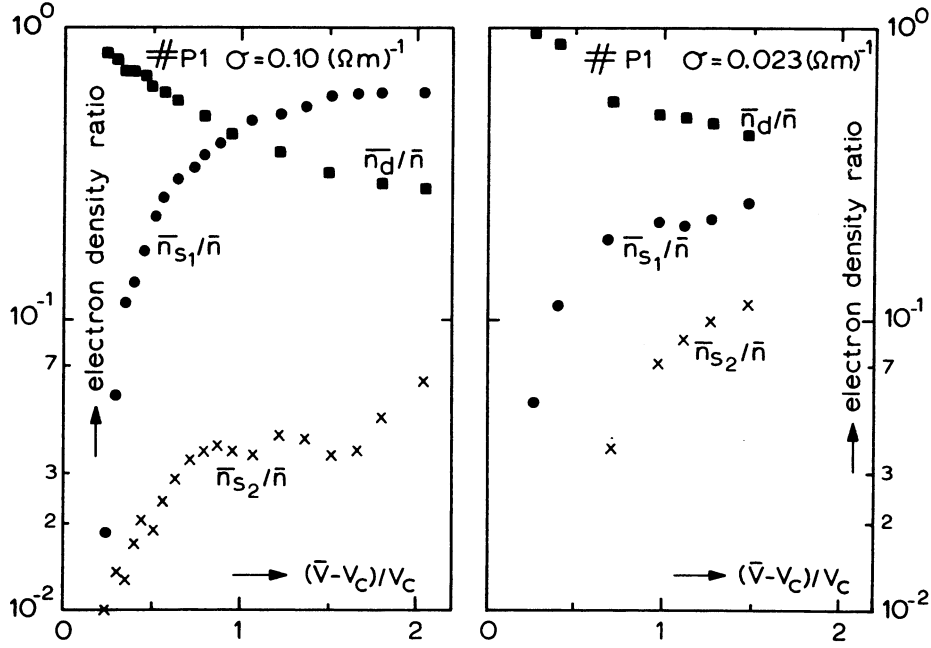
Figure 9. The relative densities of free and trapped electrons as a function of $(\bar{V} - V_c)/V_c$ for sample p_1 for two different conductivities.

In fact, an increase in electro-acoustic interaction has been found to cause an increase in the x_3-component v_{g_3} of the group velocity. Thus we can conclude that v_{g_3} will be raised with increasing voltage, due to electro-acoustic dispersion. Although Keller used White's theory, which is certainly not applicable in our case, his estimate of electro-acoustic dispersion provides a qualitative explanation for the observed shift in the resonance frequencies. The explicit calculation of electro-acoustic dispersion effects, when starting from the potential-trough model [8], is beyond the scope of this paper.

It should be noted that similar effects were found for the semiconducting samples s_2, s_5 and s_6. Apparently, in the case of sample s_3 these two competing effects compensated each other.

The solid lines in figure 8 were calculated with the help of eq. (6), as indicated before. The solid line at $(\bar{V} - V_c)/V_c = 0.33$ could not be fitted very well. The dashed line represents another possible solution. The values of the various parameters are listed in table 2 (Appendix).

In figure 9 the results obtained from the IV-characteristic and the impedance-plateau values for $\bar{n}_d/\bar{n}$, $\bar{n}_{s_1}/\bar{n}$ and $\bar{n}_{s_2}/\bar{n}$ are shown as a function of
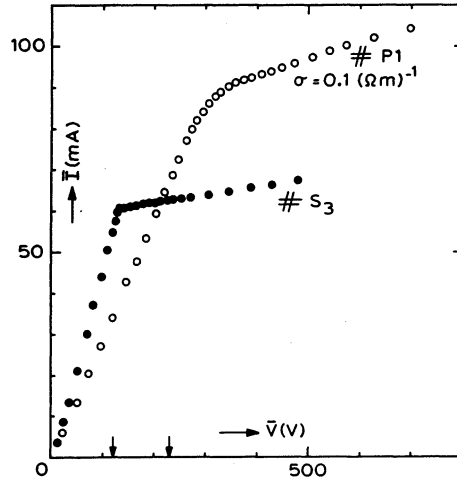
Figure 10. The current-voltage characteristics of the photoconducting sample p_1 ($\sigma = 0.1$ $(\Omega m)^{-1}$) and of the semiconducting sample s_1. The threshold voltages obtained from the onset of the electro-acoustic current fluctuations are indicated by arrows. The samples have equal contact spacings.

$(\overline{V} - V_c)/V_c$ for sample p_1, for two different conductivities. Qualitatively the voltage behaviour of the electron densities is similar to that of semiconducting crystals (cf. figure 6). The trapping is observed to decrease with decreasing conductivity, although $\overline{n}_{s_2}/\overline{n}$ increases somewhat. Since $\overline{n}_{s_2}/\overline{n}$ is very sensitive to a small change in the IV-characteristic data we can conclude that the spread in $\overline{n}_{s_2}/\overline{n}$ is caused by the inaccuracy of the measurements.

As already might be noticed from figure 7 we found for sample p_1 that the threshold voltage for the electro-acoustic effect is much larger than the value we would expect for the amplification of transverse waves. To illustrate this figure 10 shows the IV-characteristics of sample p_1 at $\sigma = 0.1$ $(\Omega m)^{-1}$ and of sample s_3. From table 1 it is seen that these samples are almost equal in length. In figure 10 the threshold voltages obtained from the onset of the current fluctuations are indicated by arrows. In fact, it was found that $V_c = (119 \pm 5)$ V for sample s_3 and $V_c = (230 \pm 10)$ V for sample p_1. From these results one might easily be tempted to conclude that it is transverse waves which are amplified in sample s_3 ($v_{s_0}(0) = 1.77 \times 10^3$ ms^{-1}) and longitudinal waves in sample p_1 ($v_{s_0}(0) = 4.41 \times 10^3$ ms^{-1}) (cf. eq. (3)). Indeed several authors [1, 4, 9] have concluded from the high value they obtained for the threshold voltage in some photoconducting CdS crystals that longitudinal waves are amplified. However, no physical reason can be given as to why the transverse waves, which even have a higher electro-mechanical coupling factor than longitudinal waves, are not excited in these samples.
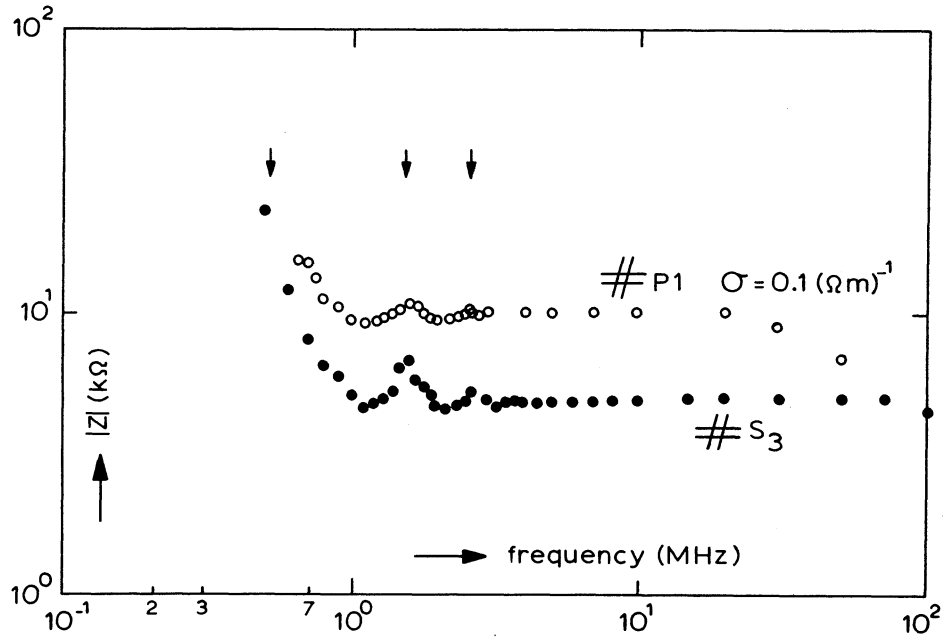
62

Figure 11. Measurements of the absolute value of the ac impedance $|Z|$ of sample p_1 (at $\sigma = 0.1$ $(\Omega m)^{-1}$) and sample s_3. The vertical arrows represent the odd harmonics of 5.15×10^5 Hz.

Therefore others [3, 10] suggested that the high value of the threshold field was due to the trapping of free charge carriers in bound-electron states. Already in 1962 White [3] showed that these carrier-trapping effects could be accounted for by multiplying the carrier mobility by a factor f_0, where $0 \leq f_0 \leq 1$. Only a fraction f_0 of the electro-acoustically produced space charge is free and contributes to the conductivity. A fraction $(1 - f_0)$ of the space charge is produced by electrons trapped at states in the forbidden gap and is immobile. When μ_{33} is replaced by $f_0 \cdot \mu_{33}$ in eq. (3), it is found that these trapping effects give rise to an increase in the threshold voltage.

This controversy can be removed if one measures the ac impedance, because the position of the resonances allows one to determine the trough transit-velocity. Figure 11 shows typical impedance measurements for both samples. Although the resonances for sample s_3 are somewhat more pronounced than those for sample p_1, it is clear that the resonances appear at the same frequencies. The arrows indicate the odd harmonics of 5.15×10^5 Hz, yielding a trough transit-velocity of about 1.7×10^3 ms^{-1}. Thence, it is concluded that it is

essentially transverse off-axis waves which are amplified in both semiconducting and photoconducting samples.

The experimental results, discussed above, strongly support the suggestion that the effect of carrier trapping in bound electron states plays an important role in some photoconducting CdS samples.

III.4.3. *Boundary-scattering effects*

In the calculation summarized in section III.2 [8] the effect of the scattering of acoustic waves at the boundaries was not taken into account. In fact, in the calculation [8] the cross-sectional area A was assumed to be large with respect to L^2. In most experimental circumstances this assumption certainly does not hold, and considerable losses due to boundary scattering have been observed [14, 15].

The acoustic scattering losses at the side-faces of our samples will affect acoustic waves with large off-axis angles most. This explains why in practice the observed off-axis angles of maximum sound amplification were smaller than 30°.

Since the off-axis angle of maximum sound amplification can be determined from the resonance frequencies in the impedance, our ac-impedance measurements provide a convenient but indirect tool for studying these boundary-scattering effects.

To investigate the effect of the boundary scattering we measured the ac impedance of sample s_1 at a certain electric field strength. As can be seen from table 1, all faces of sample s_1 are unpolished. Subsequently two side-faces of sample s_1 were polished to a flatness of $\frac{1}{4}$ μm. This sample is renamed s_4, and is also listed in table 1. Since the wavelengths of the amplified acoustic waves are typically of the order of 2 μm (at 1 GHz) [3, 15], we expect a considerable reduction in the boundary-scattering losses.

Again we measured the impedance at the same electric field strength as before.

In figure 12 part of the impedance spectra is shown for both samples. The resonances observed for sample s_1 could be interpreted as the odd harmonics of 4.93×10^5 Hz (arrows), whereas for sample s_4 we found the odd harmonics of 4.60×10^5 Hz (arrows). If we neglect electro-acoustic dispersion effects these results yield $\delta \simeq 7°$ for sample s_1 and $\delta = 17°$ for sample s_4.

It is concluded that the off-axis angle of maximum sound amplification is strongly influenced by the sound-wave scattering-losses at the side-faces.
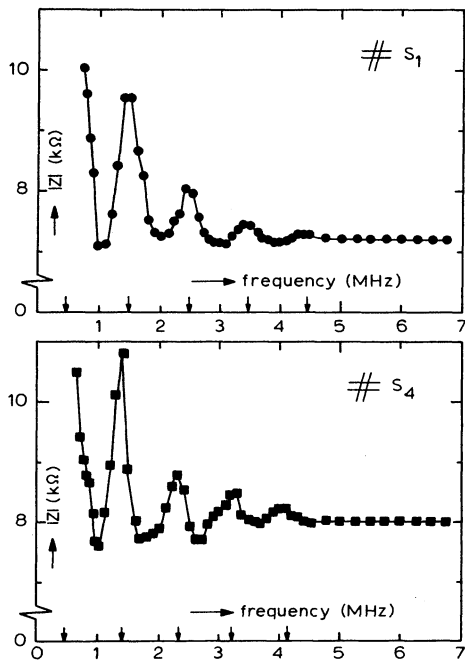
Figure 12. The absolute value of the ac impedance $|Z|$ for sample s_1 and sample s_4 at the same voltage. Resonance frequencies are indicated by arrows. The solid lines have been drawn to guide the eye.

No conclusions could be drawn from the experimental data about the influence of polished end-surfaces on the current saturation and the ac impedance.

III.4.4. Temperature effects

As the input of the sound-amplification process is determined by the thermal acoustic-energy distribution, we felt it was worth while to carry out measurements at different temperatures. Moore et al. [9, 19] found a strong increase in the ohmic slope in the IV-characteristic of semiconducting CdS when the temperature was changed from 293 K to 77 K. This was caused by an increase in the carrier mobility, whereas the carrier density remained almost constant. They found that the saturation current remained almost constant, as expected since it depends on the sound velocity, which is nearly temperature independent. The results plotted as $\bar{I}$ vs. $\bar{V}/V_c$ were almost identical at different temperatures.

So far no reports have appeared in the literature about the temperature dependence of the ac impedance.

To carry out measurements at 77 K sample s_2 was simply immersed in liquid nitrogen.
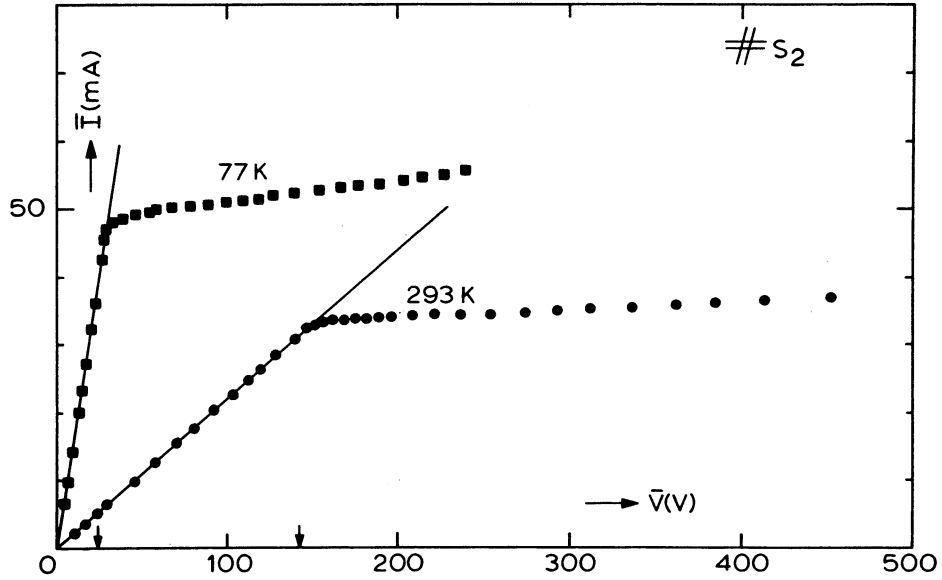
65

Figure 13. Current-voltage relationships of sample s_2 at 293 K and 77 K. The arrows indicate the threshold voltages obtained from the onset of electro-acoustic current fluctuations. The solid lines represent Ohm's law.

Figure 13 shows the IV-characteristics of sample s_2 at 293 K and at 77 K. The arrows indicate the threshold voltages obtained from the onset of the electro-acoustic current fluctuations. If we assume the carrier concentration to be temperature independent [19] we find from the ohmic slopes that $\mu_{33}(77$ K$)/\mu_{33}(293$ K$) \approx 7.4$. This is in agreement with the results obtained for the threshold voltages. From $V_c(293$ K$) = (142 \pm 5)$ V and $V_c(77$ K$) = (21 \pm 3)$ V it follows that (cf. eq. (3)) $\mu_{33}(77$ K$)/\mu_{33}(293$ K$) = 6.8 \pm 1.0$. This ratio is not in agreement with literature values for the Hall mobility μ_H; these give values between 10 [20] and 15 [12] for $\mu_H(77$ K$)/\mu_H(293$ K$)$.

Moore et al. [19], who obtained from the threshold voltages a mobility ratio between 3 and 5.2, found from Hall measurements on the same samples $\mu_H(77$ K$)/\mu_H(293$ K$) = 11$. They explained that this disagreement was due to the trapping of carriers in bound-electron states in the forbidden gap. In fact, according to [3, 10] μ_{33} should be replaced by $f_0 \cdot \mu_H$, where f_0 is the fraction of the electro-acoustically produced space charge that is free (cf. section III.4.2). Moore et al. [19] concluded that $f_0 = 1$ at room temperature and $f_0 = 0.3 - 0.5$ at 77 K.

66

It follows that the discrepancy between our data and the Hall-mobility data in [20] can be removed by setting $f_0 = 1$ at room temperature and $f_0 \simeq 0.67$ at 77 K.

Furthermore the saturated current in figure 13 is observed to be somewhat larger at 77 K than at 293 K. We found from the IV-characteristic and the impedance-plateau values that the trapping in potential troughs is less strong at 77 K. This was not reported by Moore et al. [9, 19]. However, it should be noted that the CdS samples used by Moore et al. had conductivities 20-200 times larger than sample s_2, and therefore showed stronger current saturation.

Another explanation for the observed reduction in the current saturation at 77 K may be a decrease in the sound-amplification coefficient, which depends essentially on the carrier mobility. Furthermore the ultimate magnitude of the acoustic-energy density may be reduced somewhat by the reduced input of the sound amplification process at 77 K. Another possible explanation is a change in the acoustic reflection and transmission properties of the boundaries. Since the sample is immersed in liquid nitrogen a considerable amount of acoustic
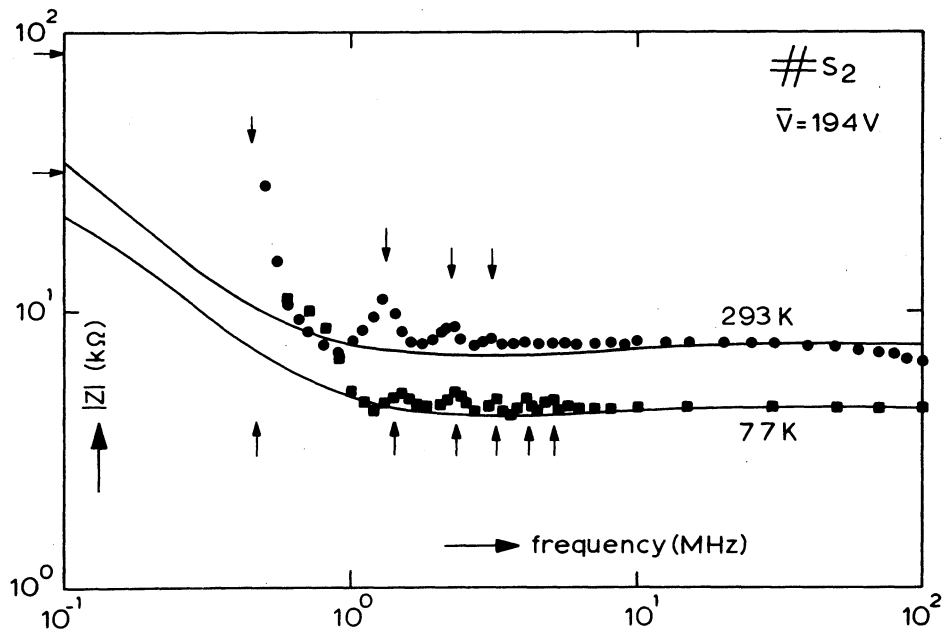

Figure 14. The absolute value of the ac impedance $|Z|$ of sample s_2 at 194 Volt for two temperatures. The values of the differential resistances are indicated by arrows on the vertical scale. The solid lines have been calculated with eq. (6). The parameters used are listed in table 2 (Appendix). The lower arrows indicate the odd harmonics of 4.67×10^5 Hz; the upper arrows represent the odd harmonics of 4.50×10^5 Hz.

67

energy may be transferred into the ambient nitrogen.

In figure 14 ac-impedance data at $\overline{V}$ = 194 Volt are plotted for two tempe-
ratures. The solid lines have been calculated as indicated before, with the
help of eq. (6) (cf. section III.4.1). The behaviour of the ac impedance at
77 K is seen to be similar to that at room temperature. At 293 K the resonance
frequencies, obviously the odd harmonics of 4.50 ± 10^5 Hz, yield
$v_{g_3} = 1.66 \times 10^3$ ms^{-1} and $\delta = 15°$. At 77 K the resonances can be associated with
the odd harmonics of 4.67×10^5 Hz, yielding $v_{g_3} = 1.72 \times 10^3$ ms^{-1} and $\delta = 9°$.
It should be noted that the effects of electro-acoustic dispersion are not
taken into account in the determination of δ.

We conclude that no fundamental changes occur in the current-voltage and
impedance data when the temperature is changed from 293 K to 77 K.

References

[1] R.W. Smith, Phys. Rev. Lett. 9 (1962) 87.
[2] A.R. Hutson, J.H. McFee and D.L. White, Phys. Rev. Lett. 7 (1961) 237.
[3] D.L. White, J. Appl. Phys. 33 (1962) 2547.
[4] P.A. Gielen and R.J.J. Zijlstra, Physica 95B (1978) 347.
[5] W. Westera, R.J.J. Zijlstra and M.A. van Dijk, Phys. Lett. 78A (1980) 371.
[6] W. Westera and R.J.J. Zijlstra, Physica 106B (1981) 33.
[7] W. Westera, Chapter IV of this thesis.
[8] W. Westera, Chapter II of this thesis.
[9] A.R. Moore, J. Appl. Phys. 38 (1967) 2327.
[10] I. Uchida, T. Ishiguro, Y. Sasaki and T. Suzuki, J. Phys. Soc. Japan 19 (1964) 674.
[11] B. Pödör, J. Balázs and M. Hársy, Phys. Stat. Sol. (a) 8 (1971) 613.
[12] J.D. Zook and R.N. Dexter, Phys. Rev. 129 (1963) 1980.
[13] A.R. Moore, R.W. Smith and P. Worcester, IBM J. Res. Developm. 13 (1969) 503.
[14] O. Keller, Phys. Rev. B 10 (1974) 1585.
[15] M. Yamada, C. Hamaguchi, K. Matsumoto and J. Nakai, Phys. Rev. B 7 (1973) 2682.
[16] O. Keller, Phys. Stat. Sol. 16 (1973) 87.
[17] D. Berlincourt, H. Jaffe and L.R. Shiozawa, Phys. Rev. 129 (1963) 1009.
[18] I.B. Kobiakov, Sol. State Commun. 35 (1980) 305.
[19] A.R. Moore and R.W. Smith, Phys. Rev. A 138 (1965) 1250.
[20] B. Pödör, Act. Phys. Ac. Sc. Hung. 36 (1974) 431.

(Chapter III)

A P P E N D I X

In table 2 we listed the parameter values used in the impedance calcu-
lations of figures 3, 4, 8 and 14.

Table 2.

Sample	Figure	$\dfrac{(\overline{V}-V_c)}{V_c}$	α_1 $(\Omega^{-1}m^{-1}s^{-1})$	τ_1 (s)	α_2 $(\Omega^{-1}m^{-1}s^{-1})$	τ_2 (s)	$q\mu_{33}\overline{n}_d$ $(\Omega^{-1}m^{-1})$
s_6	3	0.19	-3.4×10^6	2.8×10^{-7}	5.5×10^6	5.7×10^{-8}	1.14
	3*)	0.19	-1.6×10^6	5.0×10^{-7}	2.0×10^6	5.7×10^{-8}	1.14
s_3	4	0.44	-2.0×10^6	2.6×10^{-7}	1.9×10^6	8.4×10^{-8}	0.39
s_3	4	0.94	-1.2×10^6	2.4×10^{-7}	1.0×10^6	8.0×10^{-8}	0.24
s_3	4	1.94	-6.5×10^5	2.5×10^{-7}	5.7×10^5	7.6×10^{-8}	0.15
s_3	4	2.96	-4.7×10^5	2.2×10^{-7}	2.4×10^5	5.5×10^{-8}	0.13
p_2	8	0.33	-1.1×10^6	8.0×10^{-7}	5.0×10^6	1.1×10^{-8}	1.06
p_2	8*)	0.33	-6.5×10^5	1.6×10^{-6}	2.2×10^7	1.1×10^{-8}	1.06
p_2	8	0.53	-3.4×10^6	2.0×10^{-7}	4.2×10^6	1.1×10^{-8}	0.75
p_2	8	1.39	-1.5×10^6	1.8×10^{-7}	1.7×10^6	1.1×10^{-8}	0.32
p_2	8	3.73	-1.8×10^6	7.8×10^{-8}	1.3×10^6	1.1×10^{-8}	0.20
s_2	14	0.36	-1.1×10^6	3.1×10^{-7}	2.4×10^6	1.6×10^{-8}	0.33
s_2	14†)	8.1	-2.4×10^6	2.2×10^{-7}	3.5×10^6	2.0×10^{-8}	0.55

*) dashed line.
†) 77 K.

69

C H A P T E R   I V

ELECTRO-ACOUSTIC CURRENT FLUCTUATIONS IN CdS

Abstract — Experimental data on electro-acoustic current fluctuations, in the
frequency range 500 kHz to 100 MHz, are presented for semiconducting and photo-
conducting CdS single crystals. The measurements were carried out under pulsed-
bias conditions to avoid excessive Joule heating of the samples. The experi-
mental results are discussed in terms of our previously published theory. The
latter is based on a model where bunches of conduction electrons can be trapped
and detrapped in potential troughs associated with acoustic waves which are
amplified from the thermal background. The experimental current-noise spectra
showed local minima which can be related to the potential-trough transit-time.
These transit-time effects are not described by the theory, because it did not
take space charge into account. Apart from these effects, however, in most
cases the current-noise data for both semiconducting and photoconducting samples
can be described by one or two Lorentzian spectra, in accordance with the theo-
ry. In some cases, however, deviating spectra showing minima and maxima which
could not be related to potential-trough transit-times were observed.
    Values for the electron drift-mobility obtained from voltages marking the
onset of electro-acoustic current fluctuations lie well within the range of the
values published by others.

IV.1. Introduction

    If a dc electric field applied to a piezoelectric semiconducting crystal

causes the carrier drift-velocity to exceed the sound velocity, travelling

acoustic waves may be amplified. The first experiments on this effect were re-

ported in 1961 by Hutson et al. [1], who observed the amplification of injected

ultrasonic waves in photoconducting CdS single crystals under pulsed-bias con-

ditions. In addition they found that if the duration of the drift-field pulse

was made somewhat longer than the round-trip transit-time for acoustic waves

spontaneous growth of acoustic waves originating from the thermal background

occurred. In 1962 White [2] derived an expression for the sound-amplification

coefficient using a linear classical continuum description. White predicted

that a maximum in the sound amplification coefficient would occur at angular

frequency $\omega_m = (\omega_C \omega_D)^{\frac{1}{2}}$, where ω_C is the angular dielectric-relaxation frequency

71

and ω_D is the angular carrier-diffusion frequency. For CdS the value of ω_m generally lies in the GHz-range. Furthermore White showed that the amplification of an RF acoustic wave gives rise to a corresponding RF current. Preliminary measurements of the RF components of the current in a photoconducting CdS crystal by Blötekjaer et al. [3] showed a maximum near ω_m, as predicted by White. Subsequent Brillouin-scattering studies of the growth of the acoustic flux in CdS [4, 5], have shown that White's theory only applies in the weak-flux limit. With increasing acoustic flux intensities many nonlinear effects have been observed [4, 5]. These effects may include parametric generation of subharmonics, current oscillations, current saturation, current fluctuations, travelling electro-acoustic domain formation, and so on.

The first systematic measurements of electro-acoustic current fluctuations in CdS were reported by Moore [6]. Experimental data in the frequency range 1.5 MHz to 900 MHz did not show a maximum in the current-noise spectrum; instead, the noise spectrum turned out to be flat at low frequencies, and to decrease approximately as $1/f^2$ at high frequencies. This type of current noise cannot be described by a linear theory. Moore avoided the need to use nonlinear equations in that he suggested that the observed current fluctuations are caused by the trapping of bunches of free charge carriers in potential troughs, associated with the amplified acoustic waves. Assuming that the creation and annihilation of potential troughs occurs at random throughout the crystal, Moore found that the observed current fluctuations can be described by a trough creation-annihilation process. The thus obtained expression for the noise spectrum gave a reasonable explanation for his experimental data. Additional experimental results of current-noise measurements have been reported by Baibakov [7] in CdSe and by Gielen and Zijlstra [8, 9] in CdS. Moreover, Schulz et al. [10, 11] observed this trapping noise in GaAs, although their attention was mainly focussed on the parametric generation of subharmonic frequencies in the RF current.

In 1978 Zijlstra and Gielen [12] modified Moore's calculation by accounting for transit-time effects in a local description. Since, however, the boundary conditions they used imply an internal inconsistency at low frequencies their results should be considered doubtful.

In [13] we extended this local description by introducing two types of potential troughs, related to forward-travelling (i.e. towards the anode) and backward-travelling (i.e. towards the cathode) acoustic waves, respectively. The backward-travelling potential troughs were introduced to remove an inconsistency which arises when the relaxation time obtained from the current-noise

72

spectrum is compared with that obtained from the ac impedance (cf. [14]). It was assumed that space charge, diffusion and the dielectric-displacement current can be neglected, and that the kinetics of the two types of troughs are statistically independent. Furthermore the crystal anisotropy was taken into account, and consistent boundary conditions were applied. If the spontaneous fluctuations in the potential-trough creation and annihilation rates are assumed to be statistically independent, the current-noise spectrum can be described by two Lorentzian components.

The aim of this paper is to compare experimental current-noise data for photoconducting and semiconducting CdS with the calculations given in [13]. A summary of the results of these calculations is given in section IV.2, the experimental arrangement is described in section IV.3, and experimental results are presented and discussed in section IV.4.

IV.2. Theory

In this section we shall summarize the results of the calculation of the spectral current-noise intensity as given in [13].

Consider an n-type homogeneous piezoelectric semiconducting crystal where the electric field is applied along a symmetry axis, the x_3-axis. In the case of CdS the x_3-axis coincides with the c-axis. Together with the x_1- and x_2- axis the x_3-axis forms a Cartesian coordinate system. The sample is supplied with Ohmic contacts at $x_3 = 0$ (cathode) and $x_3 = L$ (anode). If the drift velocity of the electrons exceeds the sound velocity, acoustic waves, originating from the thermal background and travelling in the direction of the drifting electrons, are amplified. As a result potential troughs which propagate with the sound velocity are spontaneously created and annihilated throughout the crystal. Note that the creation and annihilation occurs at random because of the incoherent nature of the thermal background waves. The electro-acoustic current fluctuations are thought to be caused by the sudden trapping and detrapping of whole groups of free charge carriers in these potential troughs. If charge carriers become trapped in these potential troughs, their velocity is changed from the drift velocity to the trough velocity. We have assumed that two types of potential troughs occur: one type of trough is associated with acoustic waves travelling towards the anode (forwards) and the second type with waves travelling towards the cathode (backwards). The two types of troughs, having opposite velocity components, v_{g_3} and $-v_{g_3}$ respectively,

73

along the x_3-axis, have been assumed to be statistically independent. In [14] we showed that the trough velocity $\vec{v}_g$ can be associated with the group velocity of the acoustic waves. As a result of the elastic anisotropy in CdS the direction and magnitude of the group velocity may differ considerably from the direction and magnitude of the acoustic phase velocity. For reasons of simplicity we neglected space-charge, and assumed that each forward-travelling trough contains N_1 electrons, and each backward-travelling trough contains N_2 electrons, where N_1 and N_2 are independent of x_3. In addition we neglected diffusion and the displacement current.

The current noise was calculated with the Langevin method. Spontaneous fluctuations in the potential-trough creation and annihilation rates were used as Langevin source-functions. On the assumption that the spatial correlation for each Langevin source-function can be described by a delta-function, we found the following expression for the spectral current-noise intensity S_I:

$$S_I(f) = 4qN_1(q\bar{n}_{s_1}v_{g_3}A)\left(\frac{\bar{v}_{d_3} - v_{g_3}}{v_{g_3}}\right)^2 \frac{\tau_1/\tau_t}{1 + \omega^2\tau_1^2}$$

$$+ 4qN_2(q\bar{n}_{s_2}v_{g_3}A)\left(\frac{\bar{v}_{d_3} + v_{g_3}}{v_{g_3}}\right)^2 \frac{\tau_2/\tau_t}{1 + \omega^2\tau_2^2} \quad , \tag{1}$$

where $-q$ is the electron charge,

A is the contact area,

ω is the angular frequency,

$f = \omega/2\pi$ is the frequency,

$\bar{n}_{s_1}, \bar{n}_{s_2}$ are the time-averaged local densities of electrons, trapped in forward- and backward-travelling troughs, respectively,

τ_1, τ_2 the mean lifetimes of the fluctuations in the numbers of forward- and backward-travelling troughs, respectively,

$\tau_t = L/v_{g_3}$ is the potential-trough transit-time, and

$\bar{v}_{d_3}$ is the time-averaged drift-velocity component along the x_3-axis.

As a consequence of the assumption of space-charge neutrality in the steady state, $\bar{v}_{d_3}$ can be related directly to the applied voltage $\bar{V}$ by:

74

$$\bar{v}_{d_3} = \mu_{33} \frac{\bar{V}}{L} \quad ,$$

where μ_{33} is an element of the mobility tensor.

As we pointed out in [13] the threshold voltage V_c for the amplification of sound waves is determined by the phase velocity $v_s(0)$ of on-axis waves:

$$V_c = \frac{v_s(0) \cdot L}{\mu_{33}} \quad . \tag{3}$$

As a final result of the calculations given in [13] we mention the occurrence of maxima in the ac impedance at frequencies that are related to the potential-trough transit-time. The resonance frequencies are given by

$$f = f_1 = \frac{(2l + 1)}{2} \tau_t^{-1} \quad ; \quad l = 0, 1, 2, 3, \ldots \quad . \tag{4}$$

IV.3. Experimental Arrangement

For our measurements we used semiconducting and photoconducting single crystals of hexagonal n-type CdS, obtained from Eagle Picher Industries, Inc..

So that Brillouin-scattering experiments could possibly be carried out at a later stage we polished some of the crystal side-faces mechanically to a flatness of $\frac{1}{4}$ μm. In some cases the two contact faces were also polished to a flatness of $\frac{1}{4}$ μm. Unpolished surfaces, being several orders of magnitude less flat than polished ones, can be expected to cause considerable acoustic scattering losses, since the wavelengths of the amplified acoustic waves having frequencies around 1 GHz are about 2 μm [2, 4].

The samples were supplied with two In-evaporated Ohmic contacts in such a way that the applied electric field was orientated along the c-axis (the longitudinal configuration). The In-contacts covered the end-surfaces completely. For details we refer to [14].

The dimensions, dark-conductivity at room temperature and surface characteristics of the semiconducting (s) and photoconducting (p) CdS crystals are listed in table 1. Data on current saturation and ac impedances for these samples have been presented in [14]. All measurements were carried out at room temperature.

Table 1. Characteristics of the semiconducting (s) and photoconducting (p) CdS samples.

Sample	L (mm)	A (mm^2)	Dark-conductivity ($\Omega^{-1}m^{-1}$)	Polished faces (mm^2)
s_1	1.76	1.24×0.55	6.6×10^{-1}	--
s_2	1.84	1.27×0.59	5.6×10^{-1}	--
s_3	1.63	1.78×0.48	9.5×10^{-1}	1.78×1.63 — faces 1.78×0.48 — faces
s_4	1.76	1.24×0.43	6.6×10^{-1}	1.76×1.24 — faces
s_5	2.79	1.43×0.37	2.3	all faces
s_6	1.76	2.53×0.97	1.3	--
p_1	1.65	2.14×2.20	2.3×10^{-3}	--
p_2	1.14	1.81×0.76	5.5×10^{-1}	--

To control the conductivity of photoconducting crystals the samples were illuminated from the side with filtered light from a quartz–halogen lamp or with light from a Krypton laser. The optical wavelengths were such that no band-to-band transitions were induced but carriers from local centres were generated. Therefore the absorption coefficient of the light was small and it can be assumed that the samples were homogeneously illuminated.

To avoid excessive Joule heating of the samples the high voltage was applied in pulses of 40 µs at a repetition rate of 4 Hz. The rise-times of these pulses were about 5 µs. The duration of these pulses was sufficient for the samples to reach a stationary state. In addition, a room temperature nitrogen or air flow was made to pass over the sample during operation.

The height of the voltage pulses was measured with a sample-and-hold circuit.

The experimental set-up for the current-noise measurements under pulsed-bias conditions is shown in figure 1. Voltage pulses from the pulse generator, which passed through a low-pass filter to suppress higher harmonics of the pulses, were fed into an RF coaxial 50 Ω power termination. The CdS crystal (impedance Z) in series with a 50 Ω termination was connected in parallel. (The value of |Z| was always much larger than 50 Ω.) The current fluctuations generated by the electro-acoustic effect developed voltage fluctuations across the latter 50 Ω resistor. Our noise-measuring circuit, which performed the
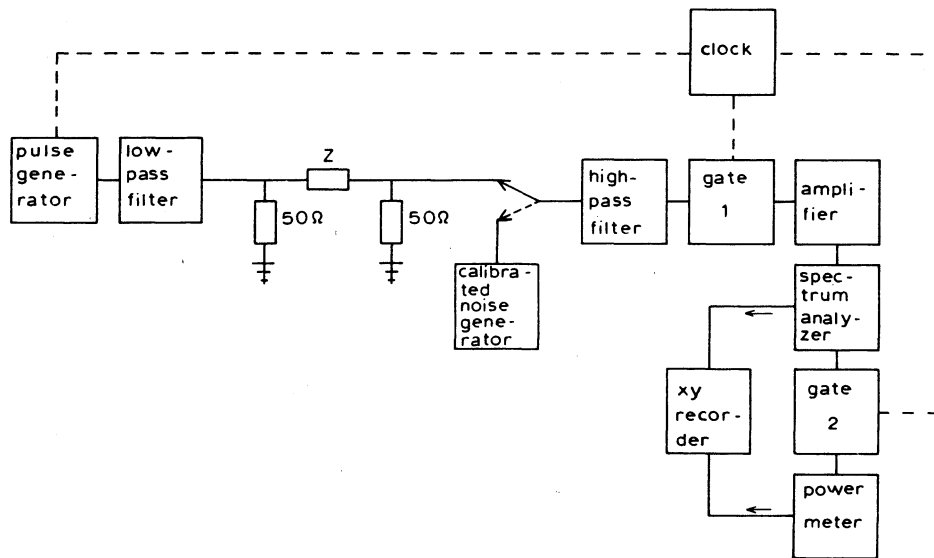
Figure 1. Experimental set-up for measuring the spectral current-noise intensity under pulsed-bias conditions.

frequency selection and noise-power measurement, was made up of several components. The input impedance of this circuit was approximately 50 Ω. The high-pass filter served to separate the dc part of the pulse from the ac part. It should be noted that the voltage fluctuations to be analyzed had typical amplitudes of a few micro-Volts, whereas the transient voltages at the input of the noise-measuring circuit were several Volts. Therefore, to prevent overloading the amplifiers we used an electronically-controlled RF gate (gate 1 in figure 1), which transmitted the noise signal only between 5 μs and 35 μs after the onset of the voltage pulse. Subsequently the noise signal was amplified and fed into an HP 8558 B spectrum analyzer. Since the power detector of the spectrum analyzer could not be used under pulsed-bias conditions, the intermediate-frequency output of the spectrum analyzer (21.4 MHz) was fed into a power meter consisting of an HP 435 A and an HP 8484 A. In this way the spectrum analyzer served only as a frequency band-filter and a mixer. A second gate (gate 2 in figure 1) was used to remove the (amplified) transients from the first gate (gate 1). The gate width of the former was slightly below 30 μs. The gates and the pulse generator were synchronised by the clock.

To determine the spectral current-noise intensity S_I we measured the power P_1 of the voltage fluctuations with bias applied to the sample, and the power P_2 without bias. This background power P_2 was caused by the noise of our measuring circuit. To calibrate the measured noise power a calibrated noise generator was connected to the noise-measuring circuit (cf. figure 1). In addition we measured P_3 (noise generator connected) and P_4 (noise generator connected, but with zero output). It can be shown [8, 9] that under these conditions the spectral current-noise intensity S_I is given by

$$S_I = \frac{P_1 - P_2}{P_3 - P_4} S_{I_0} \quad , \tag{5}$$

where S_{I_0} is the known spectral current-noise intensity of the calibrated noise generator (output resistance 50 Ω).

With the help of calibrated attenuators we verified that during the measurements the power-meter deflection was always linearly related to the input noise.

The pulse length of 40 µs determined a fundamental low-frequency limit for the current-noise measurements. This limit turned out to be about 500 kHz. The high-frequency limit was found to be about 100 MHz. This value was due to the electrical components in the low-pass and high-pass filters, and in some cases to parasitic capacitances parallel to Z. The bandwidth of the spectrum analyzer was set at 300 kHz at low frequencies ($\lesssim$ 10 MHz) and at 1 MHz at high frequencies ($\gtrsim$ 10 MHz).

The selected frequency of the spectrum analyzer could be swept automatically. Therefore, frequency-swept noise measurements were possible. The power-meter deflection and the horizontal output of the spectrum analyzer (a measure for the operating frequency) were connected to an XY-recorder. The power-meter deflections P_1, P_2, P_3 and P_4 were recorded successively with frequency-sweep times varying between 500 s and 1000 s.

With the procedure described above the spectral current-noise intensity S_I could be determined with an accuracy of about 10%. The lowest spectral current-noise intensity detectable was approximately 5×10^{-21} A^2s.

IV.4. Experimental Results and Discussion

In this section we present and discuss the experimental results for semi-conducting CdS (section IV.4.1) and photoconducting CdS (section IV.4.2). In section IV.4.3 electron drift-mobility values obtained from the voltage V_c marking the onset of electro-acoustic current fluctuations are compared with values from the literature.

IV.4.1. *Semiconducting CdS*

The spectral current-noise intensity S_I as measured at 10 MHz as a function of applied bias voltage $\bar{V}$ is shown in figure 2 for samples s_5 and s_6. The bandwidth for these measurements was 300 kHz. The solid lines have been drawn to guide the eye.

For sample s_6 we find that at low voltages, in fact at voltages where the current-voltage (IV-) characteristic is still ohmic, S_I increases proportionally to $\bar{V}^2$. This noise can be associated with generation-recombination noise [8, 9]. At a certain voltage V_c, S_I increases very strongly due to the occurrence of electro-acoustic current fluctuations. Since the critical voltage V_c is
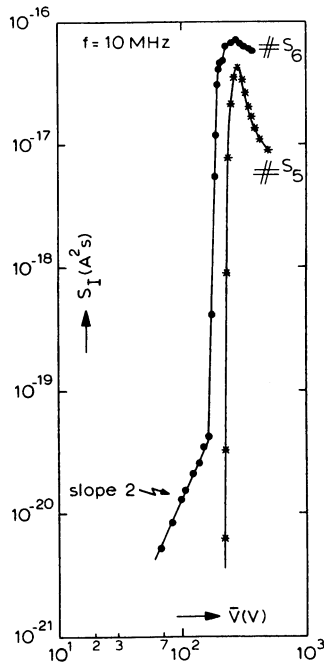
Figure 2. The spectral current-noise intensity at 10 MHz versus applied voltage for samples s_5 and s_6. The solid lines have been drawn to guide the eye.

79

closely related to the threshold voltage for electro-acoustic amplification, the strong increase in the current noise allows an accurate determination of this threshold voltage [6]. In fact, the threshold voltage can be determined much more accurately from the onset of the strong current noise than from the onset of current saturation. Moreover, in general the value of the latter is found to be somewhat higher than that of the former [8]. With increasing voltage we observe a decrease in the current noise. This is contrary to the results of Moore [6], who found experimentally $S_I \sim (\bar{V} - V_c)^2$, in accordance with his theoretical model. Gielen en Zijlstra [8, 9] compared their experimental data with calculations given by Zijlstra and Gielen [12], which predicted $S_I \sim (\bar{V} - V_c)^2$ as well, at voltages well above the curvature in the IV-characteristic (in our samples for $(\bar{V} - V_c)/V_c \gtrsim 0.5$). Their experimental data showed $S_I \sim (\bar{V} - V_c)^m$ with m varying between 1.6 and 4.0. Since, however, the electrical contacts on their CdS platelets covered only a small part of the crystal end-faces, the assumption of a homogeneous electric field strength was probably invalidated by the existence of stray electric fields in the fringe area. So far we have no explanation for the discrepancy between our data and those of Moore [6].

As can be seen from figure 2 the behaviour of sample s_5 above V_c is similar to that of sample s_6. For sample s_5, however, no generation-recombination noise could be observed.

Upon inspection of eq. (1) we can conclude that in general the voltage dependence of S_I will be very complex because of the voltage dependences of the
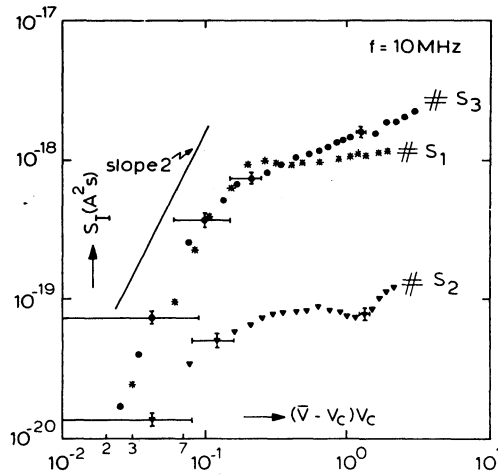

Figure 3. The spectral current-noise intensity at 10 MHz versus $(\bar{V} - V_c)/V_c$ for several samples. The solid line represents a line with slope 2.
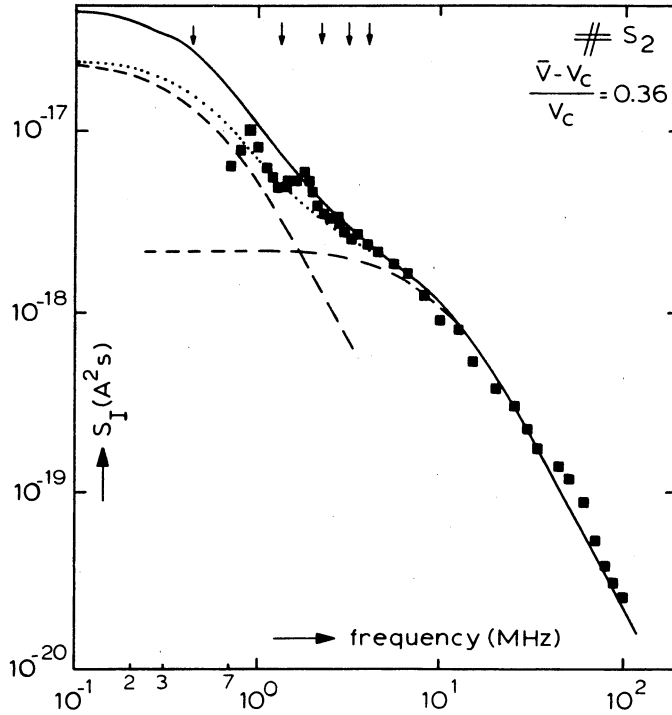
80

Figure 4. Spectral current-noise intensity for sample s_2 at $(\bar{V} - V_c)/V_c = 0.36$. Black squares represent the experimental data. The solid line and dotted line have been calculated with eq. (1). The parameters used are listed in table 2 (Appendix). The dashed lines represent the separate contributions made by the single Lorentzian spectra occurring in eq. (1) to the dotted line. The vertical arrows correspond to maxima in the ac impedance.

parameters N_1, N_2, v_{g_3}, $\bar{v}_{d_3}$, τ_1, τ_2, $\bar{n}_{s_1}$ and $\bar{n}_{s_2}$.

Figure 3 shows the spectral current-noise intensity at 10 MHz plotted versus the reduced voltage $(\bar{V} - V_c)/V_c$ for samples s_1, s_2 and s_3. At voltages slightly above V_c, S_I is approximately proportional to $(\bar{V} - V_c)^2$. With increasing voltage, however, substantial deviations from a quadratic relationship are again observed. It should be noted that the data for $(\bar{V} - V_c)/V_c$ below 10^{-1} may be quite inaccurate due to the fact that V_c could not be determined very accurately. Therefore, the errors in $(\bar{V} - V_c)/V_c$, as indicated in figure 3, will be systematic rather than accidental.

Figure 4 shows a current-noise spectrum for sample s_2. The experimental data are represented by black squares. Apparently these data cannot be described by a single Lorentzian, although such a shape was predicted in [6].

81

At low frequencies the noise spectrum shows some structure, which is not de-
scribed by the theoretical expression for the current noise (eq. (1)). Struc-
ture appearing in the ac impedance measured under the same conditions was pre-
dicted theoretically [13] and can be ascribed to potential-trough transit-time
effects. Maxima in the ac impedance occur at frequencies given by eq. (4). The
vertical arrows in figure 4 correspond to these resonance frequencies as ob-
tained from the ac-impedance data. From figure 4 we conclude that maxima in
the ac impedance correspond to minima in the current noise. It should be noted
that such transit-time effects in the expression for the ac impedance are only
found if space charge is taken into account. However, for reasons of simplicity
we neglected space charge in our calculation of the current noise [13]. There-
fore no transit-time effects are included in our expression for the current
noise (eq. (1)). We conclude that the structure observed in the current-noise
spectrum is also caused by potential-trough transit-time effects. We expect
that it will be possible to describe the current noise apart from the structure
by eq. (1). The most accurate way to determine the resonance frequencies (cf.
eq. (4)) is to use the ac-impedance data, because the bandwidth in the measure-
ments of the current-noise spectra is finite.

Moore [6], who used a non-local description, in terms of total numbers of
free and trapped carriers, accounted for transit-time effects in an ad hoc
manner by using an expression for the auto-correlation function of the current
fluctuations, originally derived by Hill et al. [15] for the case of ambipolar
carrier drift. In the transit-time-dominated case Moore's calculation yielded
a noise spectrum of the form $(\sin(X)/X)^2$ where $X = \frac{1}{2}\omega\tau_t$; this in turn yields
minima at frequencies that are multiples of $1/\tau_t$ and maxima at frequencies
given by eq. (4). Moore's experimental data, however, showed no distinct
transit-time effects. Figure 4 demonstrates that Moore's expression for the
transit-time effects cannot be correct, because the positions of experimental
minima and maxima are precisely the reverse of Moore's. The only correct way
to account for transit-time effects is to calculate the current noise in a
local description without assuming space-charge neutrality. So far no such
calculation has been published.

It was not possible to fit eq. (1) directly to the current-noise data by
adjusting τ_1, τ_2 and the plateau values. Therefore we used the following pro-
cedure to fit eq. (1) to the data in figure 4. We estimated a relaxation time
(the smaller of the two) from the noise spectrum and we fitted the expression
for the ac impedance to the experimental ac-impedance data by adjusting the

82

other relaxation time [14]. Subsequently we adjusted the plateau values of the Lorentzians in eq. (1) to the current-noise data with a least-squares fitting procedure. From the ac-impedance data it follows that τ_2 is always much smaller than τ_1 [14].

The numbers of electrons, N_1 and N_2, per trough can be determined from the adjusted plateau-values, because $\bar{n}_{s_1}$ and $\bar{n}_{s_2}$ can be calculated from the ac impedance and the IV-characteristic [14], v_{g_3} is known from the resonance frequencies in the ac impedance (cf. eq. (4)), and $\bar{v}_{d_3}$, or rather μ_{33}, is known from V_c (cf. eq. (3)). Although the value of τ_1 as found from the ac impedance is rather inaccurate [14], the procedure described above proved to give acceptable fits.

The solid line in figure 4 shows the result of the fitting procedure. Here, at low frequencies it is only the current-noise data at the local maxima which have been used in the fitting procedure. From this fit we obtained $N_1 \simeq 1.3 \times 10^5$, $N_2 \simeq 1.6 \times 10^4$, $\tau_1 \simeq 3.1 \times 10^{-7}$ s and $\tau_2 \simeq 1.6 \times 10^{-8}$ s. The parameters used are listed in table 2 (Appendix). It should be noted that the numerical values of N_1, N_2, τ_1 and τ_2 suggest a higher accuracy than can be obtained with the available experimental data. First of all, in most cases τ_1 cannot be obtained very accurately from the ac-impedance data [14]; in the second place at low frequencies the Lorentzian spectra are concealed by the transit-time resonances; in addition at low frequencies the magnitudes of the selected frequencies become comparable with the magnitude of the bandwidth (300 kHz) of our measuring circuit; there is a lack of data at low frequencies; lastly, since no expression for the transit-time resonances has been derived we are not sure whether in our fitting procedure we should use the data at the local maxima, those at the local minima, or even those in between. Therefore we adjusted the plateau values again, this time using all experimental data occurring in figure 4. The dotted line in figure 4 represents the result of this fitting procedure. The dashed lines show the separate contributions of the two single Lorentzian spectra. We found $N_1 \simeq 6.5 \times 10^4$ and $N_2 \simeq 1.8 \times 10^4$. The parameters used for this calculation are listed in table 2 (Appendix).

From further investigations we estimated the error in τ_2 to be about 20%, in τ_1 about 50% [14], in N_2 about 30% and in N_1 about 100%. We conclude that the numerical values of the parameters τ_1, N_1 and N_2 obtained from the fitting procedure are indicative only of the order of magnitude.

Figure 5 shows the current-noise spectrum of sample s_4 at $(\bar{V} - V_c)/V_c = 0.35$. The solid line has been calculated with the help of eq. (1),
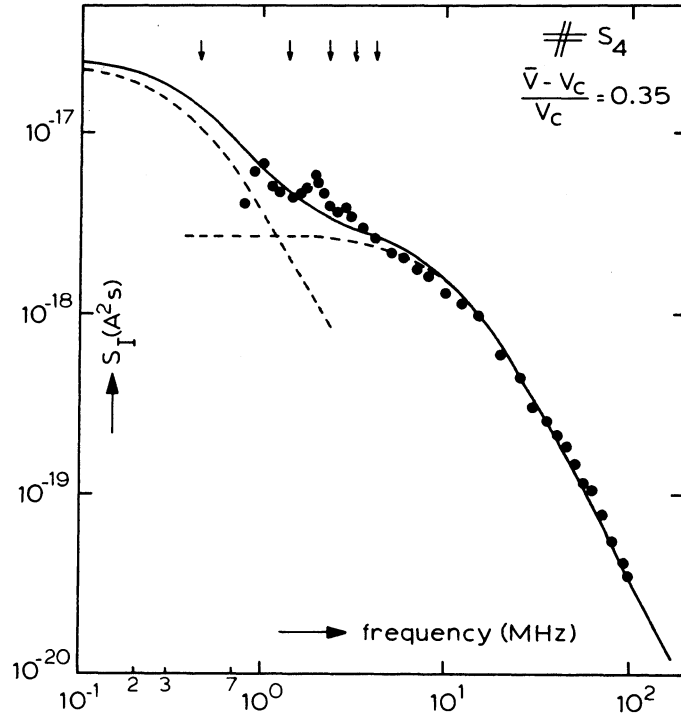
83

Figure 5. Spectral current-noise intensity of sample s_4 at $(\overline{V} - V_c)/V_c = 0.35$. The black dots represent the experimental data. The solid line has been calculated with eq. (1). The parameters used are listed in table 2 (Appendix). The separate contributions of the Lorentzians in eq. (1) are indicated by the dashed lines. The vertical arrows correspond to maxima in the ac impedance.

using all experimental data. For details we refer to table 2 (Appendix). From figures 4 and 5 we conclude that expression (1) can be fitted quite reasonably to the experimental current-noise data, apart from the transit-time resonances. Noise spectra of similar shape were obtained for sample s_1.

In some cases the current-noise spectrum is dominated by one Lorentzian spectrum in the frequency range considered. Figure 6 shows such current-noise spectra for sample s_3 at two different applied voltages. The solid lines represent hand-fitted Lorentzian spectra. Here, again we used all experimental data. From these curves we obtained $N_2 \simeq 2 \times 10^4$ at $(\overline{V} - V_c)/V_c = 0.94$ and $N_2 \simeq 5 \times 10^3$ at $(\overline{V} - V_c)/V_c = 2.96$. It is observed that an increase in the applied bias voltage hardly affects the current-noise spectrum for this sample. Only a slight broadening of the noise spectrum and a decrease of the transit-time effects are observed. The relatively low value of the roll-off frequency
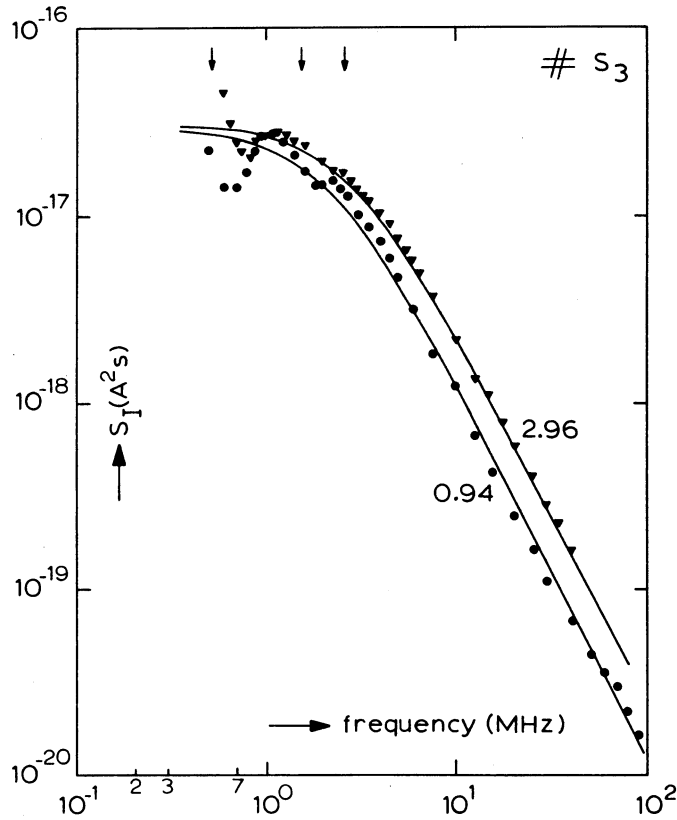
84

Figure 6. Spectral current-noise intensity of sample s_3 at two different applied voltages. The values of $(\overline{V} - V_c)/V_c$ are indicated. The solid lines represent hand-fitted Lorentzian spectra. The parameters used are listed in table 2 (Appendix). The vertical arrows correspond to maxima in the ac impedance.

(i.e. $(2\pi\tau_2)^{-1}$) compared to the values obtained in figures 4 and 5, cannot be related to the fact that the contact surfaces of sample s_3 have been polished, because similar small roll-off frequencies were observed for unpolished samples (cf. figure 7). Since the creation and annihilation of potential troughs are closely related to the spatial, angular and frequency distributions of the acoustic energy, and to the dispersion of the acoustic waves, the magnitude of the relaxation times will be mainly determined by the geometrical conditions for each sample. Manifest structure in the current-noise spectra resulting from polished end-surfaces, as reported by Gielen and Zijlstra [8, 9], was not observed in our case.
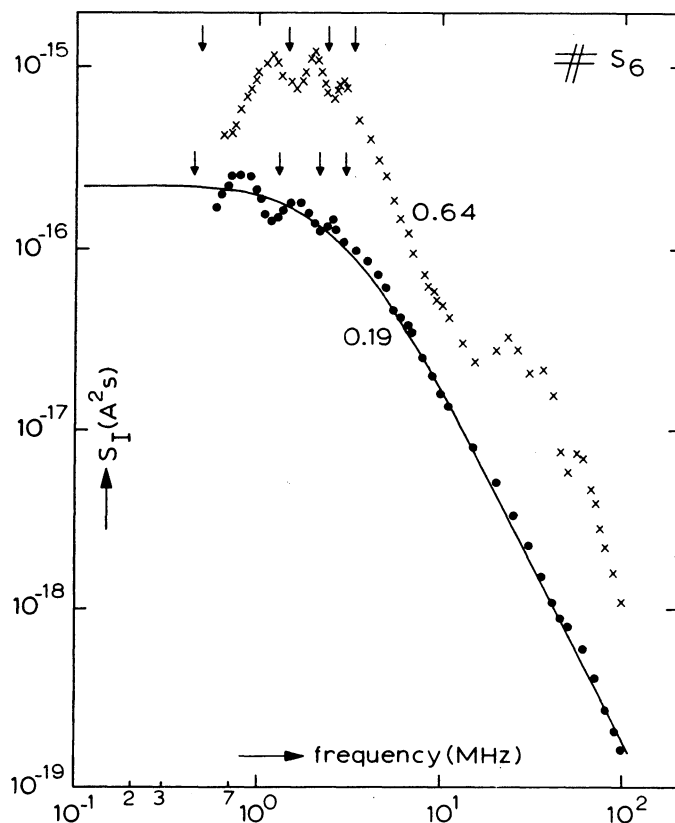
Figure 7. The spectral current-noise intensity of sample s_6 at two different applied voltages. The values for $(\overline{V} - V_c)/V_c$ are indicated. The arrows correspond to maxima in the ac impedance. The solid line represents a hand-fitted Lorentzian spectrum. Details are listed in table 2 (Appendix).

In some cases, however, the shapes of the noise spectra differed considerably from those of the noise spectra discussed previously. Figure 7 shows spectra of sample s_6 at two different applied voltages. At $(\overline{V} - V_c)/V_c = 0.19$ the spectrum apart from the transit-time resonances, can be described by a single Lorentzian spectrum (solid line). At $(\overline{V} - V_c)/V_c = 0.64$ the shape of the current-noise spectrum has changed considerably, showing additional maxima and minima at high frequencies, which cannot be related to potential-trough transit-times. Since no deviating behaviour of the corresponding ac impedance was found in this high-frequency range, a possible explanation may be that the assumptions for the spectral cross-intensities of the Langevin source-functions do not hold here [13]. Another explanation could be that the additional peaks

86

in the current-noise spectrum result from parametric amplification of sub-harmonic acoustic waves, as reported by Schulz et al. [10, 11] for GaAs. Indeed these contributions to the current noise, which are associated with subharmonic waves, have been found to become more important with increasing applied voltage. So far we cannot explain why these deviations occur in this particular sample. Similar deviations from the theory were observed for sample s_5.

The arrows in figure 7 correspond to the resonance frequencies in the ac impedance. With increasing voltage we observe a decrease in the potential-trough transit-time. This effect can be ascribed to electro-acoustic dispersion [14].

IV.4.2. *Photoconducting CdS*

Figure 8 shows the spectral current-noise intensity at 10 MHz plotted versus the reduced voltage $(\overline{V} - V_c)/V_c$ for the photoconducting sample p_1 at two different values of the conductivity. Note that $\sigma = 0.023 \ \Omega^{-1}m^{-1}$ corresponds to the dark-conductivity. Marked deviations from a quadratic relationship are observed. At $(\overline{V} - V_c)/V_c \approx 1$ even a local minimum in the current noise is observed at both conductivities. Figure 9 shows corresponding results for sample p_2. The value of $\sigma = 0.55 \ \Omega^{-1}m^{-1}$ corresponds to the dark-conductivity. The behaviour of the photoconducting samples in figures 8 and 9 is similar to that of the semiconducting samples in figure 3. It is concluded that in general the current noise at a fixed frequency is not proportional to $(\overline{V} - V_c)^2$, which is contrary to the predictions in [6] and [12]. The more complicated voltage
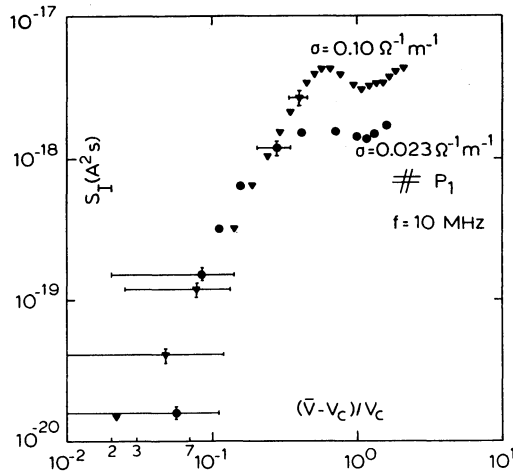

Figure 8. The spectral current-noise intensity at 10 MHz versus $(\overline{V} - V_c)/V_c$ for sample p_1 at two different conductivities (σ). The value of $\sigma = 0.023 \ \Omega^{-1}m^{-1}$ corresponds to the dark-conductivity.
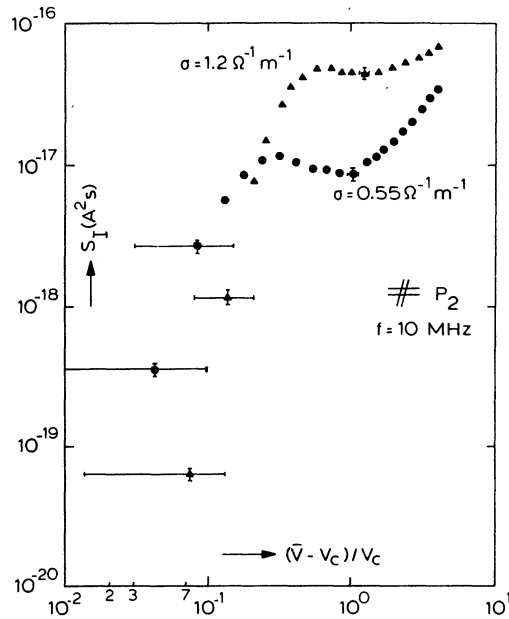
Figure 9. The spectral current-noise intensity at 10 MHz versus $(\overline{V} - V_c)/V_c$ for sample p_2 at two different conductivities (σ). The value of $\sigma = 0.55$ $\Omega^{-1}m^{-1}$ corresponds to the dark-conductivity.

dependence we found might be connected with the voltage dependence of the parameters τ_1, τ_2, N_1, N_2, v_{g3}, $\overline{v}_{d_3}$, $\overline{n}_{s_1}$ and $\overline{n}_{s_2}$, according to eq. (1).

Figure 10 shows a current-noise spectrum for sample p_1. The solid line was calculated with the fitting procedure discussed in section IV.4.1. Thus, the value of τ_1 that we used was obtained from the corresponding ac-impedance data. The dashed lines represent the separate contributions of the two Lorentzians in eq. (1), and the arrows correspond to the maxima in the ac impedance. We found that the numbers of electrons per trough N_1 and N_2 are of the same order of magnitude as those obtained for semiconductors. For details we refer to table 2 (Appendix).

Figure 11 shows current-noise spectra for sample p_2 at two different applied voltages. The solid lines represent hand-fitted single Lorentzian curves. The parameters used are listed in table 2 (Appendix). Again the arrows correspond to maxima in the ac impedance. It is concluded from figure 11 that in the frequency range considered the current noise is dominated by the kinetics of the backward-travelling troughs.
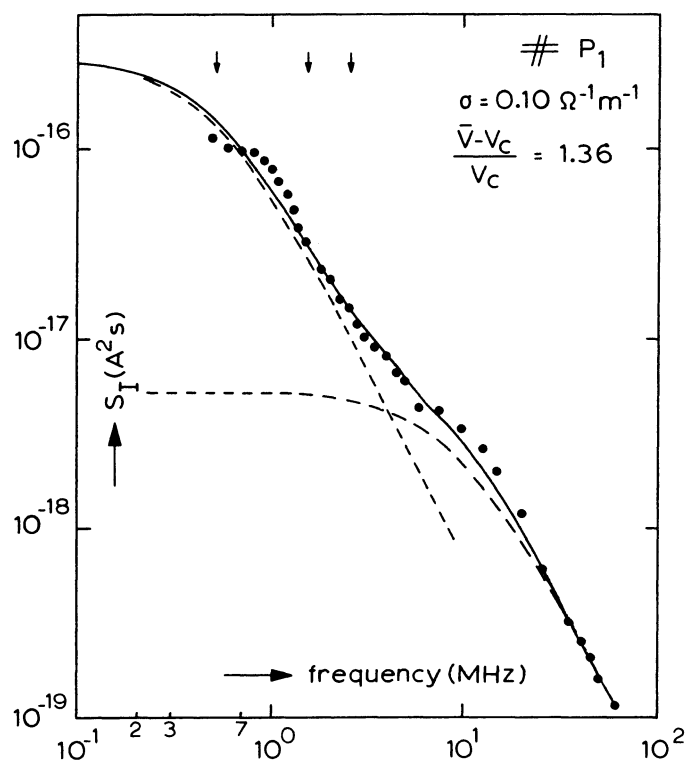
88

Figure 10. The spectral current-noise intensity for sample p_1 at $\sigma = 0.10 \ \Omega^{-1}m^{-1}$ for $(\overline{V} - V_c)/V_c = 1.36$. The solid line has been calculated with eq. (1). The parameters used are listed in table 2 (Appendix). The dashed lines represent the separate contributions of the Lorentzians in eq. (1). The vertical arrows correspond to maxima in the ac-impedance.
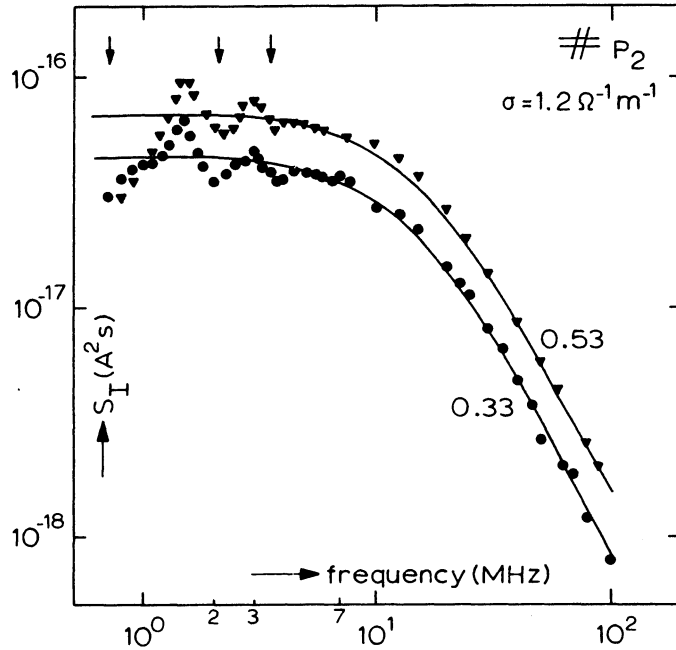
Figure 11. Current-noise spectra of sample p_2 at $\sigma = 1.2 \ \Omega^{-1}m^{-1}$ at $(\overline{V} - V_c)/V_c = 0.33$ and 0.53, respectively. The solid lines are hand-fitted single Lorentzian curves. Details are given in table 2 (Appendix). The arrows correspond to maxima in the ac-impedance.

Figure 12 shows two current-noise spectra for sample p_2 at $\sigma = 0.55 \ \Omega^{-1}m^{-1}$ (dark-conductivity). The transit-time effects are less pronounced and the roll-off frequencies are slightly lower than those in figure 11.

We conclude that electro-acoustic current noise of photoconducting CdS samples and semiconducting CdS samples is similar. Furthermore it seems that the particular shape of the current-noise spectrum of a certain sample is not predictable. So far we have not succeeded in finding how the parameters oc-curring in the expression for the current noise depend on the experimental conditions. We conclude, however, that in most cases the current noise apart from transit-time resonances can be described by eq. (1).

IV.4.3. *The electron mobility*

Several authors [16-18] have reported that the electron mobility in dif-ferent CdS crystals can differ considerably due to different impurity
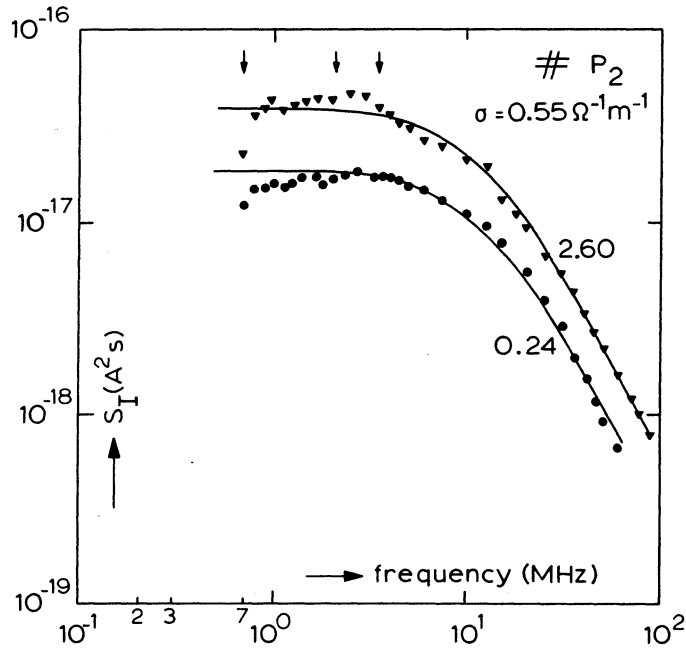
90

Figure 12. Current-noise spectra for sample p_2 at $\sigma = 0.55\ \Omega^{-1}m^{-1}$ (dark-con-
ductivity) at $(\bar{V} - V_c)/V_c = 0.24$ and 2.60, respectively. The solid lines are
hand-fitted single Lorentzians. The parameters used are listed in table 2
(Appendix). The arrows correspond to maxima in the ac impedance.

concentrations and crystal imperfections. The mobility values for CdS reported
in the literature lie between $1.25 \times 10^{-2}\ m^2V^{-1}s^{-1}$ [17] and $3.88 \times 10^{-2}\ m^2V^{-1}s^{-1}$
[19] at room temperature. Thus, unfortunately, we cannot rely on the literature
to obtain the mobility values for our particular CdS samples, necessary for
the calculations. From table 1 we find that all CdS samples discussed in this
paper have different (dark-) conductivities and therefore different impurity
concentrations and crystal imperfections. No detailed information about these
concentrations and imperfections, and about the possible associated donor-
levels and traps was available.

However, the mobility can be obtained from the onset voltage for the
electro-acoustic current fluctuations with the help of eq. (3), if the phase
velocity $v_s(0)$ of the on-axis waves is known. In our samples only the trans-
verse waves are amplified [14]. When the elastic constants given in [20, 21]
are used $v_s(0)$ for transverse waves is found to be $1.77 \times 10^3\ ms^{-1}$.
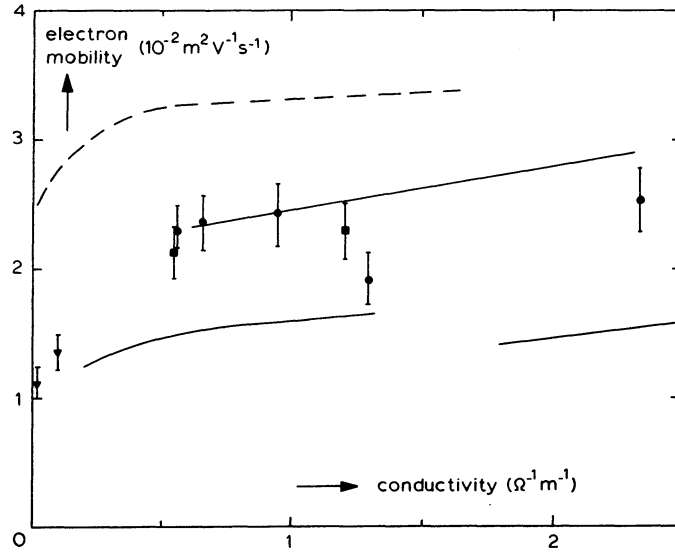
Figure 13. The electron mobility obtained from the onset voltage of electro-acoustic current fluctuations for the samples discussed in this paper plotted versus the conductivity. Data for the semiconducting samples are indicated by black dots. Data for the photoconducting samples p_1 and p_2 are indicated by triangles and squares respectively. The conductivities $\sigma = 0.02~\Omega^{-1}m^{-1}$ and $\sigma = 0.55~\Omega^{-1}m^{-1}$ correspond to the dark-conductivities of samples p_1 and p_2, respectively. The solid lines represent Hall mobilities of several photoconducting CdS crystals reported in [16]. The dashed line represents mobility data obtained from ultrasonic amplification measurements [18].

In figure 13 we have plotted the electron mobilities at room temperature obtained with eq. (3) for the samples discussed in this paper versus the conductivity. The results for the semiconducting samples have been indicated by black dots; the results for the photoconducting samples p_1 and p_2 have been indicated by triangles and squares, respectively. For comparison we have shown the results of Bube et al. [16] obtained from Hall measurements and conductivity measurements on several photoconducting CdS crystals (solid lines). The dashed line represents mobility values obtained by Krischer [18] from ultrasonic amplification measurements.

From figure 13 we conclude that the electron mobilities obtained from the onset voltage of electro-acoustic current fluctuations are well within the range of mobility values reported in the literature. Furthermore we observe that the mobility data, apart from those for sample p_1, are almost independent of the conductivity, in spite of different concentrations of possible carrier

scattering-centres. This result indicates that in our samples scattering of electrons by phonons is much more important than impurity scattering. From the temperature dependence of the Hall mobility in CdS Pödör et al. [17, 22] concluded that polar optical-phonon scattering is indeed the dominant scattering mechanism at room temperature for conductivities smaller than 50 $\Omega^{-1}m^{-1}$.

The relatively low values for the mobility obtained for sample p_1 may be caused by the trapping of electro-acoustically produced space charge in bound-electron states in the forbidden gap. According to White [2] these carrier-trapping effects can be taken into account by multiplying the carrier mobility by a factor f_0, where $0 \leqq f_0 \leqq 1$. Only a fraction f_0 of the electro-acoustically produced space charge is free and contributes to the conductivity. A fraction $(1 - f_0)$ of the space charge is produced by electrons trapped in states in the forbidden gap and is immobile. As the conductivity of sample p_1 is relatively low compared to that of the other samples, a certain number of electron trapping-centres will be empty. Thence, these centres will be able to trap part of the electro-acoustically produced space charge. The mobility data for sample p_1 may thus be interpreted as an apparent mobility given by $f_0 \cdot \mu_{33}$, where μ_{33} is the real mobility resulting from polar optical-phonon scattering.

References

[1] A.R. Hutson, J.H. McFee and D.L. White, Phys. Rev. Lett. 7 (1961) 237.
[2] D.L. White, J. Appl. Phys. 33 (1962) 2547.
[3] K. Blötekjaer and C.F. Quate, Proc. IEEE 52 (1964) 360.
[4] W. Wettling and M. Bruun, Phys. Stat. Sol. 34 (1969) 221.
[5] B.W. Hakki and R.W. Dixon, Appl. Phys. Lett. 14 (1969) 185.
[6] A.R. Moore, J. Appl. Phys. 38 (1967) 2327.
[7] V.I. Baibakov, Sov. Phys.-Semic. 3 (1969) 274.
[8] P.A. Gielen and R.J.J. Zijlstra, Physica 95B (1978) 347.
[9] P.A. Gielen and R.J.J. Zijlstra, Physica 103B (1981) 165.
[10] M. Schulz and B.K. Ridley, Phys. Lett. 29A (1969) 17.
[11] M. Schulz, Sol. St. Comm. 8 (1970) 355.
[12] R.J.J. Zijlstra and P.A. Gielen, Physica 95B (1978) 190.
[13] W. Westera, Chapter II of this thesis.
[14] W. Westera, Chapter III of this thesis.
[15] J.E. Hill and K.M. van Vliet, Physica 24 (1958) 709.
[16] R.H. Bube and H.E. MacDonald, Phys. Rev. 121 (1961) 473.
[17] B. Pödör, J. Balázs and M. Hársy, Phys. Stat. Sol. (a) 8 (1971) 613.
[18] C. Krischer, Phys. Rev. B 8 (1973) 3908.
[19] J.D. Zook and R.N. Dexter, Phys. Rev. 129 (1963) 1980.
[20] D. Berlincourt, H. Jaffe and L.R. Shiozawa, Phys. Rev. 129 (1963) 1009.
[21] I.B. Kobiakov, Sol. St. Comm. 35 (1980) 305.
[22] B. Pödör, Act. Phys. Acad. Sc. Hung. 36 (1974) 431.

A P P E N D I X

Table 2. Parameter values used in fitting eq. (1) to the experimental current-noise data.

Sample	Fig.	Conductivity $(\Omega^{-1}m^{-1})$	$\frac{\overline{V}-V_c}{V_c}$	N_1	N_2	$\overline{n}_{s_1}$ (m^{-3})	$\overline{n}_{s_2}$ (m^{-3})	τ_1 (s)	τ_2 (s)	v_{g_3} (ms^{-1})
$s_2^{\dagger}$	4	5.6×10^{-1}	0.36	1.3×10^5	1.6×10^4	5.1×10^{19}	1.1×10^{19}	3.1×10^{-7}	1.6×10^{-8}	1.66×10^3
$s_2^{\dagger\dagger}$	4	5.6×10^{-1}	0.36	6.5×10^4	1.8×10^4	5.1×10^{19}	1.1×10^{19}	3.1×10^{-7}	1.6×10^{-8}	1.66×10^3
s_4	5	6.6×10^{-1}	0.35	7×10^4	3×10^4	5.3×10^{19}	1.3×10^{19}	3.6×10^{-7}	1.4×10^{-8}	1.62×10^3
s_3	6	9.5×10^{-1}	0.94		2×10^4		1.7×10^{19}		8.0×10^{-8}	1.68×10^3
s_3	6	9.5×10^{-1}	2.96		5×10^3		2.8×10^{19}		5.5×10^{-8}	1.68×10^3
s_6	7	2.3	0.19		7×10^5		2.8×10^{18}		5.9×10^{-8}	1.53×10^3
p_1	10	1.0×10^{-1}	1.36	1.6×10^4	1.4×10^4	2.6×10^{19}	1.8×10^{18}	3.3×10^{-7}	1.9×10^{-8}	1.70×10^3
p_2	11	1.2	0.33		1.6×10^5		1.2×10^{19}		1.2×10^{-8}	1.60×10^3
p_2	11	1.2	0.53		2.2×10^5		1.2×10^{19}		1.1×10^{-8}	1.60×10^3
p_2^*	12	5.5×10^{-1}	0.24		2.3×10^5		3.4×10^{18}		1.3×10^{-8}	1.60×10^3
p_2^*	12	5.5×10^{-1}	2.60		7.7×10^4		4.7×10^{18}		1.4×10^{-8}	1.60×10^3

†) solid line.

††) dotted line.

*) dark-conductivity.

C H A P T E R V

BRILLOUIN-SCATTERING STUDY OF THE STATIONARY,

ELECTRO-ACOUSTICALLY AMPLIFIED ACOUSTIC FLUX IN CdS

Abstract — We investigated the acoustic-energy density of electro-acoustically
amplified transverse off-axis waves in single crystals of semiconducting CdS
in the frequency range 0.25-1.8 GHz with the help of a Brillouin-scattering
technique. The electric field was applied parallel to the c-axis in pulses of
40 μs duration with a rise-time of about 5 μs. The repetition rate was 4 Hz.
The excited acoustic flux appeared to be stationary about 5 μs after the onset
of the bias pulse. All measurements were carried out at room temperature. The
conductivities of the various samples ranged from 0.66 $\Omega^{-1}m^{-1}$ to 2.3 $\Omega^{-1}m^{-1}$.
The spectral acoustic-energy distribution appeared to peak at a frequency con-
siderably lower than that predicted by White's linear small-signal gain theory.
With increasing voltage this peak was found to shift towards lower frequencies,
which could be as much as 4 times lower than predicted by White's theory. This
down-shift with increasing voltage was discussed in terms of an adapted linear
theory: we took into account acoustic-scattering losses at the crystal side-
faces and a decrease of the conductivity. The latter effect is thought to be
caused by the trapping of free charge carriers in deep potential troughs which
are associated with the amplified acoustic waves. We found that the down-shift
of the peak-frequency with increasing voltage can be described quite well by
this adapted linear theory.
    The off-axis angle of maximum acoustic-energy density as obtained from
Brillouin-scattering experiments appeared to be in good agreement with the
off-axis angle as calculated from resonances in the ac impedance.

V.1. Introduction

   Amplification of travelling acoustic waves as a result of their interac-

tion with supersonically drifting charge carriers in piezoelectric semi-

conductors has been a subject of continuous interest for many years. Many

authors [1-16] have used the technique of Brillouin-scattering, i.e. inelastic

scattering of light by acoustic waves, for the study of the electro-acoustically

excited acoustic flux, as this technique provides a unique tool for the in-

vestigation of plane-wave components in a complex acoustic-wave distribution.

The electro-acoustically excited flux in piezoelectric semiconductors has

usually been found to be concentrated in macroscopic travelling domains starting at the carrier-injecting contact and propagating with the sound velocity in the direction of carrier drift. The occurrence of such travelling acoustic domains involves macroscopic electrical current oscillations with a period equal to the domain transit-time, and a highly non-uniform distribution of the electric field. So far most Brillouin-scattering studies reported in the literature have focussed on the growth of the acoustic flux in these domains. The frequencies of maximum acoustic amplification have been found to be [2, 5-7, 14] an order of magnitude lower than predicted by the linear theory of electro-acoustic amplification, given by White [17] in 1962. Several authors [1, 6, 10-12] have attributed the failure of this linear theory to the occurrence of essential nonlinearities in the interaction between strain waves and space-charge waves. The observed down-shift of the frequency of maximum amplification is thus thought to be caused by parametric down-conversion of the acoustic waves. Yamada et al. [10-12] have observed both down-conversion and up-conversion in the amplified acoustic flux in CdS, which indicates that nonlinear frequency-mixing may indeed play an important role. Others [5, 14], however, have argued that the trapping of free charge carriers in deep potential troughs that are associated with the amplified acoustic waves is responsible for the observed down-shift with increasing acoustic flux intensities, i.e. with increasing electric field strengths. They have proposed that the electro-acoustic amplification can still be described by the linear theory, if the reduction in the free charge-carrier concentration is taken into account. Since according to White's theory [17] the frequency of maximum amplification was predicted to be proportional to the square root of the free carrier concentration, the trapping of free carriers should indeed result in a down-shift.

Brillouin-scattering data on the amplified acoustic flux without the occurrence of travelling acoustic domains have been reported by Zemon et al. [2] in CdS. The amplified acoustic flux again appeared to be located around frequencies considerably lower than predicted by the linear theory. However, Zemon et al. [2] could not make a quantitative comparison with the linear theory applicable to samples with uniform conductivities only, because this condition was not met in their samples.

The formation of travelling acoustic domains is probably due to shock excitation, caused by the application of short rise-time electrical bias-pulses (rise times < 1 μs) [2, 8, 18]. Domain formation can be suppressed by using bias pulses with relatively long rise-times (> 1 μs); some authors [19, 20]

96

have argued that the use of relatively short samples ($\lesssim$ 3 mm) may also be helpful in avoiding domain formation. In the absence of these travelling acoustic domains the acoustic flux will be built up by the amplification of acoustic waves originating from the thermal background [2, 8, 19, 20].

We wanted to prevent the occurrence of these travelling acoustic domains in our study, as it involves the injection of a large, poorly defined acoustic disturbance. Many et al. [8] have observed that the down-shift of the peak-frequency of the acoustic flux within a domain is much more pronounced than in cases where no domains occur. They have proposed that the parametric down-conversion of the acoustic waves is strongly stimulated by the shock-excited flux, the latter acting as the stimulating signal [3]. Therefore the effects of nonlinear frequency-mixing may be of importance mainly in acoustic domains. If the acoustic flux is continuously distributed over the sample, i.e. in the absence of domains, the down-shift may possibly be described by the linear theory, in the sense indicated above.

The aim of this paper is to present an extended set of experimental data on the continuously distributed amplified acoustic flux in CdS. We shall discuss experimental data in terms of the linear theory, taking the reduction of the free carrier concentration into account. In section V.2 we shall review the results of this theory and summarize the Brillouin-scattering formulas from the literature. In section V.3 the scattering configuration and experimental arrangement will be described. Experimental Brillouin-scattering data will be presented in section V.4. In section V.5 conclusions will be summarized.

V.2. Theory

In section V.2.1 we summarize some theoretical results concerning the description of electro-acoustic effects. In section V.2.2 a brief review of Brillouin-scattering is given.

V.2.1. *Electro-acoustic attenuation*

Although the electro-acoustic effect refers to the *amplification* of acoustic waves, White [17] would have preferred the term *attenuation*, because the process of amplification (negative attenuation) can be regarded as anomalous behaviour. In some cases, however, the term attenuation is quite confusing. In this paper we shall use both the term amplification and the term (negative) attenuation, giving some preference to the latter.

In [21] we presented a theoretical model for the description of electro-acoustic current saturation, current noise and ac-impedance effects in an n-type piezoelectric semiconductor where the electric field is parallel to the c-axis. These electro-acoustic effects arise essentially from nonlinearities in the interaction between free charge carriers and amplified acoustic waves. To avoid the need for nonlinear equations we have assumed that the observed electro-acoustic effects can be described by the random trapping and de-trapping of free charge carriers in potential troughs. These potential troughs are associated with the amplified acoustic waves. In fact, the *cause* of potential troughs (i.e. the amplified acoustic flux) has been disregarded in the theoretical description; only the *effect* of the flux (i.e. potential troughs) has been taken into account. We could do this only if we made certain assumptions about the properties of these troughs. It should be noted that the current noise and ac-impedance effects usually occur at frequencies far below the frequencies of the amplified acoustic waves [20, 22, 23]. Although this model is a much simplified representation of the complex electro-acoustic effects, its theoretical predictions appeared to be consistent with the experimental current-noise and ac-impedance data [22, 23]. This trough model has also been used to derive expressions for the wave attenuation coefficients [21]. Experimental data on the frequency distribution of the acoustic energy, which are presented here, are connected in some way with the wave attenuation coefficients.

The expressions for the wave attenuation coefficients obtained with the potential-trough model contain various parameters; these include parameters related to the electric field dependence of the potential-trough creation and annihilation rates, potential-trough lifetimes, parameters related to electro-acoustic dispersion, etc. [21]. As we pointed out before [22, 23], these parameters, which are obtained from current-noise and ac-impedance data, cannot be determined very accurately. Due to these inaccuracies the frequency and voltage dependence of the associated wave attenuation coefficients cannot be determined unambiguously. Besides, it is doubtful whether the potential-trough model still holds at frequencies close to the frequencies of the amplified acoustic waves. For these reasons we prefer to discuss our Brillouin-scattering results not in terms of the previously published potential-trough model, but rather in terms of White's linear small-signal gain theory, taking a reduction of the free carrier concentration into account.

According to the potential-trough model [21] electrons become trapped in potential troughs and thereby can no longer participate in the sound-amplification process. The remaining average free electron conductivity, denoted by σ_1, can be calculated at each applied electric field strength from the measured plateau-value Z_{pl} of the ac impedance [23] by using

$$\sigma_1 = \frac{L}{AZ_{pl}} \quad , \tag{1}$$

where L is the contact spacing, and A is the cross-sectional area.

Instead of using the Ohmic conductivity, as did White [17] to calculate the electro-acoustic attenuation coefficients, we consider it more appropriate to use the reduced conductivity σ_1. It should be noted that generally Z_{pl} is found to differ from the differential resistance as obtained from the current-voltage characteristic [23].

Once the reduction of the free carrier concentration resulting from nonlinear effects has been taken into account, it is assumed that the amplification of acoustic waves under current-saturation conditions can be described by the linear theory.

According to the modified linear theory the electro-acoustic attenuation coefficient α_e for an acoustic wave of frequency ω having an off-axis angle δ (the angle between the acoustic wave-vector and the c-axis) is given by [17, 24, 25]:

$$\alpha_e(\omega,\delta) = \frac{K_e^2(\delta)}{2v_{so}(\delta)} \; \frac{\gamma\omega_c'}{\gamma^2 + (\frac{\omega_c'}{\omega} + \frac{\omega}{\omega_D})^2} \quad , \tag{2}$$

where K_e is the electro-mechanical coupling factor,

v_{so} is the unstiffened acoustic phase velocity,

$\omega_c' = \frac{\sigma_1}{\epsilon}$ is the modified angular dielectric-relaxation frequency,

ϵ is the permittivity of the material,

$\gamma = 1 - \frac{\overline{v}_d \cos\delta}{v_s}$ is the drift parameter,

$\overline{v}_d$ is the electron drift-velocity,

v_s is the stiffened acoustic phase velocity (slightly different from v_{so}),

$\omega_D = \dfrac{v_s^2}{D_n}$ is the angular electron-diffusion frequency, and

D_n is the electron-diffusion constant.

Amplification occurs if α_e is negative. This happens when the drift parameter γ is negative, i.e. when the component of the drift velocity $\vec{v}_d$ along the acoustic phase velocity $\vec{v}_s$ exceeds v_s. From eq. (2) we find that maximum amplification occurs at an angular frequency given by

$$\omega = \omega_m \equiv (\omega_D \cdot \omega_c')^{\frac{1}{2}} \quad . \tag{3}$$

The frequency of maximum sound amplification is thus found to be directly proportional to the square root of the free electron conductivity σ_1. Since the ac-impedance plateau-value Z_{p1} is usually found to increase monotonously with increasing applied voltage [23], this modified linear theory predicts a down-shift of ω_m with increasing voltage (cf. eq. (1)).

It should be noted that the expression for the attenuation coefficients obtained from the potential-trough model [21] reduce to eq. (2) in the extreme limit $1/\tau_1 = 1/\tau_2 = 0$, where τ_1 and τ_2 are mean lifetimes of fluctuations in the numbers of troughs. Physically this means that no trapping and de-trapping occur. However, it should be noted that expression (2) cannot be derived from the potential-trough model by putting only $\omega\tau_1 \gg 1$ and $\omega\tau_2 \gg 1$.

In practice the net amplification of acoustic waves will be reduced somewhat due to the occurrence of lattice attenuation. Lattice attenuation has been studied extensively in CdS [9, 11, 26-31]. Several authors [9, 30, 31] have found experimentally that electro-acoustically amplified acoustic waves originating from the thermal background undergo lattice attenuation which is proportional to ω^2. Thus, the lattice attenuation coefficient α_L can be written as

$$\alpha_L = A_0 \omega^2 \quad , \tag{4}$$

where A_0 is a material constant. These results are in accordance with the theoretical predictions of Akhiezer [32].

100

In addition a second loss process may be of importance: in most practical cases off-axis waves will suffer from acoustic losses due to scattering at the crystal side-faces. This effect can formally be taken into account by introducing an attenuation coefficient α_s. Yamada et al. [11] showed that α_s can be written as

$$\alpha_s = \frac{2\pi \ s^2 \omega^2}{\sqrt{A} \ v_s^2(\delta)} \ \sin^2\delta \qquad , \tag{5}$$

where s is a measure for the surface flatness. Experimental observations have been found to be in agreement with eq. (5) [11]. Since this attenuation coefficient is proportional to $\sin^2\delta/v_s^2(\delta)$, and $v_s(\delta)$ is only weakly dependent on δ, boundary-scattering losses become more important with increasing off-axis angle δ.

The net attenuation coefficient α_N is given by

$$\alpha_N = \alpha_e + \alpha_L + \alpha_s \qquad , \tag{6}$$

and shows a frequency and angular dependence which is different from that of α_e (cf. eq. (2)).

As we pointed out before [21, 23], resonances appearing in the ac impedance can be used to estimate the off-axis angle of maximum sound amplification. Resonances appear in the ac impedance at frequencies given by

$$f = f_l = \frac{(2l + 1)}{2} \cdot \frac{v_{g3}}{L} \qquad ; \quad l = 0, 1, 2, 3, \ldots \ldots \qquad , \tag{7}$$

where v_{g3} is the component of the acoustic group velocity along the c-axis. As a result of the elastic anisotropy in CdS the direction and magnitude of the group velocity may differ markedly from the direction and magnitude of the phase velocity. However, from the value of v_{g3}, obtained with eq. (7), we can calculate the associated off-axis angle of maximum sound amplification unambiguously, if the values of the elastic constants are known. Thence, the off-axis angle of maximum amplification can be obtained in two independent ways: from Brillouin-scattering as well as from ac-impedance measurements.

V.2.2. *Brillouin-scattering*

If the inter-atomic distance in a medium is small compared to the optical wavelength, the theory of light scattering can be given in a classical continuum description. It can be shown that the scattering of light in dielectric media is caused by local fluctuations in the dielectric properties, or rather by local fluctuations in the refractive properties [33, 34]. In a thermodynamical treatment these fluctuations are thought to be caused by non-propagating temperature fluctuations [33-35] and by propagating strain fluctuations [36]. The non-propagating fluctuations produce quasi-elastically scattered radiation with a central frequency equal to that of the incident radiation. The frequency width of this quasi-elastic scattering is determined by the mean lifetime of the scattering fluctuations. The propagating fluctuations give rise to a Brillouin doublet, located approximately symmetrically on either side of the unshifted line and separated from it by a frequency interval equal to the frequency of the propagating strain waves. The presence of this doublet was predicted by Brillouin [37] in 1922, and first observed by Gross [38] in 1930. The linewidth of the Brillouin doublet is determined by the mean lifetime of the scattering strain waves. The intensity of the Brillouin-scattered light is directly related to the energy density of the scattering strain wave.

The use of Brillouin-scattering as an optical probe for studying the electro-acoustically excited acoustic flux requires detailed knowledge of the kinematics of the scattering process, and the scattering efficiency.

In optically isotropic media the kinematics of the scattering process is conditioned by the normal Bragg condition. The scattering geometry in optically anisotropic media such as CdS is determined by the generalized Bragg relations, first derived by Dixon [39]. These relations can be derived from the conservation laws for energy and pseudo-momentum. Let $\vec{k}_{in}$ be the wave vector of the monochromatic, plane polarized incident light inside the medium (angular frequency ω_{in}), $\vec{k}_{sc}$ the wave vector of the scattered light (angular frequency ω_{sc}) and $\vec{k}$ that of the acoustic wave (angular frequency ω). Then the conservation laws for the anti-Stokes process read (cf. figure 1):

$$\vec{k}_{in} + \vec{k} = \vec{k}_{sc} \quad , \tag{8}$$

and

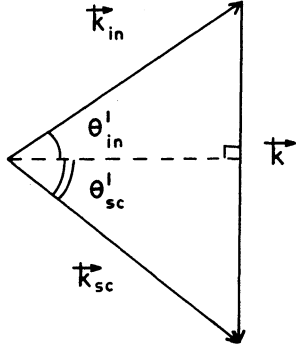$$\omega_{in} + \omega = \omega_{sc} \quad . \tag{9}$$

102

Figure 1. Schematic diagram showing the
wave-vector construction for an anti-
Stokes process. The figure also serves
to define the angles θ_{in}' and θ_{sc}'.

Note that eqs. (8) and (9) only hold for a single scattering process. As the scattering is only weak in our experiments, multiple scattering can be neglected. In this paper we restrict ourselves to the formulas for the anti-Stokes process. Similar relations apply to the Stokes process [36, 39, 49].

From eqs. (8) and (9) we obtain the following relations for the angles shown in figure 1 (if $\omega \ll \omega_{in}$):

$$\sin \theta_{in}' = \frac{\lambda_0}{2n_{in}v_s} \left[f + \frac{v_s^2}{f\lambda_0^2} (n_{in}^2 - n_{sc}^2) \right] \quad , \tag{10}$$

and

$$\sin \theta_{sc}' = \frac{\lambda_0}{2n_{sc}v_s} \left[f - \frac{v_s^2}{f\lambda_0^2} (n_{in}^2 - n_{sc}^2) \right] \quad . \tag{11}$$

Here v_s is the phase velocity and $f = \omega/2\pi$ the frequency of the acoustic wave, λ_0 the wavelength of the incident light in free space, and n_{in} and n_{sc} are the polarization-dependent refractive indices for the incident and scattered light, respectively. Note that θ_{in}' and θ_{sc}' are angles inside the medium.

Expressions (10) and (11) are known as the generalized Bragg relations. In the isotropic case ($n_{in} = n_{sc}$) these relations reduce to the well-known normal Bragg relation (corresponding to first-order diffraction):

$$\sin \theta_{in}' = \sin \theta_{sc}' = \frac{\lambda_0 f}{2n_{in}v_s} \quad . \tag{12}$$

103

From eqs. (10) and (11) we find an upper limit for the acoustic frequency, above which no Brillouin-scattering occurs. This upper limit is given by

$$f_{max} = \frac{v_s}{\lambda_0} (n_{in} + n_{sc}) \quad , \tag{13}$$

which holds for the case of collinear interaction with $\theta_{in}' = \theta_{sc}' = \pi/2$. For example, let $n_{in} = n_\perp$ and $n_{sc} = n_{//}$, where $n_\perp$ and $n_{//}$ are the refractive indices for light polarized perpendicular to and parallel to the c-axis respectively. Then, using $\lambda_0 = 632.8$ nm, $v_s \simeq 2 \times 10^3$ ms^{-1}, $n_\perp = 2.453$ and $n_{//} = 2.471$ [4], $f_{max} \simeq 15$ GHz for transverse waves in CdS. Furthermore, in the anisotropic case a lower limit for the acoustic frequency, below which no interaction occurs, is given by

$$f_{min} = \frac{v_s}{\lambda_0} \cdot |n_{in} - n_{sc}| \quad . \tag{14}$$

This case corresponds to the collinear interaction with $\theta_{in}' = -\theta_{sc}'$ and $|\theta_{in}'| = |\theta_{sc}'| = \pi/2$. In CdS $f_{min} \approx 57$ MHz for transverse waves. Note that in the isotropic case there is no positive low-frequency limit.

Once the angles θ_{in}' and θ_{sc}' have been chosen, the frequency f of the acoustic waves that are to be investigated by Brillouin-scattering is uniquely determined by the generalized Bragg relations. Thus the adjustment of θ_{in}' and θ_{sc}' provides a simple tool for the selection of the acoustic wave-vector to be studied. To be useful in the experiment the internal angles θ_{in}' and θ_{sc}' should be translated into external angles. This translation for our particular geometrical conditions will be carried out in section V.3.

Recently Mishra and Bray [41] have established that the power of Brillouin-scattered light provides a linear measure for the acoustic-energy density, even in the case of the very intense acoustic flux which is generally attained in electro-acoustically active crystals. Because the acoustic-energy density of thermal waves is known, the measurement of the power of the light scattered by these thermal waves would provide an absolute calibration of the measured acoustic-energy density. However, the sensitivity of the experimental set-up (cf. section V.3) did not allow the measurement of the light power scattered by thermal acoustic waves. Yet, the power scattered by electro-acoustically amplified waves could still be compared with the power scattered by thermal

104

waves, because the latter is known theoretically. This enabled us to give absolute values for the measured acoustic-energy densities.

The efficiency of Brillouin-scattering by thermal strain waves has been calculated by Benedek and Fritsch [36] for the case of cubic crystals. Hamaguchi [40] extended the calculation to the case of crystals with hexagonal symmetry. In these calculations it was assumed that the dielectric fluctuations are linearly related to fluctuations in the strain. The coefficients in this linear relationship are known as the photoelastic, elasto-optical or Pöckels-tensor elements p_{ijkl} (the subscripts i, j, k and 1 run from 1 to 3).

Let the power of the incident radiation be P_0; the power dP_{th} of the radiation scattered by thermal acoustic waves while it travels over the path-length 1, into an internal solid angle $d\Omega'$, is then given by:

$$dP_{th} = P_0 \cdot \sigma_{th} \cdot 1 d\Omega' \cdot \beta \qquad , \qquad (15)$$

where σ_{th} is the scattering efficiency per unit length per (internal) unit solid angle; β is a factor describing the influence of the attenuation of the incident and scattered radiation by absorption and scattering inside the medium, and by reflection at the crystal boundaries. This factor will be discussed in section V.3.4. In the range of acoustic frequencies much smaller than $k_B \cdot T/h$, where k_B is Boltzmann's constant, T is temperature and h is Planck's constant, the scattering efficiency σ_{th} for a Stokes or an anti-Stokes process is given by [40]:

$$\sigma_{th} = \frac{\pi^2 k_B T}{2\lambda_0^4 \rho v_s^2} |\vec{\xi}|^2 \qquad . \qquad (16)$$

Here ρ is the mass density of the medium and $\vec{\xi}$ is a vector which determines explicitly the polarization of the scattered light. When $\vec{\pi}$ is a unit vector indicating the polarization of the sound wave, $\vec{p}_{in}$ a unit vector indicating the polarization of the incident radiation, $\vec{\kappa} = \vec{k}/|\vec{k}|$ is a unit vector along the acoustic wave-vector, and $\vec{\kappa}_{sc} = \vec{k}_{sc}/|\vec{k}_{sc}|$ is a unit vector along the wave vector of the scattered light, the vector $\vec{\xi}$ is given by

$$\vec{\xi} = \vec{\kappa}_{sc} \times (\vec{\kappa}_{sc} \times \vec{\pi}) \qquad , \qquad (17)$$

105

where

$$\eta_i = \frac{\varepsilon_{ii}}{\varepsilon_0^2} \sum_{j,k,l=1}^{3} \varepsilon_{jj} P_{ijkl} P_{in_j} \kappa_{sc_k} \pi_l \qquad (i = 1, 2, 3) \qquad , \qquad (18)$$

where ε_0 is the vacuum permittivity. Note that generally $\vec{\xi}$ is not a unit vector.

Now, by measuring the power dP of the light scattered by the geometrically selected acoustic waves, we can calculate the spectral acoustic-energy density w per unit solid angle of these waves with the help of the equation

$$w = \frac{dP}{dP_{th}} w_{th} \qquad , \qquad (19)$$

where w_{th} is the acoustic energy per unit frequency per unit volume per unit solid angle of thermal waves; this is given by

$$w_{th} = \frac{f^2 k_B T}{v_s^{\ 3}} \qquad . \qquad (20)$$

By substituting eqs. (15), (16) and (20) into eq. (19) we find:

$$w = \left(\frac{dP}{P_0}\right) \cdot \frac{2\rho \lambda_0^{\ 4} f^2}{\pi^2 \beta |\vec{\xi}|^2 l d\Omega'} \qquad . \qquad (21)$$

V.3. Experimental Arrangements

In section V.3.1 we shall specify the characteristics of the samples used in the experiments. In section V.3.2 the experimental set-up is described. In section V.3.3 we discuss the scattering configuration. In section V.3.4 some correction formulas are given. In section V.3.5 we present some estimates of the acoustic wave-vector resolution.

V.3.1. *The samples*

For our experiments we used semiconducting single crystals of hexagonal n-type CdS obtained from Eagle Picher Industries, Inc. . To make Brillouin-

106

scattering experiments possible two opposite side-faces were mechanically
polished to a flatness of about ¼ μm. In some cases the two other side-faces or
the two contact faces were polished as well. Unpolished surfaces, being several
orders of magnitude less flat than polished ones, can be expected to cause con-
siderable acoustic scattering losses, since the wavelengths of the amplified
acoustic waves, having frequencies around 1 GHz, are about 2 μm [24].

The samples were supplied with two In-evaporated Ohmic contacts in such a
way that the electric field was orientated along the c-axis (the longitudinal
configuration). The In-contacts covered the end-surfaces completely. For details
we refer to [23].

Table 1. Characteristics of the CdS samples.

Sample	L (mm)	A (mm^2)	Dark-conductivity at room temp. ($\Omega^{-1}m^{-1}$)	Polished faces (mm^2)
s_3	1.63	1.78×0.48	0.95	1.78×1.63 — faces 1.78×0.48 — faces
s_4	1.76	1.24×0.43	0.66	1.24×1.76 — faces
s_5	2.79	1.43×0.37	2.3	all faces
s_7	1.96	1.99×0.58	1.4	1.99×1.96 — faces 1.96×0.58 — faces

In table 1 the dimensions, dark-conductivity at room temperature and sur-
face characteristics of the samples have been listed. Data on current satu-
ration, ac impedance and current noise for samples s_3, s_4 and s_5 have been
presented in [22, 23].

V.3.2. *Experimental set-up*

In the Brillouin-scattering experiments we selected acoustic wave-vectors
directed parallel to the polished crystal side-faces (cf. figure 2). Then, the
internal angles θ_{in}' and θ_{sc}' are related to the external angles θ_{in} and θ_{sc}
by Snell's law as follows:

$$\sin \theta_{in} = n_{in} \sin \theta_{in}' \qquad , \qquad (22)$$

and

$$\sin \theta_{sc} = n_{sc} \sin \theta_{sc}' \quad . \tag{23}$$

Note that for this geometry the operational frequency-interval suitable for Brillouin-scattering experiments, which is related to the limiting frequencies f_{min} and f_{max} (cf. eqs. (13) and (14)), is reduced due to the occurrence of total internal reflections. From figure 2 we find that the path-length 1, as occurring in eq. (15), is equal to $b/\cos \theta_{in}'$, where b is the sample thickness.
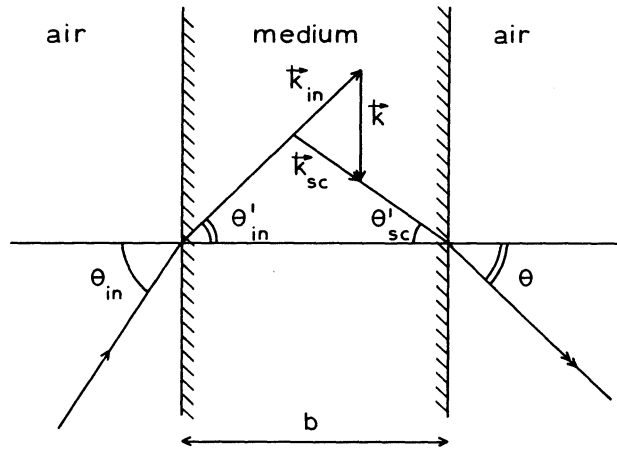

Figure 2. Refraction of the incident and scattered light at the medium/air interfaces. The selected acoustic wave-vector was always parallel to the side-faces.

To avoid excessive Joule heating of the samples the voltage was applied in pulses of 40 µs with a repetition rate of 4 Hz. The duration of these pulses was sufficient for the samples to reach a stationary state. To suppress travelling acoustic-domain formation we used rise-times of about 5 µs. Under these conditions only a continuous type of acoustic flux was amplified.

The height of the voltage pulses was measured with a sample-and-hold circuit.

The experimental set-up for the Brillouin-scattering experiments was similar to that in the original paper of Zucker et al. [1] (cf. figure 3). A helium-neon (He-Ne) laser (output $\lesssim$ 1 mW; λ_0 = 632.8 nm) was used as a light source. The laser beam was polarized by a Glan-Thomson prism and focussed to a diameter of about 0.1 mm on the sample. The sample was placed on a translatable and rotatable sample-mount. Light scattered into an external solid angle $d\Omega$,

108

polarizer   +lens diaphragm   sample

laser

θ_{in}

θ_{sc}

diaphragm
+lens

analyzer

photomultiplier

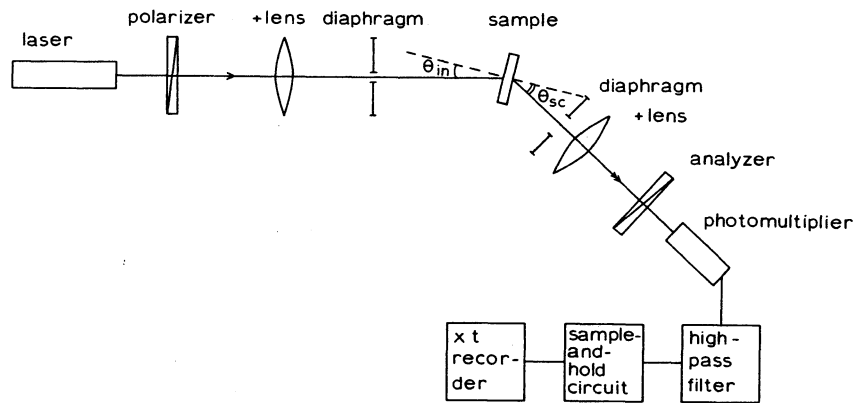| x t recorder	sample-and-hold circuit	high-pass filter

Figure 3. The experimental set-up for the measurement of Brillouin-scattered light.

defined by the aperture angle of a circular diaphragm, passed through a col-
limating lens and a second Glan-Thomson polarizer before it was detected by an
EMI 9558 B photomultiplier. The laboratory angles θ_{in} and θ_{sc} could be varied
independently ,to select the acoustic wave-vector. The apparatus needed for the
investigation of the scattered light (consisting of a photomultiplier, analyzer,
lens and diaphragm) was placed on an optical rail connected to a turntable.

Since the radiation scattered by the electro-acoustically excited flux is
present only during the application of the voltage pulse to the sample, it
causes a synchronous modulation of the detector current. The quasi-elastically
scattered light, mainly resulting from static crystal defects [34] produces a
stationary detector current. Thus, the ac part of the detector current provides
a measure for the intensity of the light scattered by the amplified acoustic
waves. This part of the detector current was measured with a synchronized
sample-and-hold circuit and recorded on an xt-recorder.

V.3.3. *Scattering configuration*

In [23] we pointed out that transverse off-axis waves are amplified in
our samples. The polarization vector of these waves lies in the plane through
the acoustic wave-vector, which is parallel to the c-axis (T_2-mode); T_1-waves
(polarization perpendicular to the c-axis) produce no piezo-electric fields
[24, 25].

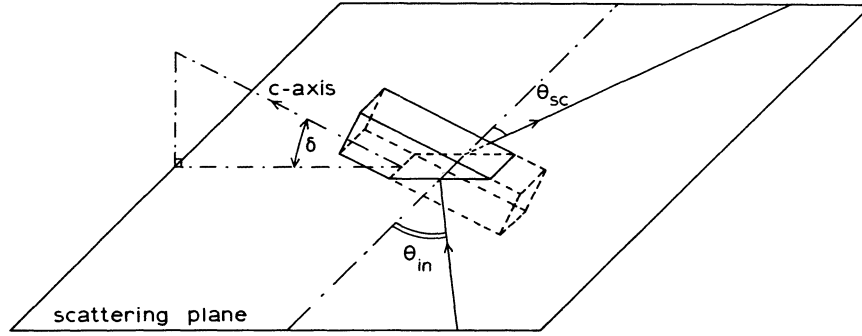To make Brillouin-scattering measurements possible for off-axis angles of

Figure 4. Brillouin-scattering configuration suitable for the study of off-axis waves.

up to 30° or more, we used the scattering configuration introduced by San'ya et al. [13] (cf. figure 4). The sample was mounted on the scattering table in such a way that it could be inclined with respect to the scattering plane. In this way any desirable off-axis angle could be selected.

The polarization of the incident light was chosen perpendicular to the c-axis. So we can put

$$n_{in} = n_\perp \quad . \tag{24}$$

The Brillouin-scattered light contained various components of polarization, defined by the vector $\vec{\xi}$ in eq. (17). To minimize the disturbing effect of the quasi-elastically scattered radiation, which in general shows no change of polarization, we detected only the extraordinary component of the Brillouin-scattered light by adjusting the analyzer. It can be shown that the associated extraordinary refractive index is given by [13, 42]:

$$n_{sc} = n_\perp n_{//}[n_\perp^2 + (n_{//}^2 - n_\perp^2)\sin^2\theta_{sc}'\cos^2\delta]^{-\frac{1}{2}} \quad . \tag{25}$$

From eqs. (10), (11), (22)-(25) a unique relationship can be obtained between the acoustic frequency f and the laboratory angles θ_{in} and θ_{sc}. Under these conditions we were able to select acoustic waves with frequencies ranging from about 0.25 GHz to 3 GHz, without the angle $|\theta_{in}|$ ever exceeding 25°. Still larger angles of incidence would give rise to an unacceptable reduction in the spatial resolution.

110

V.3.4. *Scattered power outside the scattering medium*

The power of the incident light as well as that of the Brillouin-scattered light may be reduced by scattering and absorption inside the medium. In addition, (multiple) reflections at the air/solid interfaces reduce the power that is received by the detector.

Let $\sigma_{T_{in}}$ be the total scattering coefficient per unit path-length and α_{in} the absorption coefficient per unit path-length of the incident light, respectively; let the corresponding coefficients for the Brillouin-scattered light be denoted by $\sigma_{T_{sc}}$ and α_{sc}. We derived an expression for the correction factor β, introduced in eq. (15), which accounts for the power reduction of the incident and scattered light due to scattering, absorption and multiple reflections. The factor β is given by:

$$\beta = \frac{\left\{ \exp\left(\frac{(\sigma_{T_{sc}} + \alpha_{sc})b}{\cos \theta_{sc}'} - \frac{(\sigma_{T_{in}} + \alpha_{in})b}{\cos \theta_{in}'}\right) - 1 \right\} \cdot \exp\left(-\frac{(\sigma_{T_{in}} + \alpha_{in})b}{\cos \theta_{in}'}\right)}{\left(\frac{(\sigma_{T_{sc}} + \alpha_{sc})}{\cos \theta_{sc}'} - \frac{(\sigma_{T_{in}} + \alpha_{in})}{\cos \theta_{in}'}\right) \cdot b}$$

$$\times \frac{(1 - R_{in})(1 - R_{sc})}{\left\{1 - R_{in}^2 \exp\left(\frac{-2(\sigma_{T_{in}} + \alpha_{in})b}{\cos \theta_{in}'}\right)\right\} \cdot \left\{1 - R_{sc}^2 \exp\left(\frac{-2(\sigma_{T_{sc}} + \alpha_{sc})b}{\cos \theta_{sc}'}\right)\right\}} \quad , \tag{26}$$

where R_{in} and R_{sc} are reflection coefficients given by Fresnel's law [42]. In fact, if the angle between the polarization vector $\vec{p}_{in}$ of the incident light and the plane of refraction (or scattering) is denoted by ϕ_{in}, and the angle between the polarization vector $\vec{p}_{sc}$ of the analysed, scattered light and the refraction plane by ϕ_{sc}, then R_{in} and R_{sc} are given by

$$R_{in} = \frac{tg^2(\theta_{in} - \theta_{in}')}{tg^2(\theta_{in} + \theta_{in}')} \cos^2\phi_{in} + \frac{\sin^2(\theta_{in} - \theta_{in}')}{\sin^2(\theta_{in} + \theta_{in}')} \sin^2\phi_{in} \quad , \tag{27}$$

and

$$R_{sc} = \frac{tg^2(\theta_{sc} - \theta_{sc}')}{tg^2(\theta_{sc} + \theta_{sc}')} \cos^2\phi_{sc} + \frac{\sin^2(\theta_{sc} - \theta_{sc}')}{\sin^2(\theta_{sc} + \theta_{sc}')} \sin^2\phi_{sc} \quad . \tag{28}$$

If we were to omit the effects of reflections at the crystal boundaries by putting $R_{in} = R_{sc} = 0$, eq. (26) would reduce to the result obtained by Ando et al. [43]. In our samples the attenuation of the laser light due to scattering and absorption appeared to be of little importance.

For small cone angles the internal solid angle $d\Omega'$ is related to the external solid angle $d\Omega$ by [40]:

$$d\Omega' = \frac{\cos \theta_{sc}}{n_{sc}(n_{sc}^2 - \sin^2\theta_{sc})^{\frac{1}{2}}} \cdot d\Omega \quad . \tag{29}$$

If we realize that only the component of $\vec{\xi}$ parallel to $\vec{p}_{sc}$ is detected, eq. (21) can be rewritten as (we used eqs. (20) and (29)):

$$w = \frac{dP}{P_0} \cdot \frac{2\rho\lambda_0^4 f^2 n_{sc}(n_{sc}^2 - \sin^2\theta_{sc})^{\frac{1}{2}}\cos \theta_{in}'}{\pi^2\beta \ |\vec{\xi}\cdot\vec{p}_{sc}|^2 b \cos \theta_{sc} d\Omega} \quad . \tag{30}$$

The lowest value of w we could measure turned out to be about $5 \times 10^3 \ w_{th}$. This detection limit was set by the noise in the detector current which was due to the intensity of the quasi-elastically scattered light still passing through the crossed polarization filters. However, the energy density of the electro-acoustically amplified acoustic waves was usually much higher than this detection limit.

V.3.5. *Acoustic wave-vector resolution*

In our experiments the acoustic wave-vector resolution was limited due to the finite extent of the solid angle $d\Omega$ of detection. If a wave vector with a frequency f and off-axis angle δ is selected in the way discussed before, acoustic waves with frequencies in the interval $(f \pm \Delta f)$ and off-axis angles in the interval $(\delta \pm \Delta\delta)$ scatter light into the solid angle $d\Omega$ as well. From geometrical considerations we found the frequency resolution Δf to be given by

$$(\Delta f)^2 \approx \frac{v_s^2}{\lambda_0^2} \frac{d\Omega}{\pi} \quad . \tag{31}$$

The angular resolution $\Delta\delta$ of acoustic waves is given by

$$\Delta\delta^2 \approx \frac{v_s^2}{f^2\lambda_0^2} \frac{d\Omega}{2\pi} \quad . \tag{32}$$

It should be noted that Δf and $\Delta\delta$ are not half-power band-widths, but in-dicate the maximum deviations from the selected frequency f and off-axis angle δ, respectively.

In our case $d\Omega$ was always smaller than 1.8×10^{-3} sr. Inserting this value in eq. (31) we obtain $\Delta f \approx 8 \times 10^7$ Hz. The angular resolution $\Delta\delta$ is a function of the acoustic frequency. For $f = 10^9$ Hz we find from eq. (32) that $\Delta\delta \approx 3°$; at $f = 3 \times 10^8$ Hz we even find $\Delta\delta \approx 9°$.

V.4. Experimental Results and Discussion

When investigating the propagation characteristics of an acoustic dis-turbance that is formed by a collection of plane acoustic waves with wave vectors centred in a narrow cone around a certain central wave-vector, one should realize that the direction of the acoustic-energy flow is determined by the acoustic group velocity. As a result of the elastic anisotropy in CdS the magnitudes and directions of the group velocity and the phase velocity may be quite different [15]. This elastic dispersion effect is illustrated in figure 5: an acoustic disturbance originating from 0 will propagate along the direc-tion of the group velocity $\vec{v}_g$, if the associated phase velocities are centred around $\vec{v}_s$. For instance, for $\delta = 30°$ the angle between the group velocity and the c-axis appears to be $45°$ in CdS [15].

In preliminary measurements we were able to verify the predicted frequency-shift of the Brillouin-scattered light using a Spectra Physics 470 spectrum analyzer (a Fabry-Perot interferometer).

The possible laser-induced generation of free charge carriers from local centres was investigated by varying the laser-light intensity. Photo-excitation would locally change the electro-acoustic properties of the crystal. The in-tensities of the incident light in our experiments were always such that the
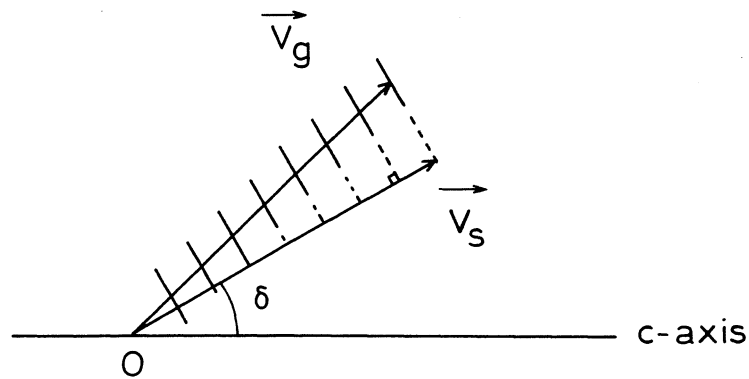
Figure 5. Elastic dispersion in CdS. $\vec{v}_s$ is the phase velocity, $\vec{v}_g$ is the group velocity. Wavefronts are indicated by parallel lines perpendicular to $\vec{v}_s$.

power of the Brillouin-scattered light was proportional to the power of the incident light. From this result we concluded that effects of local photo-excitation could be neglected in our case.

Figure 6 shows acoustic spectra for sample s_7, at various collinear positions. The selected off-axis angle was 30°; the positions were chosen along the direction of the acoustic-energy flow (i.e. at 45°). The position coordinate r = 0.8 mm was found to be quite close to the anode. (Note that the origin r = 0 was chosen arbitrarily.) The position of the anode could not be determined very accurately due to the finite cross-section of the laser beam and to the oblique angles of incidence and scattering. All spectra in figure 6 were obtained at the same reduced voltage $(\overline{V} - V_c)/V_c = 0.69$, where $\overline{V}$ is the applied voltage and V_c is the voltage defined by the onset of electro-acoustic current fluctuations [22]. The external solid angle of detection was fixed at 5×10^{-4} sr. The intensity of the Brillouin-scattered light reached a constant level about 5 μs after the onset of the bias pulse. The current and current noise appeared to remain constant after 5 μs as well. These observations indicate that after 5 μs the sample reached a stationary state.

From figure 6 we observe that the spectral acoustic-energy density increases monotonously the closer one measures to the anode, whereas the shape of the spectra remains almost unchanged. In addition, each spectrum shows a maximum at about 0.6 GHz. It is expected that this frequency will somehow be related to the frequency of maximum acoustic amplification. To find the latter frequency we should take into account that the number of acoustic modes in the
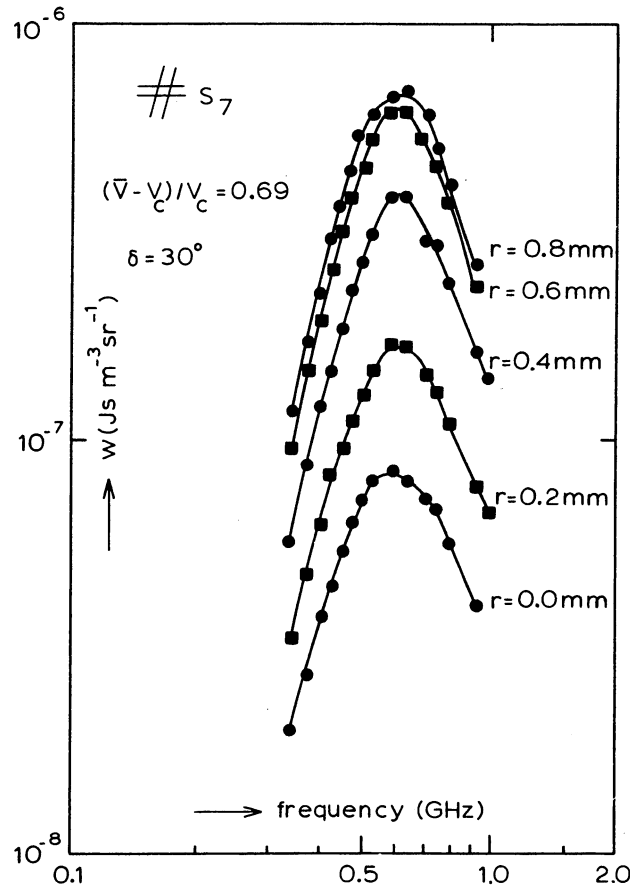
114

Figure 6. Acoustic spectra for sample s_7 at various collinear positions. The off-axis angle was $30°$. The position vector $\vec{r}$ was directed along the acoustic group velocity (at $45°$). The origin, $r = 0$, was chosen arbitrarily. The position $r = 0.8$ mm is near the anode.

frequency interval between f and $f + df$ is proportional to f^2. The frequency of maximum acoustic amplification will coincide with the frequency where a maximum occurs in the quantity $w(f)/f^2$, which is proportional to the acoustic energy of a single acoustic mode. From the data in figure 6 we derive that the maximum of $w(f)/f^2$ lies at 0.5 GHz. White's theory [17] predicts a maximum at 1.8 GHz, a value too large compared with the measured 0.5 GHz. Better agreement with the theory is obtained if we use eq. (1) combined with eq. (3). Then we find a maximum at 0.95 GHz (using $Z_{pl} = 4.3$ kΩ). Lattice attenuation (cf. eq. (4)) is of little importance. Taking lattice attenuation ($A_0 \simeq 3 \times 10^{-17}$ dBs^{2}m^{-1}rad^{-2}
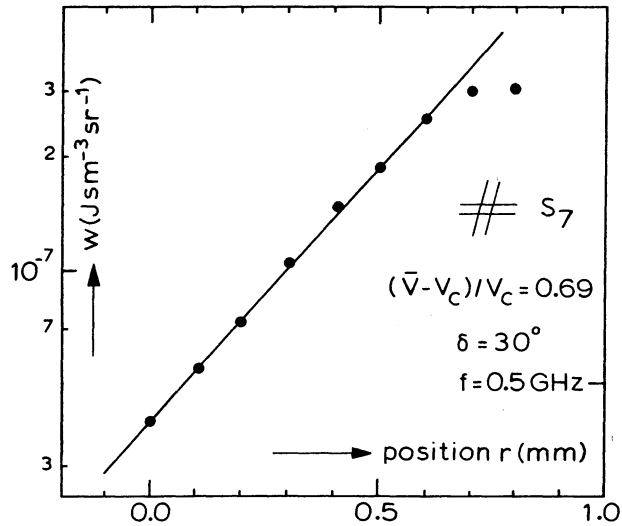
Figure 7. The spectral acoustic-energy density for $\delta = 30°$ at 0.5 GHz versus position. The position vector was in the direction of the associated acoustic group velocity (at 45°). The origin was chosen arbitrarily.

[29-31]) into account the maximum in the amplification coefficient is still found to be located at 0.95 GHz. The theoretical frequency of maximum net amplification (cf. eq. (6)) can be fitted to the experimental value of 0.5 GHz by inserting a value $s = 0.9$ μm for the surface-flatness parameter s (cf. eq. (5)). This value is quite acceptable: in the polishing procedure we used diamond powder with a fineness of about $\frac{1}{4}$ μm. The value of α_N at 0.5 GHz was found to be -8.4×10^3 dB m^{-1}.

Figure 7 shows the data of figure 6 and some supplementary data at 0.5 GHz plotted versus position r. We observe that the local acoustic-energy density varies approximately exponentially with position. At positions close to the anode (r = 0.7 mm-0.8 mm) the acoustic-energy density seems to saturate somewhat. At these positions the incident and scattered light may perhaps have been partially blocked by the anode, resulting in a reduction of the detector current.

We might interpret the exponential position-dependence of the acoustic-energy density as some kind of electro-acoustic attenuation coefficient. From the slope in figure 7 we obtained an operationally defined negative attenuation coefficient of -6.9×10^3 dB m^{-1}, a value close to the net attenuation coefficient

116

α_N calculated before. With the help of these experimental results we were able to estimate by extrapolation the spectral acoustic-energy density at positions near the cathode. Near the cathode we found $w/w_{th} \simeq 3 \times 10^3$ (for comparison, near the anode $w/w_{th} \simeq 4 \times 10^6$). This result indicates that net round-trip gain occurred in the sample during the build-up of the acoustic flux. Net round-trip gain has been observed before in CdS by Hutson et al. [44] and McFee [45]. Finally a stationary state will be reached when the net round-trip gain is reduced to unity due to some nonlinear loss mechanism.

Figure 8 shows w/w_{th} plotted versus frequency for sample s_3 at different applied voltages. The values of the reduced voltage $(\overline{V} - V_c)/V_c$ have been indicated. Note that the dimensionless quantity w/w_{th} is proportional to w/f^2 (cf. eq. (20)). We observe that the acoustic-energy density increases with increasing voltage. Maxima in the spectra occur at frequencies much lower than predicted by White's theory (according to White's theory $f_m \simeq 1.3$ GHz). In addition, these maxima are found to shift towards lower frequencies with increasing voltage. Notice that the broadening of the spectra with increasing voltage is apparent rather than real due to the logarithmic frequency-scale. The curve at $(\overline{V} - V_c)/V_c = 0.44$ shows a small additional maximum around 1 GHz. With increasing voltage this maximum turns into a small shoulder and finally it is no longer observable. Possibly this additional maximum may be interpreted as a peak left over from the early growth-stage of the acoustic flux: during the early growth-stage the amplification can be assumed to peak around a frequency close to that predicted by White's theory [5-12]; in our case $f_m \simeq 1.3$ GHz, if the Ohmic conductivity is used.

In figure 9 the frequencies corresponding to the principal maxima in w/w_{th} (cf. figure 8) have been plotted versus the reduced voltage for sample s_3 (black dots). The solid line was calculated from maxima in the net amplification coefficient $-\alpha_N$ (cf. eq. (6)) by putting $s = 1.0$ μm, which again is quite an acceptable value. Note that the adjusted parameter s, because it takes account of boundary-scattering losses only, should be independent of the applied voltage. Therefore the voltage dependence of the frequency of maximum net amplification essentially arises from the voltage dependence of the electro-acoustic amplification coefficient $-\alpha_e$ (cf. eq. (2)). The voltage dependence of the latter is determined by the drift parameter (cf. eq. (2)), and the ac-impedance plateau-value (cf. eq. (1)). For $(\overline{V} - V_c)/V_c \lesssim 0.6$ the calculation of α_N becomes very inaccurate, because α_e and $(\alpha_L + \alpha_S)$ are almost of the same magnitude and have opposite signs (cf. eq. (6)).
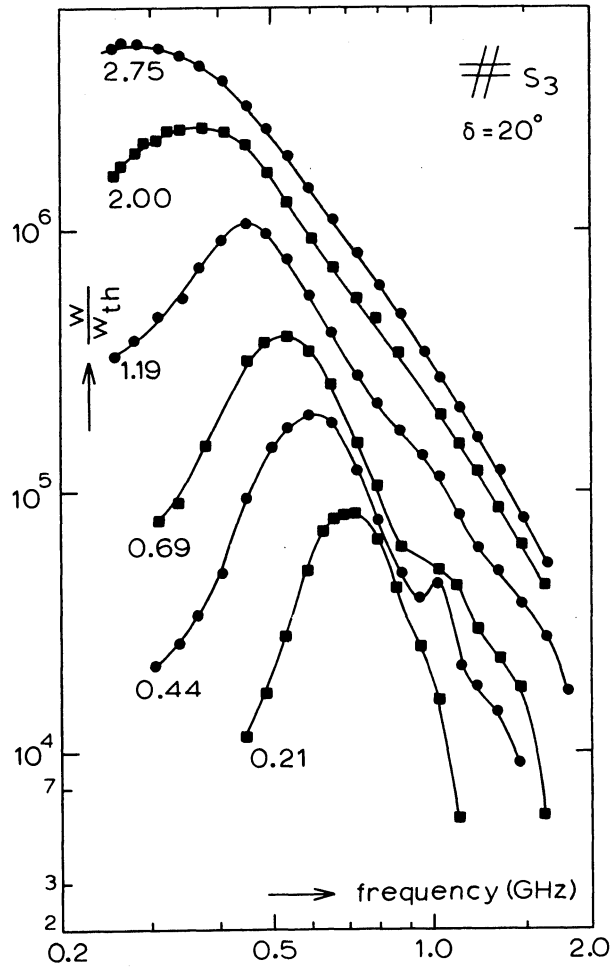
117

Figure 8. The relative spectral acoustic-energy density w/w_{th} versus frequency at different applied voltages for sample s_3. The values of the reduced voltage $(\overline{V} - V_c)/V_c$ have been indicated; V_c is the voltage marking the onset of electro-acoustic current fluctuations. The off-axis angle was $20°$.
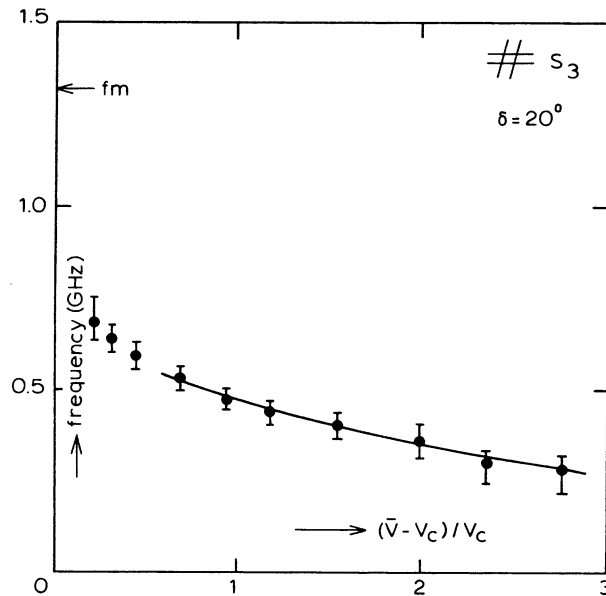
Figure 9. Experimental frequencies of maximum w/w_{th} versus the reduced voltage (dots) for sample s_3. The off-axis angle was $20°$. The solid line corresponds to maxima in the net amplification coefficient, if $s = 1.0$ µm is used (s is a measure for the surface-flatness of the crystal side-faces). The frequency of maximum amplification according to the theory of White has been indicated with an arrow on the vertical scale.

It should be noted that when the reduction of the conductivity was neglected (replacing σ_1 by the Ohmic conductivity) no acceptable curve could be fitted to the data of figure 9 with the help of eq. (6).

We conclude that the down-shift of the frequency of maximum amplification can be described quite reasonably by the linear theory, if a reduction in the conductivity, and the acoustic losses due to boundary scattering are taken into account.

From measurements of the spectral acoustic-energy distribution for sample s_3 as a function of position we again found, as in the case of sample s_7, an exponential position-dependence. The thus obtained operationally defined amplification coefficients have been plotted in figure 10 versus the reduced voltage (black dots). The data were taken at the frequencies where the ratio w/w_{th} reaches a maximum (cf. figure 8). The solid line represents the calculated net amplification coefficient, $-\alpha_N$, again using $s = 1.0$ µm.
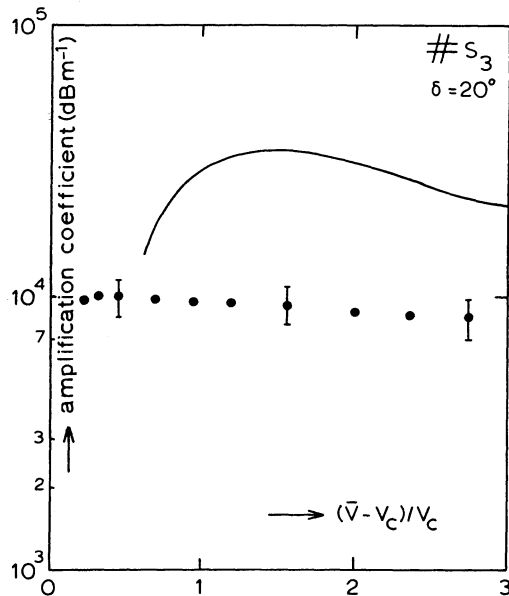
Figure 10. The operationally defined amplification coefficient for sample s_3, obtained from measurements of the spatial distribution of the acoustic energy at frequencies of maximum w/w_{th}, as a function of the reduced voltage $(\bar{V} - V_c)/V_c$ (dots). The solid line represents the calculated net amplification coefficient $-\alpha_N$, at frequencies of maximum amplification (putting $s = 1.0$ μm).

We conclude that the calculated net amplification coefficient α_N is indicative only for the order of magnitude of the operationally defined amplification coefficient which was determined from the spatial distribution of the stationary acoustic flux. There is no quantitative agreement. However, it is not clear whether we should expect such agreement. The agreement between these two amplification coefficients as found for sample s_7 (cf. figure 7) can be regarded as accidental.

Figure 11 shows acoustic spectra for sample s_4 at different applied voltages. The values of the reduced voltage $(\bar{V} - V_c)/V_c$ have been indicated. Again a pronounced down-shift is observed with increasing voltage. At voltages relatively close to the critical voltage V_c a small, additional maximum is observed, which becomes a shoulder at higher voltages. This second maximum at $(\bar{V} - V_c)/V_c = 0.23$ is found to be located close to the frequency of maximum amplification that follows from White's theory, if the Ohmic conductivity is
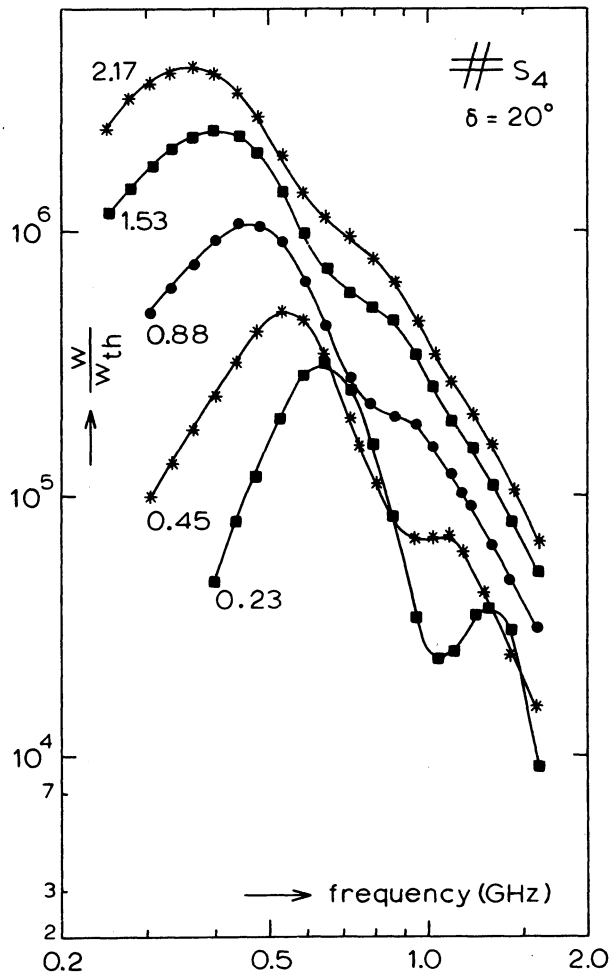
120

Figure 11. The relative spectral acoustic-energy density w/w_{th} versus frequency at different applied voltages for sample s_4. The values of the reduced voltage $(\bar{V} - V_c)/V_c$ have been indicated. The off-axis angle was $20°$.
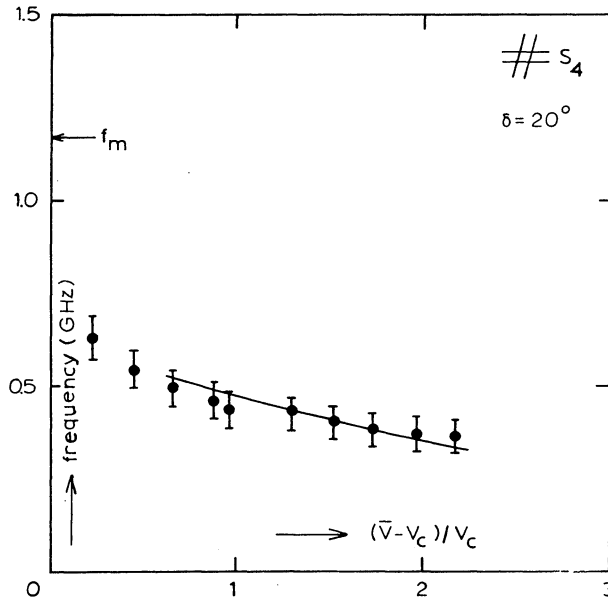
Figure 12. Experimental frequencies of maximum w/w_{th} versus the reduced voltage (dots) for sample s_4. The off-axis angle was 20°. The solid line corresponds to maxima in the net amplification coefficient, calculated if $s = 0.9$ μm is used. The frequency f_m of maximum amplification, according to the theory of White has been indicated by an arrow on the vertical scale.

used ($f_m \approx 1.2$ GHz).

In figure 12 the frequencies corresponding to the principal maxima in w/w_{th} (cf. figure 11) have been plotted versus the reduced voltage for sample s_4. The solid line was calculated from maxima in the net amplification coefficient $-\alpha_N$ (cf. eq. (6)) by putting $s = 0.9$ μm.

Measurements of the angular distribution of the acoustic-energy density for sample s_5 at $(\overline{V} - V_c)/V_c = 1.05$ are shown in figure 13. The solid lines have been drawn to guide the eye. The important feature of these experimental data is that the acoustic-energy density peaks at an off-axis angle of about 20°. As we pointed out before information about the angular distribution of the acoustic-energy density can also be obtained from resonance frequencies occurring in the ac impedance. Figure 14 shows the absolute value $|Z|$ of the ac impedance as measured for sample s_5 at $(\overline{V} - V_c)/V_c = 1.05$. For details about the measuring procedure the reader is referred to [23]. Apparently, the maxima in the ac impedance coincide with the odd harmonics of $(2.8 \pm 0.1) \times 10^5$ Hz.
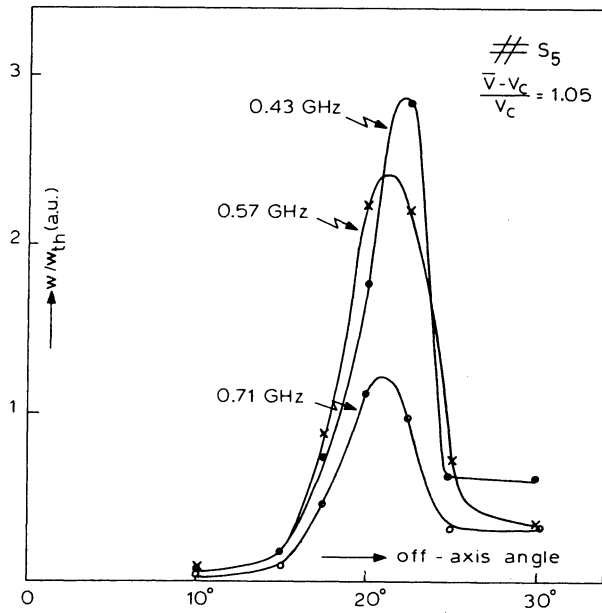
Figure 13. The angular distribution of the relative spectral acoustic-energy density for sample s_5 at $(\overline{V} - V_c)/V_c = 1.05$ for three different frequencies. The solid lines have been drawn to guide the eye.
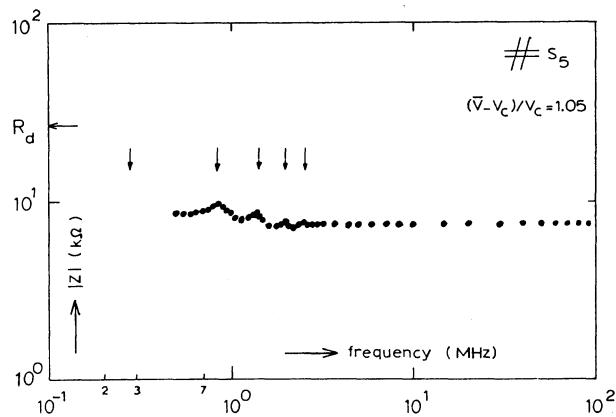

Figure 14. The absolute value of the ac impedance Z as a function of frequency for sample s_5 at $(\overline{V} - V_c)/V_c = 1.05$. The value of the differential resistance R_d has been indicated by a horizontal arrow on the vertical scale. The vertical arrows correspond to odd harmonics of 2.8×10^5 Hz.

123

As we pointed out before [21, 23], these maxima can be related to the group velocity of the amplified acoustic waves (cf. eq. (7)). Using eq. (7) we obtained for the component of the group velocity along the c-axis $v_{g_3} = (1.56 \pm 0.06) \times 10^3$ ms^{-1}. From this result and with the help of the known elastic constants [46, 47] we found the off-axis angle of the associated acoustic waves to be $\delta = 22° \pm 5°$. We conclude that this result is in good agreement with the off-axis angle of maximum acoustic-energy density as obtained from figure 13. This indicates that, as proposed before [23], the determination of resonance frequencies in the ac impedance is a useful tool for finding the off-axis angle of maximum acoustic-energy density.

V.5. Conclusion

Brillouin-scattering studies of the stationary electro-acoustically amplified acoustic flux showed that the acoustic spectra peak at frequencies which could be as much as 4 times lower than those predicted by White's linear theory [17]. The frequencies of maximum acoustic-energy density were found to be independent of position. With increasing voltage the acoustic energy was found to increase; the frequency of maximum acoustic energy was found to shift towards lower frequencies. If the effects of acoustic scattering-losses at the crystal side-faces, and a reduction of the conductivity are taken into account, this down-shift could be described by the linear theory. However, the calculated amplification coefficients appeared to be indicative only of the order of magnitude of the operationally defined amplification coefficients that were obtained from the spatial distribution of the acoustic energy.

The off-axis angle of maximum acoustic-energy density as obtained from Brillouin-scattering experiments appeared to be in good agreement with the off-axis angle as calculated from resonance frequencies in the ac impedance.

References

[1] J. Zucker and S. Zemon, Appl. Phys. Lett. 9 (1966) 398.
[2] S. Zemon, J.H. Wasko, L.L. Hope and J. Zucker, Appl. Phys. Lett. 11 (1967) 40.
[3] S. Zemon, J. Zucker, J.H. Wasko, E.M. Conwell and A.K. Ganguly, Appl. Phys. Lett. 12 (1968) 378.
[4] J. Zucker and S. Zemon, J. Ac. Soc. Am. 49 (1971) 1037.
[5] B.W. Hakki and R.W. Dixon, Appl. Phys. Lett. 14 (1969) 185.

[6]   M. Bruun, W. Wettling and N.I. Meyer, Phys. Lett. 31A (1970) 31.
[7]   D.L. Spears, Phys. Rev. B 2 (1970) 1931.
[8]   A. Many and U. Gelbart, Appl. Phys. Lett. 19 (1971) 192.
[9]   U. Gelbart and A. Many, Phys. Rev. B 7 (1973) 2713.
[10] M. Yamada, C. Hamaguchi and J. Nakai, J. Phys. Soc. Japan 33 (1972) 865.
[11] M. Yamada, C. Hamaguchi, K. Matsumoto and J. Nakai, Phys. Rev. B 7 (1973)
      2682.
[12] M. Yamada and C. Hamaguchi, J. Phys. Soc. Japan 36 (1974) 747.
[13] M. San'ya, M. Yamada, C. Hamaguchi and J. Nakai, Jpn. J. Appl. Phys. 13
      (1974) 611.
[14] J. Attal and J.P. Laurenti, J. Phys. C: Sol. St. Phys. 7 (1974) 1160.
[15] O. Keller, Phys. Rev. B 10 (1974) 1585.
[16] O. Keller, Phys. Rev. B 11 (1975) 5059.
[17] D.L. White, J. Appl. Phys. 33 (1962) 2547.
[18] M.B.N. Butler, Rep. Prog. Phys. 37 (1974) 421.
[19] R.W. Smith, Phys. Rev. Lett. 9 (1962) 87.
[20] A.R. Moore, J. Appl. Phys. 38 (1967) 2327.
[21] W. Westera, Chapter II of this thesis.
[22] W. Westera, Chapter IV of this thesis.
[23] W. Westera, Chapter III of this thesis.
[24] N.I. Meyer and M.H. Jørgensen, in "Festkörperprobleme X", ed. by
      O. Madelung, Pergamon Vieweg (1970) p. 21.
[25] A.R. Moore, R.W. Smith and P. Worcester, IBM J. Res. Developm. 13 (1969)
      503.
[26] T.B. Bateman and J.H. McFee, J. Appl. Phys. 39 (1968) 4471.
[27] F. Siebert, O. Keller and W. Wettling, Phys. Stat. Sol. (a) 4 (1971) 67.
[28] O. Keller, Phys. Lett. 39A (1972) 235.
[29] S. Furukawa and T. Hata, El. Comm. Japan. 54 C (1971) 118.
[30] T. Hata, T. Nakano, K. Koma and T. Hada, Appl. Phys. Lett. 33 (1978) 3.
[31] Y. Tokunaga, T. Hata, Y. Neda and T. Hada, Jpn. J. Appl. Phys. 19 (1980)
      379.
[32] A. Akhiezer, J. Phys. 1 (1939) 277 (in Russian).
[33] B.J. Berne and R. Pecora, "Dynamic light scattering", J. Wiley and Sons,
      Inc. (1975).
[34] W. Hayes and R. Loudon, "Scattering of light by crystals", J. Wiley and
      Sons, Inc. (1978).
[35] L. Landau and G. Placzek, Fysik Z. Sowj. 5 (1934) 172.
[36] G.B. Benedek and K. Fritsch, Phys. Rev. B 149 (1966) 647.
[37] L. Brillouin, Ann. Phys. (Paris) 17 (1922) 88.
[38] E. Gross, Nature 126 (1930) 201; 12 (1930) 400 and 126 (1930) 603.
[39] R.W. Dixon, IEEE J. Quant. El. QE-3 (1967) 85.
[40] C. Hamaguchi, J. Phys. Soc. Japan 35 (1973) 832.
[41] S. Mishra and R. Bray, Sol. St. Comm. 33 (1980) 281.
[42] M. Born and E. Wolf, "Principles of Optics", Pergamon Press, Oxford
      (1970).
[43] K. Ando and C. Hamaguchi, Phys. Rev. B 11 (1975) 3876.
[44] A.R. Hutson, J.H. McFee and D.L. White, Phys. Rev. Lett. 7 (1961) 237.
[45] J.H. McFee, J. Appl. Phys. 34 (1963) 1548.
[46] D. Berlincourt, H. Jaffe and L.R. Shiozawa, Phys. Rev. 129 (1963) 1009.
[47] I.B. Kobiakov, Sol. State Commun. 35 (1980) 305.

S U M M A R Y

Both the amplification of travelling acoustic waves in a piezoelectric
semiconductor and the effects of this amplification on the optical and elec-
trical properties of the semiconductor are referred to as *electro-acoustic
effects*. A prerequisite for the occurrence of electro-acoustic effects is the
application of an electric field that is sufficiently high to make the carrier
drift-velocity exceed the velocity of sound. In this thesis we report the re-
sults of an investigation of some electro-acoustic effects in single crystals
of hexagonal n-type CdS where the electric field was applied parallel to the
c-axis. We investigated in particular electro-acoustic current saturation,
electro-acoustic current noise and electro-acoustic effects in the ac impedance.
In addition, data on the amplified acoustic flux, which were obtained from
Brillouin-scattering experiments, are presented.

In Chapter II theoretical expressions for the current-voltage (IV-)
characteristic, spectral current-noise intensity and ac impedance are derived.
To avoid the need for solving nonlinear differential equations we made use of
a simple model. In this model free charge carriers can become trapped in deep
potential troughs that are associated with the amplified acoustic waves. We
assumed that two types of potential troughs occur, one being associated with
acoustic waves that are amplified from the thermal background, travelling in
the direction of carrier drift and the other being associated with acoustic
waves with large amplitudes travelling in the opposite direction. We assumed
that the two types of troughs are independent and that they are created and
annihilated at random throughout the crystal. In these calculations the
anisotropy of the crystal was taken into account. In addition, the potential-
trough creation and annihilation rates were allowed to depend on the electric
field strength. If space charge, diffusion and the displacement current are
neglected, the calculated current-noise spectra consist of two Lorentzians.
The ac impedance, which was calculated without making these approximations,
shows two low-frequency roll-offs, and resonances that are related to the
potential-trough transit-time.

To avoid excessive Joule heating of the CdS samples the electric field

126

was applied in pulses of only 40 μs duration with a repetition rate of 4 Hz. By using pulses with a relatively long rise-time (≃ 5 μs) the formation of macroscopic travelling acoustic domains could be prevented.

In Chapter III experimental results on the ac impedance, in the frequency range 400 kHz to 100 MHz, and on current saturation are presented. The ac-impedance data did indeed show two low frequency roll-offs obscured somewhat by potential-trough transit-time resonances. At frequencies above about 10 MHz an impedance plateau was observed. Theoretical results for the ac impedance could be fitted to the experimental data. From the positions of the observed resonance frequencies we were able to determine the potential-trough transit-time and the velocity of potential troughs. The latter was found to correspond to the group velocity of transverse off-axis waves. We concluded that in our configuration it is always transverse off-axis waves which are amplified. Furthermore it was found that the off-axis angle of maximum sound amplification is very sensitive to acoustic scattering losses at the crystal side-faces. Experimental data at 77 K did not differ essentially from data at room temperature.

In Chapter IV experimental data on electro-acoustic current noise, in the frequency range 500 kHz to 100 MHz, are presented. The measured current-noise spectra showed one or two Lorentzians, as expected from theory, and local minima at frequencies that are related to the potential-trough transit-time. The transit-time effects are not described by the noise theory, because in that theory the occurrence of space charge was neglected. Values for the electron drift-mobility obtained from the voltages marking the onset of electro-acoustic current noise lie well within the range of the values published by others.

In Chapter V experimental data on the spectral acoustic-energy density of the amplified acoustic off-axis flux in the frequency range 0.25 GHz to 1.8 GHz are given. These data were obtained with the help of a Brillouin-scattering technique. We established that no macroscopic travelling acoustic domains occurred; instead, the acoustic-energy density of the amplified acoustic waves appeared to be continuously distributed over the sample and to remain stationary about 5 μs after the moment of application of a voltage pulse of 40 μs duration. Near the carrier-injecting contact (cathode) we found that the acoustic-energy density was several orders of magnitude larger than the thermal acoustic-energy density. The spectral acoustic-energy density appeared to peak at a frequency considerably lower than that predicted by White's linear theory. With increasing voltage this peak was found to shift towards lower frequencies.

127

However, this down-shift with increasing voltage could be described quite well by White's theory, if a reduction in the free carrier concentration as resulting from trapping of carriers in potential troughs and if acoustic scattering losses at the crystal side-faces were taken into account. The off-axis angle of maximum acoustic flux as obtained from Brillouin-scattering experiments was in good agreement with the off-axis angle as calculated from resonances in the ac impedance.

SAMENVATTING

De versterking van lopende akoestische golven in een piëzo-elektrische halfgeleider, alsmede de gevolgen van die versterking voor de elektrische en optische eigenschappen van de halfgeleider worden *elektro-akoestische effekten* genoemd. Een noodzakelijke voorwaarde voor het optreden van elektro-akoestische effekten is de aanwezigheid van een elektrisch veld, dat groot genoeg is om de driftsnelheid van de ladingdragers groter te maken dan de geluidssnelheid. In dit proefschrift worden de resultaten beschreven van een onderzoek naar enkele elektro-akoestische effekten in één-kristallen van n-type CdS met het elektrisch veld evenwijdig aan de c-as. In het bijzonder zijn elektro-akoestische stroomverzadiging, elektro-akoestische stroomruis en elektro-akoestische effekten in de wisselstroom-impedantie onderzocht. Bovendien zijn, met behulp van Brillouin-verstrooiing, metingen gedaan aan de versterkte akoestische flux.

In hoofdstuk II zijn uitdrukkingen voor de stroom-spannings(IV-)karakteristiek, de spektrale stroomruis-intensiteit en de wisselstroom-impedantie afgeleid. Om de noodzaak tot het oplossen van niet-lineaire differentiaalvergelijkingen te vermijden is gebruik gemaakt van een eenvoudig model. In dat model kunnen vrije ladingdragers worden ingevangen in diepe potentiaaltroggen, die gekoppeld zijn aan de versterkte akoestische golven. Er is aangenomen, dat er twee soorten troggen kunnen voorkomen: de ene soort troggen is gekoppeld aan akoestische golven, versterkt vanuit de thermische achtergrond, die in de richting van de driftsnelheid lopen; de andere soort troggen is gekoppeld aan akoestische golven, met grote amplitudes, die in tegenovergestelde richting lopen. Er is aangenomen, dat de twee soorten troggen onafhankelijk zijn, en dat zij overal in het kristal stochastisch ontstaan en verdwijnen. In de berekeningen is rekening gehouden met de kristal-anisotropie en bovendien met een eventuele veldafhankelijkheid van het aantal troggen dat per tijdseenheid ontstaat, en verdwijnt. Indien ruimtelading, diffusie en de doorschuifstroom verwaarloosd worden, bestaat het berekende stroomruis-spektrum uit twee Lorentz-spektra. De wisselstroom-impedantie, die uitgerekend is zonder deze verwaarlozingen, vertoont twee laagfrekwente ruggen, en resonanties, die samenhangen

129

met de oversteektijd van potentiaal-troggen.

Om opwarming van de CdS-kristallen tijdens de metingen te voorkomen, wer-
den ze bekrachtigd met blokvormige spanningspulsen met een pulsduur van 40 μs
en een herhalingsfrekwentie van 4 Hz. Het optreden van makroskopische lopende
akoestische domeinen kon worden voorkomen door pulsen met een relatief lange
stijgtijd (≈ 5 μs) te gebruiken.

In hoofdstuk III worden metingen van de wisselstroom-impedantie, in het
frekwentiegebied van 400 kHz tot 100 MHz, en van stroom-spanningskarakteristie-
ken besproken. Metingen van de wisselstroom-impedantie vertonen inderdaad twee
laagfrekwente ruggen, die een beetje gemaskeerd worden door resonanties, die
samenhangen met de oversteektijd van potentiaal-troggen. Voor frekwenties boven
10 MHz is de impedantie onafhankelijk van de frekwentie. Uit de gemeten reso-
nantie-frekwenties kon de oversteektijd van potentiaal-troggen worden afgeleid.
Hieruit is gebleken, dat de snelheid van potentiaal-troggen overeenkomt met de
groepssnelheid van transversale golven, waarvan de golfvektor een hoek met de
c-as maakt (de "as-hoek"). In de gebruikte konfiguratie (elektrisch veld even-
wijdig aan de c-as) bleken in alle gevallen transversale golven, waarvan de
golfvektor een hoek met de c-as maakt, versterkt te worden. De grootte van de
as-hoek bleek sterk af te hangen van de mate van vlakheid van de zijvlakken
van de kristallen. Metingen bij 77 K verschilden niet fundamenteel van metin-
gen bij kamertemperatuur.

In hoofdstuk IV worden metingen van stroomruis-spektra, in het frekwentie-
gebied van 500 kHz tot 100 MHz, besproken. De gemeten spektra konden, in over-
eenstemming met de theorie van hoofdstuk II, beschreven worden met één of twee
Lorentz-spektra. De gemeten stroomruis-spektra vertoonden bovendien lokale mi-
nima bij frekwenties, die samenhangen met de oversteektijd van potentiaal-
troggen. Deze oversteektijdeffekten worden niet beschreven door de ruistheorie,
omdat daarin de aanwezigheid van ruimtelading verwaarloosd is. Uit metingen van
de ruis als funktie van het aangelegde elektrische veld, kon het drempelveld,
waarboven het elektro-akoestisch effect optreedt, worden bepaald. Waarden voor
de drift-beweegbaarheid van elektronen, voor verschillende kristallen afgeleid
uit het drempelveld, kwamen redelijk overeen met literatuur-waarden.

In hoofdstuk V worden metingen van de spektrale akoestische energie-dicht-
heid van de versterkte flux, in het frekwentiegebied van 0,25 GHz tot 1,8 GHz,
besproken. Deze metingen zijn verricht met behulp van Brillouin-verstrooiing.
De versterkte akoestische flux bleek ongeveer 5 μs na het aanleggen van het
elektrische veld stationair te zijn. Makroskopische lopende akoestische domei-
nen traden niet op. De spektrale akoestische energie-dichtheid bleek gepiekt

130

te zijn bij een frekwentie, die aanzienlijk lager was dan voorspeld door White's lineaire theorie. Bij toenemende veldsterkte verschoof deze piek naar lagere frekwenties. Dit verschuiven naar lagere frekwenties kon echter toch vrij goed door White's lineaire theorie beschreven worden, indien zowel een afname van het geleidingsvermogen, die ontstaat doordat ladingdragers worden ingevangen in potentiaal-troggen, als akoestische verstrooiingsverliezen aan de zijvlakken van het kristal in rekening worden gebracht. De ashoek van maximale akoestische flux, zoals verkregen uit Brillouin-verstrooiingsmetingen, bleek goed overeen te komen met de hoek, berekend uit de positie van de resonanties in de wisselstroom-impedantie.

CURRICULUM VITAE

In 1971 slaagde ik voor het examen HBS-b aan de Koninklijke Scholengemeen-
schap te Apeldoorn, en ging vervolgens natuurkunde studeren aan de Rijksuniver-
siteit te Utrecht. In september 1973 slaagde ik voor het kandidaatsexamen
natuurkunde met bijvakken wiskunde en sterrenkunde. In het studiejaar 1973-74
ben ik assistent geweest bij het praktikum medische fysika. In januari 1977
behaalde ik het doktoraal examen experimentele natuurkunde met groot bijvak
wiskunde en eerste-graads lesbevoegdheid natuurkunde, wiskunde en sterrenkunde.

Vanaf januari 1977 tot augustus 1977 gaf ik wiskunde-les op het "Nieuwe
Lyceum" te Bilthoven en van augustus 1977 tot januari 1978 natuurkunde-les op
de scholengemeenschap "F.A. Minkema" te Woerden.

In januari 1978 ben ik, in dienst van de "Stichting voor Fundamenteel
Onderzoek der Materie", begonnen met mijn promotie-onderzoek. Dit onderzoek
werd verricht binnen de vakgroep "Fysische Fluktuatieverschijnselen" van de
Rijksuniversiteit te Utrecht. Mijn onderwijstaak verrichtte ik bij het werk-
kollege natuurkunde voor scheikunde-studenten.